UNIVERSITÀ DEGLI STUDI FIRENZE

Development and Testing of Hand Exoskeletons

A dissertation submitted in partial fulfillment of the requirements for the Degree of Doctor of Philosophy in

INDUSTRIAL AND RELIABILITY ENGINEERING
Scientific Disciplinary Sector ING-IND/13

Candidate	**Advisor**
Matteo Bianchi	Prof. Benedetto Allotta

Coordinator
Prof. Maurizio De Lucia

Department of Industrial Engineering
University of Florence
Florence, Italy

XXXI Ph.D. Cycle - Years 2015/2018

To my family

Abstract

Robotics is increasingly involving many aspects of daily life and robotic-based assistance to physically impaired people is considered one of the most promising application of this largely investigated technology. However, as of today, hand exoskeletons design can still be considered a hurdle task and, even in modern robotics, providing assistance to those patients who have lost or injured their hand skills, assuring them an independent and healthy life through the design of exoskeleton technologies is, surely, one of the most challenging goal.

In this framework, the research activity carried out during the PhD period concentrated on the development of wearable devices, with special focus given to hand exoskeletons which support patients suffering from hand disabilities during the Activities of Daily Living (ADLs). The studied devices have been designed to be also used during rehabilitative sessions in specific tasks trying to restore the dexterity of the user's hands.

Starting from current solutions identified within the state of the art, the work was conducted heading to the development of portable, wearable and highly customizable devices. The last aspect will be fully endorsed by the definition of patient-centered design strategies leading to tailor-made devices specifically developed on the users' needs.

Two hand exoskeletons solutions will be presented throughout the thesis. The first consists of a compact and lightweight solution which exploits a novel 1-DOF kinematic chain of the finger mechanism to accurately reproduce the physiological finger trajectory. The applicability of topology optimization to the wearable technologies field has then been deeply investigated in the design of the second exoskeleton, which has yielded an high-performance aluminum-alloy solution.

The performance of the resulting systems was evaluated by means of simulations and tested during experimental validation campaigns by producing several prototypes which allowed to assess their effectiveness in a real-use scenario; the obtained results were satisfying, indicating that the derived solutions may constitute a valid alternative to existing hand exoskeletons so far studied in the rehabilitation and assistance fields.

Acknowledgments

The University of Florence has been giving me an incredible education throughout the last three years. It has stretched me academically and personally. I am very grateful to the people that have been with me to share this whole experience.

First and foremost, I would like to thank my advisor, Prof. Benedetto Allotta, whose knowledge and commitment allowed me to work in the field of robotics for three years, making me understand that what was a "quiescent" but long-lasting wish was coming true. These very few lines will never be enough to express my gratitude.

I also want to thank Dr. Alessandro Ridolfi for his advice, guidance, help, time, and enthusiasm. I appreciate all that I have learned from him as a teacher, mentor and especially as a friend.

I thank Dr. Enrico Meli for the significant contributions to this thesis and Dr. Roberto Conti, who paved the way of this research with tireless passion and dedication. Their direction and encouragement has been tremendous.

Special thanks go to my colleagues, past and present, of the Mechatronics and Dynamic Modeling Laboratory of the Department of Industrial Engineering of the University of Florence, which is a great place to work because of the people! Several of them have mentored me throughout this whole journey leading the distinction between colleague and friend to cease to exist. We shared with wonderful camaraderie experiences ranging from the frustration of failed attempts to the excitement of witnessing that something you spent much time and effort into works as planned.

For their loyalty, I am grateful to my lifetime friends; times may change, but the trust I have in them will always be the same.

Finally, I would like to thank my family for supporting and loving me during the highs and lows of these years. Mom and Dad are the ones who made it possible to start this journey and, along with my sister, brother and girlfriend have always been there to see me through with constant support, encouragement, and words of confidence. Their love has been overflowing.

Thanks to all the people mentioned here for shaping the person I am!

Matteo Bianchi
October 2018

Contents

List of Figures

List of Tables

Acronyms

ABS Acrylonitrile Butadiene Styrene

ADLs Activities of Daily Living

AM Additive Manufacturing

CAD Computer Aided Design

CAE Computer Aided Engineering

CMC CarpoMetaCarpal

COR Centre Of Rotation

D-H Denavit-Hartenberg

DIP Distal InterPhalangeal

DOF Degree of Freedom

EMG ElectroMyoGraphy

FDM Fused Deposition Modeling

FEA Finite-Element Analysis

FEM Finite-Element Method

GUI Graphical User Interface

HES Hand Exoskeleton System

IP Proximal Interphalangeal

LSM Level Set Method

MCP MetaCarpalPhalangeal

MoCap Motion Capture

PCA Principal Components Analysis

PIP Proximal InterPhalangeal

ROM Range Of Movement

sEMG surface ElectroMyoGraphy

SIMP Solid Isotropic Material with Penalization

SLM Selective Laser Melting

SMA Spinal Muscular Atrophy

STL Standard Tessellation Language

UM Unwanted Movement

Nomenclature

Measurement units for non-uniform quantities are not reported. A 1 in the units field denotes an unitless quantity.

C	Centrifugal and Coriolis effects	kg/s
J	Jacobian matrix	
M	System mass matrix	kg
T	Kinetic energy	kg mm^2/s^2
V	Potential energy	kg mm^2/s^2
$V(\rho)$	Volume	m^3
$V_{d,i}$	Initial design volume	m^3
V_{fr}	Volume fraction	1
$V_{n,i}$	Initial non-design volume	m^3
$V_{t,i}$	Total volume at i-th iteration	m^3
Ψ	Finger mechanism constraint equations written in vector form	
α_i	Orientation of the i-th frame	rad
$\boldsymbol{F_i}$	Forces/torques applied to the i-th body	
$\boldsymbol{Q}$	Generalized forces associated with the corresponding Lagrangian coordinate	
$\boldsymbol{\Theta}_f$	Finger rotational joints coordinates	rad

$\boldsymbol{\gamma_i}$	Spatial vector of the generalized forces acting on the i-th end-effector	
$\boldsymbol{\lambda}$	Vector collecting the Lagrange multipliers	1
$\boldsymbol{\tau_i}$	$(n \times 1)$ vector of joint forces/torques acting on the *i-th* joint for the n-degree-of-freedom mechanism	
$\boldsymbol{f_i}$	Generalized forces acting on the i-th end-effector	
$\boldsymbol{f}$	Body forces on the domain Ω	N
$\boldsymbol{r}$	Displacements of a part of the system	
$\boldsymbol{t}$	External forces acting on a body	N
$\boldsymbol{u}$	Displacements	m
$^i\boldsymbol{R_j}$	Reaction force applied to component i on joint j	N
$\mathbf{P}$	Vector collecting all the application points of the forces acting on the exoskeleton mechanism	mm
$\mathbf{R}_i^j$	Orientation of i-frame with respect to j-frame	1
$\mathbf{S}$	Vector collecting exoskeleton geometrical parameters	mm
$\mathbf{p}_f$	Fingertip pose	mm
$\mathbf{p}_i^C$	Position of object i in the camera frame	mm
$\mathbf{p}_i^F$	Position of object i in the finger frame	mm
$\mathbf{q}$	State vector of the exoskeleton system	
$\mathbf{q}_G$	Vector collecting positions and orientations of all the exoskeleton finger mechanism components	
ρ	Density	kg/m^3
ρ_f	Material density	1
σ_r	Maximum allowable values of stress	MPa
l	Strain energy	J
n_i	Generalized moment acting on the i-th end-effector	Nmm

u_r Maximum allowable displacement   m

$\widetilde{\Psi}$ Jacobian of the constraints equations system

$^1\mathbf{p}_{G,i}$ Position of the center of mass of i-th body with respect to j- frame mm

^iM_j Torque applied to component i on joint j j Nmm

$^j\mathbf{p}_i$ Position of i-frame with respect to j-frame   mm

Chapter 1

Introduction

Over the past few decades, robots have been becoming increasingly more pervasive in many aspects of the human life: industry, goods handling and transportation mostly. Lately, as other sectors, also the healthcare system has been consolidating the use of robotic devices as part of the so called "assistive technology". The World Health Organization (WHO) identifies as assistive technology the set of all the products that "enables people to live healthy, productive, independent, and dignified lives" whatever their condition. Examples of standard assistive technology are hearing aids, wheelchairs, communication aids, spectacles, prostheses, pill organizers, memory aids, etc. According to the last WHO action plan on disability [2], people who need at least one assistive device are more than 1 billion all over the world. However, only the 10% of the ones in need have access to these products due to, among the other causes, "high costs and nonexistent or inadequate funding mechanisms". The work conducted in the framework of the presented research activity was born with the intention of intervening in this problematic, making the assistive technology more accessible and affordable by developing low-cost robotic assistive devices. In this specific case, the focus is on a hand exoskeleton to help and assist people with hand(s) impairments.

The hand is one of the most important provider of independence in carrying out the Activities of Daily Living (ADLs). From the engineering point of view, it also represents a major challenge both for the mechanical design and the control strategy because of its complex anatomy, the high dexterity tasks it can accomplish and the wide set of movements it can carry out. The attempt to integrate robotics aspects with assistive products represents, nowadays, one

of the most tricky aspect of the human-robot interaction field. As a matter of fact, robotic devices have to be designed to share the environment and to physically interact with human users affected by disabilities for long periods of time and, for these reasons, they have to meet strict requirements in terms of wearability, safety and comfort. In this complex scenario, the exploitation of topology optimization methods for the mechanical design and the use of rapid prototyping technologies for the manufacturing phase have proved to be valid tools for the development of well-performing prototypes of hand exoskeletons even in a low-cost perspective.

Throughout the thesis, two different devices will be presented. Basing upon the same fundamentals of portability, wearability and cost-effectivness, an Acrylonitrile Butadiene Styrene (ABS) and an aluminum alloy system have been designed and manufactured. The first device, meant to be an effective aid at home during the ADLs and also an efficacious rehabilitative tool within the physiotherapy sessions, has been totally thought and developed in ABS material focusing on a tailor-made and patient-oriented solution capable of replicating the specific trajectories of the user's fingers. The aluminum alloy exoskeleton, instead, has been designed focusing on the dynamic interaction between the hand and the device. The whole design process of this second prototype, exploiting a topology optimization-based technique, yielded an as lightweight as robust system, which exerts suitable forces on the hand to carry out daily manual operations.

While the high costs have been avoided in the first device by choosing cheap materials and components, in the second exoskeleton, even if the price surely results higher due to the material and the motion system (the exoskeleton must guarantee higher level performances), the employment of a compact actuation and the exploitation of an additive manufacturing[1] technique let to keep costs reduced, compared to other solutions present in literature.

Unlike passive prostheses, which, as the name suggests, do not present active elements (e.g. motors), assistive robotic devices generally incorporate power supply circuits, electronics (e.g. sensors, micro-processors) and actuators and, thus, need to be carefully controlled in order to provide an intuitive and safe utilization. Even though the control strategy of the exoskeleton will not be discussed in this work, in the whole design process this issue played a key role.

---

[1] Differently from subtractive manufacturing techniques, additive manufacturing allows to produce components avoiding different steps of machining and to save material since the processing powder does not represent a proper waste, but it can be almost totally re-used. That results in a reduction of costs when complicated geometries, as in this case, need to be produced.

Resorting to a single-DOF mechanism per finger allows for the control of only one variable and results in the exploitation of less sensors and a reduction of the computational burden. On the other hand, replicating finger flexion/extension by means of only 1-DOF kinematic architecture required several choices and a specific optimization procedure which deeply affected the design of the system.

1.1 Overall framework

The research activity was conducted at the Mechatronics and Dynamic Modeling Laboratory (MDM Lab) of the Department of Industrial Engineering of the University of Florence (DIEF). The MDM Lab has been active in the field of wearable robotics since 2013. In that year, the very first prototype started to be developed. A patient affected by Spinal Muscular Atrophy (SMA) was the first user of the device, which was specifically developed for his needs and basing on his requirements. This first version of the hand exoskeleton prototype represented a first embodiment of the novel 1-DOF kinematic mechanism architecture which has then been later developed during the following years. In 2016, a collaboration with the Don Carlo Gnocchi Foundation Rehabilitation Center of Florence allowed to enlarge the target of possible users of the device. This scenario demands for the adaptation of the designed robotic system to different patients' hands. Exploiting the MoCap system available at the Don Gnocchi Rehabilitation Center, several studies focusing on the hand kinematics were carried out and a new ABS exoskeleton was developed in accordance with the necessity of tailoring different fingers gestures. Currently, the collaboration with the Don Gnocchi Foundation deals with the study of innovative control strategies for hand exoskeleton systems based on surface ElectroMyoGraphy (sEMG) signals. Even though the exploitation of sEMG signals represents a non-invasive technique in straightforwardly controlling wearable devices and such approach results deeply studied in literature, it has not been deeply tested on real patients yet. Preliminary studies have been successfully concluded and some patients have already been enrolled for the testing campaign, which is about to start.

At the time of writing, two projects are ongoing: Hand exoskeleton system, for rehabilitation and activities Of daily Living, specifically Designed on the patient anatomy (HOLD) project, funded by the University of Florence and the project Brain Machine Interface in space manned missions: amplifying FOCUSed attention for error counterbalancing (BMIFOCUS), funded by the Tuscany region. HOLD project, in the context of fully endorsing the robotic approach for the

rehabilitation and assistive issues, aims at developing a portable, wearable and highly customizable device that can be used both as an assistive hand exoskeleton and as a rehabilitative one. In view of the practical spirit of HOLD project, the hand exoskeleton configuration is based on the real requirements of patients affected by hand disabilities. The assistive use of the exoskeleton aims at satisfying the requirements concerning ADLs and, in particular, at increasing the social interaction capabilities. On the other hand, the rehabilitative exploitation aims at enhancing the therapeutic approach for addressing the sensorimotor issues of the patients. HOLD project heads to improve the wearability and portability of the current ABS device in order to make it capable of being easily transportable and easily worn for a long period thanks to its lightweight, small size, high comfort and ergonomics. Its lightness shall also allow to avoid tiredness and undesired arm fatigue as well. The devices shall be very inexpensive compared to the commercial devices, ease of use (it should be autonomously used by the patients themselves both for home rehabilitation and for ADLs assistance). In addition, different solutions of active and/or passive actuation are assessed both for opening and closing gestures. Finally, the optimization of the compliance/stiffness of the interface between the hand back and the fixed part of the exoskeleton is carried out to improve not only the ergonomics of the system but also to maximize the effect of the exoskeleton actuation by a solid connection with the hand. Since contact pressure distribution is recognized to be strictly related to comfort perception, the contact occurring between these components is simulated (by means of a finite element solver) as well as splints with different material stiffness/distribution, which are also simulated and optimized. In order to validate the numerical model, pressure distribution measurements are performed using capacitive sensors such as Novel Pliance®, available within DIEF labs. The outcome will be a comfort-oriented optimized model of the aforementioned interface.

BMIFOCUS project aims to develop a training platform to study the cognitive, sensory and locomotor systems to train pilots in managing emotions and stress in extreme environments such as piloting spacecraft and planetary extravehicular activities. The training platform will be comprised of three systems: Neurostimulation System (NSS) to monitor and enhance cognitive and physiological capacities, Simulation System (SIS) to reproduce a variety of immersive experiences (tactile, visual, auditory) and Robotic Rover (ROR) to validate the effectiveness of the system. In this framework, an hand-exoskeleton-based solution has to be integrated in the training platform to interact with a virtual and augmented reality which simulates the interaction with various objects during space vehicle piloting activities.

1.2 State of the art of hand exoskeletons

Robotic devices, such as Hand Exoskeleton Systems (HESs), provide effective solutions in assisting and improving the mobility of the patients' hands [3] and they are currently been more frequently exploiting to speed up the disease recovery and to support different manipulation tasks (such as dexterous manipulation and power grasping) [4]. Robotic systems are indeed in charge of providing high-intensity rehabilitation treatments replicating a given protocol always in the same conditions. These devices are also able to evaluate the patients' progresses measuring suitable parameters and giving the possibility to deeply monitor the rehabilitation sessions. The importance in using such a tools in a medical scenario is then highlighted by considering that the aforementioned operations are difficult, and sometimes impossible, with manual therapy.

In many cases, unfortunately, hand functions are not totally replaced after the treatment either. As reported in [5], [6], [7] and [8], up to 66% of post-stroke patients cannot regain the dexterity of their affected arm after 6 months from the stroke. In these cases the hand exoskeletons can be used to assist the users during the ADLs increasing the hand performances or automating some functional gestures.

Because of strict requirements in terms of weight and size of the mechanism, of the actuation system and of mounted sensors, and also in terms of manipulation capabilities, actually portable hand exoskeletons have not been developed as well as the exoskeleton robots for lower and upper limbs and their use does not show an outcome as positive as expected. All these reasons have made the design of a support for the hand function, based on exoskeleton technologies, one of the most influential challenges in modern robotics.

An accurate state of the art assessment has been conducted, in the first phase of the research activity, to define the underpinnings which the design process in based on, and, throughout the PhD, the critical evaluation of the wearable technologies in literature has been kept on to understand the research trends in designing exoskeletons responding to the patients' needs which, consequently, has paved the way to the development of an actually usable device.

An important aspect that must be considered at the very beginning of the literature assessment is the clustering of the aimed technology. The design phase can be thus conducted heading to the fulfilling of each request group of the whole project (i.e. the exoskeleton design).

In accordance with the state of the art [9] [10] [11] [12], HESs are classified using various criteria: linking system, Degrees Of Freedom (DOFs) and actuation type.

As regards the linking system between the hand and the exoskeleton, there are
two main different types: multi-phalanx devices [13] [14], which directly control
each phalanx separately, and single-phalanx exoskeletons [15], which actuate
only that part of the hand they are connected to. The multi-phalanx approach
exploits mechanisms made up of several parts and, thus, presents more complex
control strategies [16] [17] [18]. Usually, these devices are not totally portable
and they are supposed to be used for rehabilitative purposes [19] [20] or in
haptics [21], where the portability requirement is not a strict constraint. Nev-
ertheless, this kind of devices allows to actuate the patients' hands exactly as
well as they would do if they could by themselves. Single-phalanx devices use,
instead, simpler actuation systems and control algorithms despite of less control
capabilities than the multi-phalanx ones.

Another possible classification is based on the number of Degrees of Freedom
(DOF) of the mechanisms. Rigid multi-DOF kinematic chains are widely re-
ported [22] [23] [24], while the number of rigid single-DOF mechanisms is not
so large [25] [26]. Since exoskeletons using a rigid multi-DOF kinematic archi-
tecture demand multi-phalanx approaches, they usually present the same pros
and cons. Current single-DOF devices present a very simplified kinematics [27]
[10], which is quite far from the physiological hand kinematics.

In recent years, soft-robotic applications have, then, increasingly been develo-
ped. They present a totally different type of mechanism based on elastomeric
materials or fluid structures [28] [29] [30] [31] [32]. These devices result very
lightweight and safe for the user because of their limited stiffness.

Concerning the type of actuator, hand exoskeletons may be driven by electric
actuators [33] [34] [35] or pneumatic actuators [36]. The former actuation pro-
vides smaller forces to the hand than the latter, which, in turn, leads to higher
weight and size due to its actuation system.

Considering the aforementioned research scenario, the researchers of the MDM
Lab of the DIEF have designed an assistive and rehabilitative device for the
hand focusing on the long fingers [37]. This particular prototype was born
basing on the specific requirements indicated by a patient affected by a hand
opening impairment caused by a genetic disease and exploited a novel single
phalanx, rigid, single-DOF and cable-driven mechanism especially developed
within this research activity.

The designed kinematic chain for the long fingers has then been optimized to be
specifically adapt to any user allowing to get a good trade-off between accuracy
and functionality by reproducing the patient's finger trajectories in spite of its
dependence on only 1 DOF.

In addition, in order to increase the performance of the device, an aluminum

alloy hand exoskeleton has been developed basing on topology optimization techniques which yielded a robust but light assistive and rehabilitative tool.

1.3 Contribution and thesis structure

The research activity carried out during the PhD period focused on the development of hand exoskeletons with special regard to the mechanical design based on kinematic and dynamic assessments.

Starting from the existing scientific literature, state-of-the-art hand exoskeletons solutions (and their limitations) were analyzed, in order to identify those issues that could open up for improvements or novel design strategies. In particular, the proposed contribution relies on the design of novel devices specifically developed keeping in high regard not only the users' requirements, but also the close human-robot interaction since the very first design process. In fact, as of today, one of the challenges that need to be tackled is the exploitation of a device as effective as comfortable while maintaining the portability of the whole system. During the initial phase of the research activity, a new system capable of reproducing fingers closing and opening gestures has led to the design of a new single-phalanx, rigid, single-DOF and cable-driven mechanism for hand exoskeletons aimed at patients affected by hand opening disabilities. The achievement of a trade-off between accuracy and functionality in accomplishing this crucial task has been reached through the innovative kinematic chain especially developed to reproduce the particular long fingers trajectories basing only on a 1-DOF parallel mechanism per finger itself.

On one hand, the goal was to keep the overall system as compact and lightweight as possible (that led to the choice of exploiting only one DOF); on the other hand, in light of the contributions identified within the state of the art and supported by the preliminary tests and first testing campaigns, the primary objective was to resort to a comfortable and patient-centered solution avoiding tactile hindrance during the use of the device. This second issue was satisfyingly addressed during the PhD period thanks to the development of an optimization-based strategy which uses a completely automatic scaling procedure to customize hand exoskeletons for different patients. The testing phase, conducted in collaboration with the Don Carlo Gnocchi Foundation of Florence, has showed that the optimization process leads to devices which tailor the hand of generic patients and are capable of reproducing the natural fingers kinematics even though exploiting a mechanism with only 1 DOF.

The focus was then given to the redesign of a new hand exoskeleton made of

aluminum alloy for structural parts. Since the above-mentioned exoskeleton is based on a rigid kinematic chain that guides flexion/extension finger movements, an effective usability of the device is determined by the application of suitable forces on the hand for objects handling. That results in the requirement of high-performances and structural integrity although withstanding high forces during a prolonged use.

To reach this important goal, the applicability of topology optimization techniques has been deeply investigated. Topology optimization, even if considered as one of the most challenging and promising strategy in structural optimization, is still quite new in the wearable robotics field. In this framework, this new approach allowed for the evaluation of the optimal distribution of a given amount of material in the design domain to get the optimal connectivity, shape and number of holes. This approach enables the creation of complex 3D geometries, which are usually difficult or impossible to build using traditional manufacturing methods. Exploiting the innovative topology optimization approach and resorting an Additive Manufacturing (AM) process, a proof of concept whose mechanical features strictly replicate the desired ones (i.e. high stiffness, low weight) has been developed.

The remainder of the thesis is organized as follows. Chapter 2 introduces the mathematical background reporting the kinematic and dynamic analyses developed during the PhD period, which constitute the bases to understand the interaction between the hand and the exoskeleton. In Chapter 3 the optimization-based strategy to adapt the exoskeleton kinematics to the users' one is discussed. Chapter 4 presents the experimental results, which are embodied by the manufacturing of three different prototypes leading to the final solution. Finally, throughout Chapter 5, the whole topology optimization-based design procedure, from the problem mathematical formulation to the production of the proof of concept, is presented. Chapter 6 concludes the work.

Chapter 2

Mathematical background

This chapter introduces the adopted notation and discuss the fundamental theoretical and mathematical concepts used throughout the thesis to characterize the kinematic and dynamic behavior of the developed exoskeleton.

The kinematic and kineto-static modeling of the 1-DOF mechanism is proposed organized as follows, then, the last section is dedicated to the lagrangian dynamics formulation, which has been adopted to study the motion of the multibody system.

Section 2.1 discusses the exoskeleton kinematic analysis and synthesis: a forward kinematic study has been carried out to obtain a suitable mechanism which will be capable, once suitably modified and optimized (as detailed in Chapter 3), of accurately following the patient's finger trajectories. The mechanism has been thought to be adaptable to different hand sizes with a few variations of its geometrical parameters.

Section 2.2 reports the kineto-static study leading to the definition of the torque required to the actuation system. Starting from the kinematic characterization of the system, the relationship between the generalized forces applied to the end-effector (i.e. the finger-exoskeleton connection points) and the generalized forces applied to the joints (i.e. the demanded torque for the actuation) are determined.

Both the kinematic and the kineto-static studies are proposed in a closed form. Finally, section 2.3 presents a dynamic assessment exploited to characterize each finger mechanism behavior during the use of the device. In this study, the lagrangian formulation has been adopted to define, given the external load configuration (determined by the interaction with the hand), forces and torques

9

that the exoskeleton parts exert one to each other. This study revealed itself mandatory to the structural analysis which will be discussed in vhapter 5.
In the following sections, the notation reported in [9] will be adopted.

2.1 Kinematic analysis and synthesis

In this section, the proposed 1-DOF mechanism for the exoskeleton fingers is presented and analyzed from the kinematic viewpoint. The accurate development of a novel mechanism, characterized by a single DOF per finger, which follows the natural fingers trajectory, allowed to precisely and comfortably reproduce the complex hand kinematics without being forced to use an equally complex robotic device. That results in a designed mechanism representing a successful solution in term of functionality and manufacturability.
The choice of a single controlled DOF has led, in fact, to reduced costs, weight and encumbrance, so that the whole system (mechanism, actuation and control) could be directly placed on the back of the hand yielding a quite compact system.
An in-depth analysis of the kinematics of the single-DOF finger mechanism is detailed in the following. For sake of brevity, what reported below is related to one finger mechanism, but the same analysis can be applied to all long fingers mechanisms as well.
Fig. 2.1 shows the exoskeleton 1-DOF kinematic chain. The center of the reference system $x_1 y_1$ related to the body A is fixed to the hand. The other reference systems $x_2 y_2$, $x_3 y_3$, $x_4 y_4$, $x_5 y_5$ and $x_6 y_6$ are related to the bodies C, B, E, D and F. Component F represents a thimble which has been added in the first version of the presented hand exoskeleton. Its mounting on the system does not modify the 1-DOF kinematic chain of the device. For this reason, even if the thimble introduces a second connection point with the hand, this will not be considered a proper end-effector.
The kinematic synthesis, defining the trajectory of the exoskeleton connection point (which represents, de facto, the end effector of the planar mechanism trajectory), will pave the way to the optimization strategy, presented in Chapter 3.
The forward kinematics equations of the mechanism can be obtained starting from the revolute constraints, identifying rotational joints, in $Ox_1 y_1$, $Ox_2 y_2$, $Ox_4 y_4$:

$$\mathbf{0} = {}^1\mathbf{p}_2 + \mathbf{R}_2^1 \, {}^2\mathbf{p}_1 \tag{2.1}$$
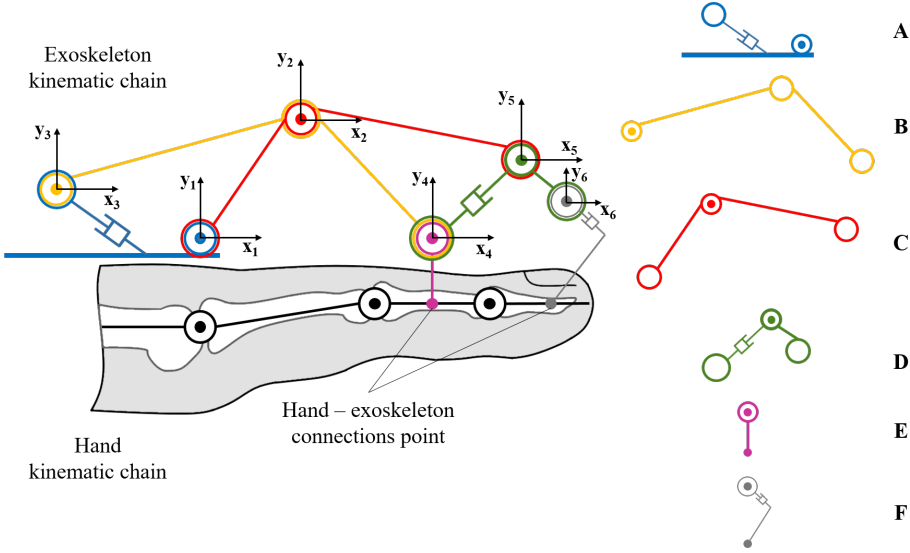
Figure 2.1: 1-DOF mechanism kinematic architecture.

$$^1\mathbf{p}_2 = {}^1\mathbf{p}_3 + \mathbf{R}_3^1 \; {}^3\mathbf{p}_2 \tag{2.2}$$

$$^1\mathbf{p}_4 = {}^1\mathbf{p}_3 + \mathbf{R}_3^1 \; {}^3\mathbf{p}_4. \tag{2.3}$$

Where, referring to Fig. 2.1 and according with the mathematical notations reported in [9], the position of the origin of i-frame[1] with respect to j-frame has been denoted by the vector ${}^j\mathbf{p}_i = \left({}^jp_i^x \; {}^jp_i^y\right)^T \in \mathbb{R}^2$ (the component on $\mathbf{z_i}$ axis has been omitted as the proposed mechanism acts on a plane) and $\mathbf{R}_i^j$ represents the orientation of i-frame with respect to j-frame, which, in this case, results in a rotation about $\mathbf{z_i}$ axis through an angle α_i.

By analyzing the two mechanical guides related to joints 3 and 5, constraints equations are:

$$a_1 \, {}^1p_3^x + b_1 \, {}^1p_3^y + c_1 = 0 \tag{2.4}$$

$$a_2 \, {}^4p_5^x + b_2 \, {}^4p_5^y + c_2 = 0 \tag{2.5}$$

---

[1]This chapter and those that follow it make frequent use of coordinate *reference frames* or simply *frames*.

where

$$^1\mathbf{p}_5 = \, ^1\mathbf{p}_2 + \mathbf{R}_2^1 \, ^2\mathbf{p}_5 \tag{2.6}$$

and

$$^1\mathbf{p}_5 = \, ^1\mathbf{p}_4 + \mathbf{R}_4^1 \, ^4\mathbf{p}_5. \tag{2.7}$$

In Eq. 2.4 and 2.5, a_1, b_1, c_1 and a_2, b_2, c_2 are respectively coefficients of Eq. 2.4 and Eq. 2.5, which represent the two linear constraints of the mechanism.

Eq. 2.6 and 2.7 have been obtained considering the rotational joint in 5.

Finally, as reported above, another interesting point has to be added to the forward kinematic analysis: since a thimble will be mounted on the presented mechanism (without altering the kinematics of the device) and it will be linked to point 6, an additional reference system (i.e. $x_6 y_6$) has been considered in the kinematic synthesis.

$$^1\mathbf{p}_6 = \, ^1\mathbf{p}_4 + \mathbf{R}_4^1 \, ^4\mathbf{p}_6. \tag{2.8}$$

Referring to Eq. 2.1-2.8, the state of the system is represented by the vector

$$\mathbf{q} = \begin{bmatrix} ^1\mathbf{p}_2^T \, ^1\mathbf{p}_3^T \, ^1\mathbf{p}_4^T \, ^1\mathbf{p}_5^T \, ^1\mathbf{p}_6^T \, \alpha_2 \, \alpha_3 \, \alpha_4 \end{bmatrix}^T \; \in \; \mathbb{R}^{13} \tag{2.9}$$

and depends on the control variable α_2. The unknowns representing the state of the system can be thus calculated as a function of only α_2 by solving Eq. 2.1-2.8. All the interesting points of the mechanism (included in the state vector $\mathbf{q}$) are in fact completely described as functions of the angle α_2 and of the geometrical parameters $\mathbf{S} \; \in \; \mathbb{R}^{16}$:

$$\mathbf{S} = [^2\mathbf{p}_1^T, \, ^3\mathbf{p}_2^T, \, ^2\mathbf{p}_5^T, \, ^3\mathbf{p}_4^T, \, ^4\mathbf{p}_6^T, a_1, b_1, c_1, a_2, b_2, c_2]^T. \tag{2.10}$$

All these parameters are completely known because they represent geometric quantities, depending only on the design of the exoskeleton parts. Consequently, it is possible to solve the extended direct kinematic model $\tilde{\mathbf{q}} = \mathbf{f}(\alpha_2, \mathbf{S}) \; \in \; \mathbb{R}^{12}$ (see Eq. 2.11) of the mechanism writing a function of α_2 and $\mathbf{S}$, where $\tilde{\mathbf{q}}$ is the

unknown part of the state vector $\mathbf{q}$:

$$\tilde{\mathbf{q}} = \begin{bmatrix} {}^1p_2^x \\ {}^1p_2^y \\ {}^1p_3^x \\ {}^1p_3^y \\ \alpha_3 \\ {}^1p_4^x \\ {}^1p_4^y \\ \alpha_4 \\ {}^1p_5^x \\ {}^1p_5^y \\ {}^1p_6^x \\ {}^1p_6^y \end{bmatrix} = \mathbf{f}(\alpha_2, \mathbf{S}). \tag{2.11}$$

The closed form resolution of the aforementioned forward kinematic is given hereinafter. Each component of vector $\tilde{\mathbf{q}}$ is highlighted in blue when it is solved in terms of only α_2 and $\mathbf{S}$. Starting from Eq. 2.1, it is possible to obtain Eq. 2.12 and 2.13:

$$ {}^1p_2^x + c\alpha_2 \cdot {}^2p_1^x - s\alpha_2 \cdot {}^2p_1^y = 0 \tag{2.12}$$

$$ {}^1p_2^y + c\alpha_2 \cdot {}^2p_1^y + s\alpha_2 \cdot {}^2p_1^x = 0 \tag{2.13}$$

and then:

$$ {}^1p_2^x(\alpha_2) = -\left(c\alpha_2 \cdot {}^2p_1^x - s\alpha_2 \cdot {}^2p_1^y\right) \tag{2.14}$$

$$ {}^1p_2^y(\alpha_2) = -c\alpha_2 \cdot {}^2p_1^y - s\alpha_2 \cdot {}^2p_1^x. \tag{2.15}$$

Similarly, from Eq. 2.2 and 2.4, the following equations can be written:

$$ {}^1p_3^x + c\alpha_3 \cdot {}^3p_2^x - s\alpha_3 \cdot {}^3p_2^y - {}^1p_2^x = 0 \tag{2.16}$$

$$ {}^1p_3^y + c\alpha_3 \cdot {}^3p_2^y + s\alpha_3 \cdot {}^3p_2^x - {}^1p_2^y = 0 \tag{2.17}$$

$$ a_1 \cdot {}^1p_3^x + b_1 \cdot {}^1p_3^y + c_1 = 0 \tag{2.18}$$

or, equivalently:

$$ \begin{cases} {}^1p_2^x - {}^1p_3^x = c\alpha_3 \cdot {}^3p_2^x - s\alpha_3 \cdot {}^3p_2^y \\ {}^1p_2^y - {}^1p_3^y = c\alpha_3 \cdot {}^3p_2^y + s\alpha_3 \cdot {}^3p_2^x \\ a_1 \cdot {}^1p_3^x + b_1 \cdot {}^1p_3^y + c_1 = 0. \end{cases} \tag{2.19}$$

Summing the squares of the first and second components of Eq. 2.19 one can get:

$$\begin{cases} \left(^1p_2^x - {}^1p_3^x\right)^2 + \left(^1p_2^y - {}^1p_3^y\right)^2 = \left(^3p_2^x\right)^2 + \left(^3p_2^y\right)^2 \\ a_1 \cdot {}^1p_3^x + b_1 \cdot {}^1p_3^y + c_1 = 0 \end{cases} \tag{2.20}$$

and solving the system:

$$^1p_3^y(\alpha_2) = \frac{-\left(^1p_2^x \cdot \frac{b_1}{a_1} + \frac{b_1 \cdot c_1}{a_1^2} - {}^1p_2^y\right)}{\left(\frac{b_1}{a_1}\right)^2 + 1} + \frac{\sqrt{\left(^1p_2^x \cdot \frac{b_1}{a_1} + \frac{b_1 \cdot c_1}{a_1^2} - {}^1p_2^y\right)^2 - \left[\left(\frac{b_1}{a_1}\right)^2 + 1\right] \cdot H}}{\left(\frac{b_1}{a_1}\right)^2 + 1} \tag{2.21}$$

$$^1p_3^x(\alpha_2) = -\frac{1}{a_1} \cdot \left(b_1 \cdot {}^1p_3^y + c_1\right) \tag{2.22}$$

where

$$H = \left(^1p_2^x\right)^2 + \left(^1p_2^y\right)^2 - \left(^3p_2^x\right)^2 - \left(^3p_2^y\right)^2 + 2 \cdot {}^1p_2^x \cdot \frac{b_1}{a_1} + \left(\frac{c_1}{a_1}\right)^2 . \tag{2.23}$$

Now α_3 can be computed as:

$$c\alpha_3 = \frac{^1p_2^y - s\alpha_3 \cdot {}^3p_2^x - {}^1p_3^y}{^3p_2^y} \tag{2.24}$$

$$s\alpha_3 = \frac{1}{^3p_2^y + \frac{\left(^3p_2^x\right)^2}{^3p_2^y}} \cdot \left(-^1p_2^x + {}^1p_3^x + \frac{^3p_2^x}{^3p_2^y} \cdot {}^1p_2^y - \frac{^3p_2^x}{^3p_2^y} \cdot {}^1p_3^y\right) \tag{2.25}$$

$$\alpha_3(\alpha_2) = atan2\left(\frac{\left(-^1p_2^x + {}^1p_3^x + \frac{^3p_2^x}{^3p_2^y} \cdot {}^1p_2^y - \frac{^3p_2^x}{^3p_2^y} \cdot {}^1p_3^y\right)}{^3p_2^y + \frac{\left(^3p_2^x\right)^2}{^3p_2^y}}, \frac{^1p_2^y - s\alpha_3 \cdot {}^3p_2^x - {}^1p_3^y}{^3p_2^y}\right) . \tag{2.26}$$

At this point, Eq. 2.27 and 2.28 can be written from Eq. 2.3:

$$^1p_3^x + c\alpha_3 \cdot {}^3p_4^x - s\alpha_3 \cdot {}^3p_4^y - {}^1p_4^x = 0 \tag{2.27}$$

$$^1p_3^y + c\alpha_3 \cdot {}^3p_4^y + s\alpha_3 \cdot {}^3p_4^x - {}^1p_4^y = 0 \tag{2.28}$$

and then:

$$^1p_4^x(\alpha_2) = {}^1p_3^x + c\alpha_3 \cdot {}^3p_4^x - s\alpha_3 \cdot {}^3p_4^y \tag{2.29}$$

$$^1p_4^y(\alpha_2) = {}^1p_3^y + c\alpha_3 \cdot {}^3p_4^y + s\alpha_3 \cdot {}^3p_4^x . \tag{2.30}$$

Finally, from Eq. 2.6, one can get

$$^1p_5^x(\alpha_2) = {}^1p_2^x + c\alpha_2 \cdot {}^2p_5^x - s\alpha_2 \cdot {}^2p_5^y \tag{2.31}$$

$$^1p_5^y(\alpha_2) = {}^1p_2^y + c\alpha_2 \cdot {}^2p_5^y + s\alpha_2 \cdot {}^2p_5^x \tag{2.32}$$

and from Eq. 2.5 and 2.7:

$$^1p_5^x = {}^1p_4^x + c\alpha_4 \cdot {}^4p_5^x - s\alpha_4 \cdot {}^4p_5^y \tag{2.33}$$

$$^1p_5^y = {}^1p_4^y + c\alpha_4 \cdot {}^4p_5^y + s\alpha_4 \cdot {}^4p_5^x \tag{2.34}$$

$$a_2 \cdot {}^4p_5^x + b_2 \cdot {}^4p_5^y + c_2 = 0 \tag{2.35}$$

or, equivalently:

$$\begin{cases} {}^1p_5^x - {}^1p_4^x = c\alpha_4 \cdot {}^4p_5^x - s\alpha_4 \cdot {}^4p_5^y \\ {}^1p_5^y - {}^1p_4^y = c\alpha_4 \cdot {}^4p_5^y + s\alpha_4 \cdot {}^4p_5^x \\ a_2 \cdot {}^4p_5^x + b_2 \cdot {}^4p_5^y + c_2 = 0. \end{cases} \tag{2.36}$$

As in the previous cases, summing the squares of the first and second components of Eq. 2.36, Eq. 2.37 can be obtained:

$$\begin{cases} \left({}^1p_5^x - {}^1p_4^x\right)^2 + \left({}^1p_5^y - {}^1p_4^y\right)^2 = \left({}^4p_5^x\right)^2 + \left({}^4p_5^y\right)^2 \\ a_2 \cdot {}^4p_5^x + b_2 \cdot {}^4p_5^y + c_2 = 0 \end{cases} \tag{2.37}$$

and, consequently,

$$^4p_5^y(\alpha_2) = \frac{-(b_2 \cdot c_2) + \sqrt{(b_2 \cdot c_2)^2 - (b_2{}^2 + a_2{}^2) \cdot T}}{b_2{}^2 + a_2{}^2} \tag{2.38}$$

$$^4p_5^x(\alpha_2) = -\frac{1}{a_2} \cdot (b_2 \cdot {}^4p_5^y + c_2) \tag{2.39}$$

where:

$$T = -a_2{}^2 \cdot \left[\left({}^1p_5^x - {}^1p_4^x\right)^2 + \left({}^1p_5^y - {}^1p_4^y\right)^2\right] + c_2{}^2. \tag{2.40}$$

Considering the system 2.36, α_4 can be calculated:

$$c\alpha_4 = \frac{{}^1p_5^x + s\alpha_4 \cdot {}^4p_5^y - {}^1p_4^x}{{}^4p_5^x} \tag{2.41}$$
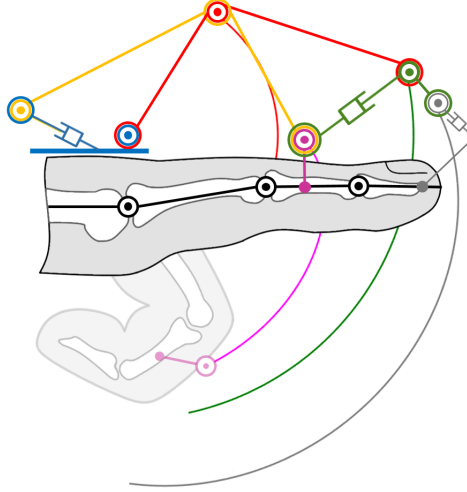
Figure 2.2: Joint trajectories of the 1-DOF finger mechanism.

$$s\alpha_4 = \frac{1}{-{}^4p_5^x + \frac{({}^4p_5^y)^2}{{}^4p_5^x}} \cdot \left(-{}^1p_4^y + {}^1p_5^y - \frac{{}^4p_5^y}{{}^4p_5^x} \cdot {}^1p_5^x + \frac{{}^4p_5^y}{{}^4p_5^x} \cdot {}^1p_4^x \right) \tag{2.42}$$

$$\alpha_4(\alpha_2) = atan2 \left(\frac{\left(-{}^1p_4^y + {}^1p_5^y - \frac{{}^4p_5^y}{{}^4p_5^x} \cdot {}^1p_5^x + \frac{{}^4p_5^y}{{}^4p_5^x} \cdot {}^1p_4^x \right)}{-{}^4p_5^x + \frac{({}^4p_5^y)^2}{{}^4p_5^x}}, \frac{{}^1p_5^x + s\alpha_4 \cdot {}^4p_5^y - {}^1p_4^x}{{}^4p_5^x} \right) \ . \tag{2.43}$$

Finally, ${}^1\mathbf{p}_6$ results:

$${}^1p_6^x(\alpha_2) = {}^1p_4^x + c\alpha_4 \cdot {}^4p_6^x - s\alpha_4 \cdot {}^4p_6^y \tag{2.44}$$

$${}^1p_6^y(\alpha_2) = {}^1p_4^y + c\alpha_4 \cdot {}^4p_6^y + s\alpha_4 \cdot {}^4p_6^x \tag{2.45}$$

All the interesting points of the mechanism (included in the state vector $\mathbf{q}$) are completely described as a function of the angle α_2 and of the geometrical parameters collected in $\mathbf{S} \in \mathbb{R}^{16}$.

At this point, the motion is completely described and the relative positions of any joint is given. Fig. 2.2 shows the trajectories of the 1-DOF finger mechanism joints., providing a qualitative overview of the resulted kinematics of the mechanism when fingers are actuated.

Please, note that, even the forward kinematic assessment lead to define the position of the end-effector, its orientation can be evaluate only considering his coupling with the hand. This point will be discussed in detail in Chapter 3.

2.2 Kineto-statics

This section lays the foundation to assess how much power will be required for the exoskeleton actuation, considering the amount of strength demanded in grasping. Hereinafter the mathematical procedure for the kineto-static analysis is described.

Let us consider the $(r \times 1)$ spatial vector of the generalized forces[2] (r is the dimension of the operational space of interest) acting on the i-th end-effector

$$\boldsymbol{\gamma_i} = \begin{pmatrix} \boldsymbol{f_i} \\ n_i \end{pmatrix}, \tag{2.46}$$

where $\boldsymbol{f_i}$ and n_i denote the force and moment, respectively (in this planar case, $\boldsymbol{f_i}$ is a two-component vector and n_i a scalar value).

By invoking the principle of virtual work, the following relation can be derived

$$\boldsymbol{\tau_i} = J^T(\mathbf{q_i})\boldsymbol{\gamma_i}, \tag{2.47}$$

where, $\boldsymbol{\tau_i}$ denote the $(n \times 1)$ vector of joint forces/torques acting on the i-th joint for the n-degree-of-freedom mechanism. Eq. 2.47 establishes, by the transpose of the manipulator geometric Jacobian, the relationship between the end-effector forces and the joint torques.

Eq.2.47 can be then generalized to the whole proposed mechanism

$$\tau_1(\alpha_2, \mathbf{S}) = J^T(\alpha_2, \mathbf{S})\boldsymbol{\gamma}. \tag{2.48}$$

Where, τ_1 is the torque acting on joint 1 and vector $\boldsymbol{\gamma}$ is the $(6r \times 1)$ vector collecting the torques and forces applied to 1 to 6 joints.

The first step of the kineto-static analysis is thus the definition of the geometric Jacobian J of the mechanism. The procedure to determine the geometric Jacobian is reported below. Essentially, J has been calculated exploiting the forward kinematic model described in Section 2.1. Considering to directly actuate joint 1 (Fig. 2.1), Eq. 2.47 has to yield, once defined the general forces the

---

[2]Generalized forces at the joints will be often called *torques*, while generalized forces at the end-effector are often called *forces*.

end-effector should exert, the torque needed at that joint itself. Through the principal of virtual work, the required torque on joint 1 is then characterized by the equation:

$$\boldsymbol{\gamma}^T \delta \mathbf{P} = \tau_1 \delta \alpha_2, \tag{2.49}$$

where $\mathbf{P}$ is the vector collecting all the application points of the forces acting on the exoskeleton mechanism. As the application points correspond to the joint positions, vector $\mathbf{P}$ is defined as follows:

$$\mathbf{P} = \left[{}^1\mathbf{p}_1^T, {}^1\mathbf{p}_2^T, {}^1\mathbf{p}_3^T, {}^1\mathbf{p}_4^T, {}^1\mathbf{p}_5^T, {}^1\mathbf{p}_6^T \right]^T. \tag{2.50}$$

Vector $\mathbf{P}$ depends only on α_2 and $\mathbf{S}$:

$$\mathbf{P} = \mathbf{P}(\mathbf{q}) = \mathbf{P}(\mathbf{q}(\alpha_2, \mathbf{S})) = \mathbf{P}(\alpha_2, \mathbf{S}). \tag{2.51}$$

Alle the components in Eq. 2.51 are completely known as vector $\mathbf{P}$ is defined by the forward kinematic (solved in closed form in the previous section).

By means of the kineto-static model of the mechanism and considering Eq. 2.49, τ_1 can be calculated:

$$\tau_1(\alpha_2, \mathbf{S}) = \left(\frac{\delta \mathbf{P}}{\delta \alpha_2}(\alpha_2, \mathbf{S}) \right)^T \boldsymbol{\gamma}, \tag{2.52}$$

where $\left(\frac{\delta \mathbf{P}}{\delta \alpha_2}(\alpha_2, \mathbf{S}) \right)$ is the geometric Jacobian of the mechanism.

2.3   Lagrangian formulation

In this Section, exploiting the kinematic analysis presented in Section 2.1, Lagrange's equations are used to analyze the motion of multibody systems consisting of interconnected rigid bodies (in this case, the exoskeleton finger mechanism) by a dynamic point of view.

The application of Lagrange dynamics to the exoskeleton, once the external loads have been defined (i.e. hand-exoskeleton interaction forces and torques provided by the actuation system) allowed to determine forces and torques which exoskeleton linked components exert one to each other during the use of the device. This information will be mandatory to design a prototype characterized by high stiffness and low weight (Chapter 5).

To maintain the generality of the formulations presented in this chapter, the Cartesian coordinates are used to describe the motion of the multibody system.

To this end, a reference coordinate system, henceforth called *body reference* or *body coordinate system*, is assigned for each body in the multibody system. The configuration of the rigid body in the system can then be identified by defining the location of the origin and the orientation of the body coordinate system with respect to an inertial global frame of reference, which is centered on its center of mass. For convenience, the notation $^1\mathbf{q}_{G,i}$ denotes the generalized coordinates of the body reference for each component, that is,

$$^1\mathbf{q}_{G,i} = \left[\begin{array}{cc} ^j\mathbf{p}_{G,i}{}^T & \alpha_i{}^T \end{array} \right]^T, \tag{2.53}$$

where $^1\mathbf{p}_{G,i}$ is the position of the center of mass of i-th body ($i = 2, 3, 4$ for, respectively, C, B, D bodies), while α_i indicates the orientation of the i-th body and it is represented by a scalar in the 2-D motion. Component A has not been included in this analysis, since it is considered fixed to the hand back. Component E and F have not been analyzed either, because their interactions with the finger will be evaluated as forces applied on joints 4 and 6.

Similarly to Eq. 2.9, $\mathbf{q}_G \in \mathbb{R}^{3n}$ denotes the vector collecting positions and orientations of all the n mechanism components.

These generalized coordinates, however, are not totally independent because of the mechanical joints between adjacent bodies. The motion of each component in the system is influenced by the motion of the others through the kinematic constraints that relate the generalized coordinates and velocities. Considering the multibody system represented by the exoskeleton finger mechanism, these $3n$ generalized coordinates are related by n_c constraint equations where $n_c \leq n$. The n_c constraint equations of the finger mechanism can be written in the following vector form:

$$\{\Psi\} = 0, \tag{2.54}$$

which, referring to the forward kinematics discussed in Section 2.1, can be explicitly written as:

$$
\begin{bmatrix}
{}^1p_{G,2}^x + c\alpha_2\,{}^2p_{G,1}^x - s\alpha_2\,{}^2p_{G,1}^y \\
{}^1p_{G,2}^y + c\alpha_2\,{}^2p_{G,1}^y - s\alpha_2\,{}^2p_{G,1}^x \\
\alpha_2 - K \\
{}^1p_{G,3}^x + c\alpha_3\,{}^3p_{G,2}^x - s\alpha_3\,{}^3p_{G,2}^y - {}^1p_{G,2}^x \\
{}^1p_{G,3}^y + c\alpha_3\,{}^3p_{G,2}^y + s\alpha_3\,{}^3p_{G,2}^x - {}^1p_{G,2}^y \\
{}^1p_{G,3}^x + c\alpha_3\,{}^3p_{G,4}^x - s\alpha_3\,{}^3p_{G,4}^y - {}^1p_{G,4}^x \\
{}^1p_{G,3}^y + c\alpha_3\,{}^3p_{G,4}^y + s\alpha_3\,{}^3p_{G,4}^x - {}^1p_{G,4}^y \\
a_1\,{}^1p_{G,3}^x + b_1\,{}^1p_{G,3}^y + c_1 \\
a_2\,{}^4p_{G,5}^x + b_2\,{}^4p_{G,5}^y + c_2
\end{bmatrix}
= 0.
\qquad (2.55)
$$

Eq. 2.55 is the set of independent (holonomic, scleronomic) constraint equations. In particular, the first two rows represent the revolute joint in 1, while the third raw does not represent a real constraints but it has been included in order to fix the pose of the mechanism defining a particular ROM K. Fourth and fifth rows are the revolute joint in 2 and sixth and seventh raws model revolute joint 3. Joints 3 and 5 are modeled by equations in the last two rows.

The dynamic description of the system is then completed by considering the kinetic energy T, the potential energy V, and the generalize forces $\boldsymbol{Q}$. Q_j is namely the component of the generalized force associated with the lagrangian coordinate q_j and can be written as:

$$
Q_j = \sum_{i=1}^{n} \boldsymbol{F}_i^T \frac{\partial \boldsymbol{r}_i}{\partial q_j},
\qquad (2.56)
$$

where n is, again, the number of the elements of the system, $j = 1, ..., 3n$, with $3n$ that denotes the number of DOF of the system (without considering constraints equations since they are included in the term $\{\Psi\}$), $\boldsymbol{F_i}$ is the force applied to the i-th body, and $\boldsymbol{r_i}$ is the i-th displacement of that part of the system.

The Lagrangian for the system is given by :

$$
\mathcal{L} = T - V - \sum_{k=1}^{n_c} \lambda_k \Psi_k,
\qquad (2.57)
$$

where λ_k is the k-th Lagrange multiplier for each constraint equation Ψ_k ($k = 1, ..., n_c$). The Lagrange's equation (first kind) is then given by:

$$\frac{d}{dt}\frac{\partial \mathcal{L}}{\partial \dot{q}_j} - \frac{\partial \mathcal{L}}{\partial q_j} = Q_j. \tag{2.58}$$

Referring to the specific application (the hand exoskeleton finger mechanism), the considered constraints $\{\Psi\}$ do not depend either on time (t) or velocity ($\dot{\boldsymbol{q}}$) and the Lagranges's equation can be thus written as:

$$\frac{d}{dt}\frac{\partial T}{\partial \dot{q}_j} - \frac{\partial T}{\partial q_j} + \sum_{k=1}^{n_c} \lambda_k \frac{\partial \Psi_k}{\partial q_j} = -C_j(q_j, \dot{q}_j)\dot{q}_j - \frac{\partial V}{\partial q_j} + Q_j. \tag{2.59}$$

Equation 2.59 can be written explicitly as follows:

$$M\ddot{\mathbf{q}} + \widetilde{\Psi}(\mathbf{q})^T \{\lambda\} = \mathbf{Q}(\mathbf{q}) - C(\mathbf{q}, \dot{\mathbf{q}})\dot{\mathbf{q}} - \left(\frac{\partial V}{\partial \mathbf{q}}\right)^T. \tag{2.60}$$

where: M is the system mass matrix referred to the generalized coordinates systems (Eq. 2.53); $\widetilde{\Psi}(\boldsymbol{q})$ is the ($n_c \times 3n$) Jacobian of the constraints equations system (referred to the generalized coordinates systems as well); $\boldsymbol{\lambda} \in \mathbb{R}^{n_c}$ is the vector collecting the Lagrange multipliers; $\boldsymbol{Q}$ is the vector collecting the generalized forces; $C(\mathbf{q}, \dot{\mathbf{q}})\dot{\boldsymbol{q}}$ is the matrix collecting the non-linear centrifugal and Coriolis effects. Equation 2.60 can be written in a compact form:

$$\begin{bmatrix} M & \tilde{\Psi}^T \\ \tilde{\Psi} & 0 \end{bmatrix} \begin{pmatrix} \ddot{\mathbf{q}} \\ \boldsymbol{\lambda} \end{pmatrix} = \begin{pmatrix} \mathbf{Q} - C\dot{\mathbf{q}} - \left(\frac{\partial \mathbf{V}}{\partial \mathbf{q}}\right)^T \\ -\dot{\tilde{\Psi}}\{\dot{\boldsymbol{q}}\} \end{pmatrix}, \tag{2.61}$$

and governs the dynamic behavior of the mechanism. In particular, once defined the geometry of the finger mechanism and the forces applied to it (i.e. the interaction forces acting during the ordinary use of the device), reaction forces on each joint and the torque applied to joint 1 can be determined by Eq. 2.61. The procedure that led to the joints reaction forces definition is reported in its closed form in the following.

Exploiting the algorithm reported in [38] and neglecting centrifugal and Coriolis effects (because of the slow rate of change of α_2), as well as the contribution of the potential energy, Lagrange multipliers and acceleration terms can be calculated:

$$\boldsymbol{\lambda} = A_{21}\boldsymbol{Q}, \tag{2.62}$$

$$\ddot{\boldsymbol{q}} = A_{11}\boldsymbol{Q}, \tag{2.63}$$

where

$$A_{22} = (\tilde{\Psi}M^{-1}\tilde{\Psi}^T)^{-1}, \tag{2.64}$$

$$A_{11} = M^{-1} - M^{-1}\tilde{\Psi}^T A_{22}\tilde{\Psi}M^{-1}, \tag{2.65}$$

$$A_{21} = \left(-M^{-1}\tilde{\Psi}^T A_{22}\right)^T. \tag{2.66}$$

Equation 2.62 allows for the definition of the Lagrange multipliers, this step is mandatory for reaction forces calculation. Reaction forces are then calculated as follows:

$$\left(\begin{array}{c} {}^1F_{xi} \\ {}^1F_{yi} \\ {}^1\tau_i \end{array}\right) = \left(\begin{array}{cc} -R_i^1(\alpha_i)^T A_i^1(\alpha_i)^T & 0 \\ {}^1\boldsymbol{d}_i{}^T V A_i^1(\alpha_i)^T & -1 \end{array}\right) min_k\left(\tilde{\Psi}\right) min_k\left(\boldsymbol{\lambda}\right). \tag{2.67}$$

In Eq. 2.67, F_{xi}, F_{yi} are, respectively, components along x- and y-axis of forces applied to the i-th joint, while τ_{zi} is the reaction torque component about z axis. $A_i^1(\alpha_i)$ represents the 3-by-3 rotation matrix mapping the transformation from i-th joint frame to the body reference frame, $R_i^1(\alpha_i)$ represents the orientation of i- joint frame with respect to the base reference frame 1 and ${}^1\boldsymbol{d}_i$ is then the distance between them expressed in the base frame. Finally, $min_k(\Psi)$ and $min_k(\boldsymbol{\lambda})$ can be defined for the k-th constraint as follows:

$$min_k\left(\tilde{\Psi}\right) = \left[\begin{array}{cc} \frac{\partial\Psi_k}{\partial q_{3i-2}} & \frac{\partial\Psi_{k+1}}{\partial q_{3i-2}} \\ \frac{\partial\Psi_k}{\partial q_{3i-1}} & \frac{\partial\Psi_{k+1}}{\partial q_{3i-1}} \\ \frac{\partial\Psi_k}{\partial q_{3i}} & \frac{\partial\Psi_{k+1}}{\partial q_{3i}} \end{array}\right]$$

and

$$min_k\left(\boldsymbol{\lambda}\right) = \left\{\begin{array}{c} \lambda_k \\ \lambda_{k+1} \end{array}\right\}.$$

Forces and torques are hence calculated with respect to joints frames.
The detailed procedure has been exploited in order to define the reaction forces and torques acting on each mechanism parts during the use of the device. Such forces played the important role of input for the topology optimization problem, which has been studied in designing a device as lightweight as possible without lowering its stiffness. The application of this particular analysis is detailed in Chapter 5.

Chapter 3

Optimization-based scaling procedure

The designed kinematic chain allows to get a good trade-off between accuracy and functionality when reproducing the patient's finger trajectories in spite of its dependence on only 1 DOF. In fact, assessing the hand exoskeletons presented in the state of the art, portability, wearability and adaptability appear as critical aspects to be considered during the design and development processes. The portability of the device regards the development of light mechanisms and actuation systems with limited encumbrances mechanisms and actuation systems themselves. Adopted solutions to reach these goals will be detailed in Chapters 4 and 5. The wearability requires an ergonomic structure and the manufacture of a comfortable device for the patient. This is demanded also for a prolonged use of the exoskeleton itself. Last but not least, the adaptability requires an exoskeleton tailored on the user. Since different users have, of course, different hand characteristics (hand sizes and anatomical dimensions due to e.g. bone positions and tissue deformations), and different disabilities, the adaptability of a device is not only important but even necessary for its use, although that complicates the design of the exoskeleton.

Bearing in mind these three important aspects, part of the research study proposed in this thesis aimed to develop a novel design strategy which leads to a totally custom-made aid for the patients' hands. The resulting mechanism is indeed not only portable and wearable but especially adaptable to the user's hand.

In this chapter, the optimization strategy yielding a completely tailor-made hand exoskeleton is reported. Exploiting the kinematic architecture of the finger mechanism presented in Section 2.1, this optimization procedure aims, therefore, to enlarge the target users of the device, extending the opportunity of its employment to every generic patient with a generic hand opening disease. To achieve this goal, a procedure to adapt the exoskeleton to the patients is needed. In literature, there are many examples of different strategies applied in finding optimum design of mechanisms. One of the first effort has been carried out in [39] more than 50 years ago. This research area was futher investigated in [40] and, then, through the work presented in [41], thanks to the increasing computational resources which are getting even more available in recent years. Even if, nowadays, this field is deeply studied, there are few examples of optimization-based strategy to design mechanism to be applied to the human body [42] [43]. The presented novel optimization-based strategy exploited to design a custom-made robotic device for hand assistance allows, starting from the hand motion analysis, to automatically generate a hand exoskeleton tailored on the patient hand itself [44] [45] [46] [47]. Its main advantages can be summarized as:

- input data are the trajectories of each finger and are provided in an easy way by means of a completely non-invasive hand motion analysis;

- obtained data lead automatically to a ready-to-use device thanks to a parametric Computer Aided Design (CAD)-Computer Aided Engineering (CAE) software and to the additive manufacturing process;

- the achieved exoskeleton is personalized on the user hand.

The remainder of the chapter is given hereinafter and follows the general architecture of the automatic scaling procedure reported in Fig. 3.1.

The first step of the scaling procedure is a hand MoCap analysis to track the natural motion of the user's fingers (Section 3.1). The SMART-DX MoCap opto-electronic system by BTS Bioengineering (BTS Bioengineering S.p.A., Milano, Italy) available at the Don Carlo Gnocchi Foundation Rehabilitation Center, Florence, Italy, has been exploited. This system is made up of infrared cameras and is capable to automatically record three-dimensional trajectories of passive reflective markers placed on the patient's hand by means of stereophotogrammetric methods.

Section 3.2 deals with the hand kinematic model, which, along with the exoskeleton kinematic synthesis, has to be used in the optimization procedure.

Section 3.3 reports how the exoskeleton mechanism has been appropriately
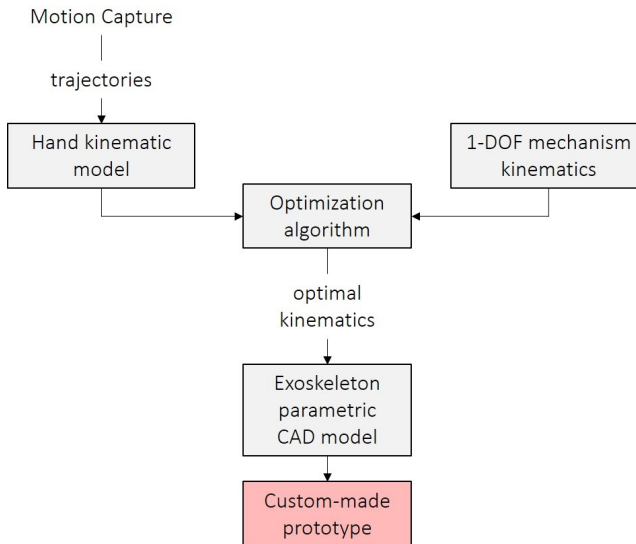
Figure 3.1: Automatic scaling procedure.

changed to match the trajectories acquired by the motion analysis. A real finger mechanism has then been designed, basing on the previously described kinematic architecture (Fig. 2.1); its overall mechanical design is reported in Fig. 3.2. The distal phalanx is generally not connected to the mechanism in order to maintain the tactile feedback during grasping. However, as anticipated in Section 2.1, a thimble can be added to the mechanism in order to help some users during the opening phase. The thimble will not been considered in the optimization process, since its addition to the mechanism does not change the kinematic interaction between the hand and the device.

Changing the relative distances between the mechanism joints position (points 1 to 6), the trajectory of the linking point (point 4) between the mechanism and the finger, i.e. exoskeleton end-effector, is modified. The purpose lies in determining such distances so that the exoskeleton replicates, when actuated, the proper natural motion of the long fingers. To reach this goal, it has been recoursed to a numerical optimization method; in particular, that one proposed in [48], which is a Nelder-Mead based optimization algorithm used to solve non convex, non linear constrained problems, has been exploited. The exploitation of this numerical algorithm led to a novel automatic procedure for mechanism
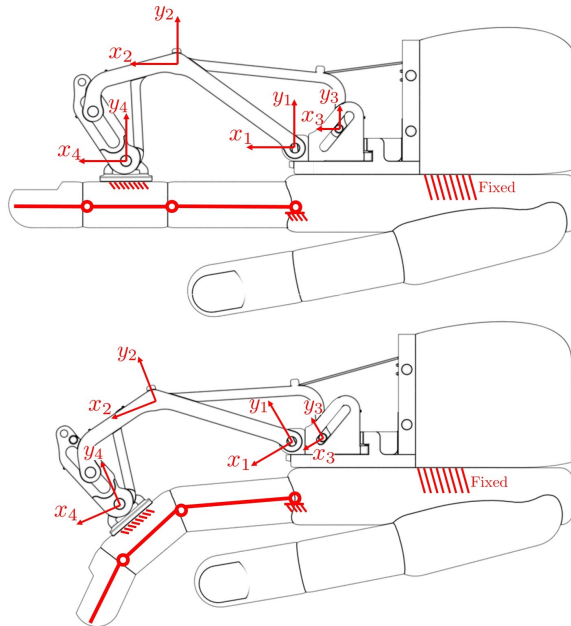
Figure 3.2: Embodiment of the finger mechanism kinematic chain: lateral view.

optimization. Taking the MoCap data as input and making use of the kinematic synthesis of the mechanism, the implemented algorithm provides the customized geometry for each user. In addition, several constraints have been added to the optimization problem in order to guarantee the physical feasibility of the device and, at the same time, to maintain the overall size limited.

A real exoskeleton prototype has, then, been designed and manufactured to validate the scaling procedure (Section 4.2). All the mechanical parts are entirely produced by means of a 3D printer in a thermoplastic polymer, ABS. The exploitation of the additive manufacturing technique allows to build even complicated geometries, which result hard to produce with subtractive processing method. In fact, this allows to design a mechanism directly from the parametric CAD model, without manufacturing constraints, providing the maximum comfort when the exoskeleton is worn.

The final phase of this part research activity, discussed in Section 3.4, consists in the evaluation of the transparency of the developed device (the capability of

the device in reproducing the real trajectories of the hand phalanges).

3.1 Hand Motion Capture

Since the input data of the scaling algorithm include the trajectories acquired by the MoCap system in order to customize the mechanical parts of the exoskeleton mechanism, a hand motion analysis has been required and is proposed in this section.

Performing a hand MoCap represents one of the main advantages in defining the object function of the proposed design procedure. Indeed, motion analysis guarantees to accurately track the physiological hand gestures through a completely non-invasive procedure. However, carrying out this analysis might be difficult, or even impossible, if the subject is not able to move both of his hands autonomously. In these cases, the authors resort to a hand kinematic model, previously presented by [1], which, starting from the anthropometry of the subject's hand, is capable of generating the finger trajectories that are mandatory to implement the proposed optimization-based scaling procedure. Even though the aforementioned kinematic model has not been entirely developed by the authors, its exploitation in this context has shown several advantages in producing hand exoskeleton for people who could not perform the mandatory gestures for the hand kinematic assessment, for this reason, an overall description of the model is reported in Appendix 6.

3.1.1 Protocol for hand motion analysis

A motion analysis technique is exploited for hand motion tracking. Joint positions are calculated (as reported in Section 3.2) by placing passive reflective 3 mm diameter markers on the right hand of some volunteers, as shown in Fig. 3.3. Markers are placed on the MCP, on thePIP joint, on the DIP joint and on the Tip (TIP). The marker positioned on the MCP joint constitutes the system reference frame for each finger. Three additional 10 mm diameter markers are, then, placed in order to determine the orientation of the hand back.

The proposed protocol [49] with the aforementioned markers positioning allows to minimize artefacts, due to skin movements and potential marker occlusion.
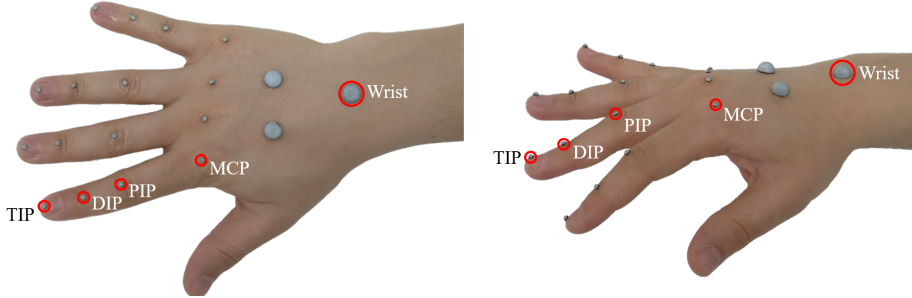
Figure 3.3: Markers positioning protocol.

3.1.2   Hand motion analysis setup

In this section, how the proposed protocol has been used to track and record the hand motion will be discussed. Such protocol was used to analyze data extracted from specific tests on healthy subjects. Then, the trajectory of the markers has been studied to define which trajectories the exoskeleton has to replicate to actuate the grasping gesture.

Thirteen right-handed human subjects (ten men and three women), aged 30.84 on average (standard deviation 10.06) have participated voluntarily in this study. Each subject was asked to grasp and release 3 times a 50 mm diameter cylindrical object. The subjects seated in front of a table and the cylindrical objects were located by the subjects themselves in a comfortable position but within a set area, as reported in Fig. 3.4, to optically track the whole gesture. The starting position (hand pose and body posture) was the same for all the participants. The hand was initially placed opened with the palm on the object with the the four long fingers completely extended and the thumb adducted. The shoulder was positioned with $0°$ in abduction on the frontal plane and flexed with an angle of about $45°$ in the sagittal plane (according to a comfortable posture for the subject). The elbow was slightly flexed in the sagittal plane in order to allow the subjects to keep the forearm on the table while they were grasping the cylindrical object. The wrist was in a neutral position ($45°$ for flexion and $0°$ for radio-ulnar deviation).

The BTS SMART-Suite MoCap System by BTS Bioengineering placed at the Don Carlo Gnocchi Foundation Rehabilitation Center has been exploited. Four infrared cameras (their setup is shown in Fig. 3.4) compose this optoelectronic
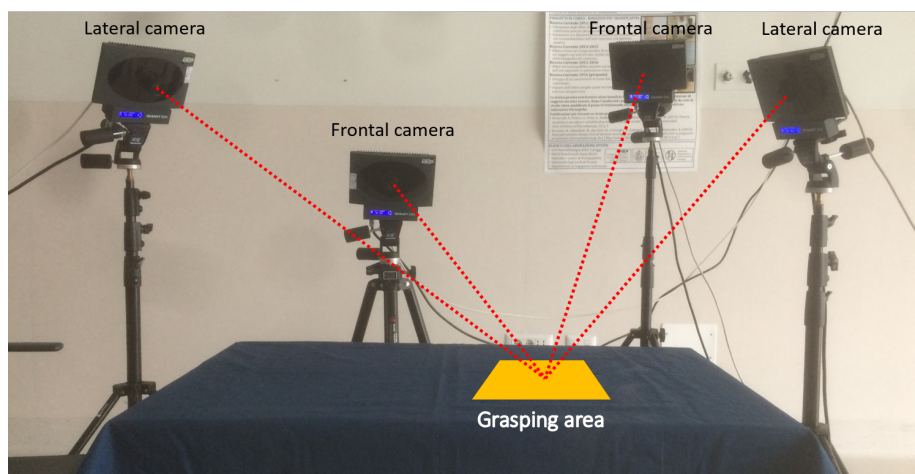
Figure 3.4: Motion analysis cameras setup.

system which automatically records 3D trajectories of passive reflective markers
with an acquisition rate of 100 Hz. In this context, the BTS Smart Analyzer
software package has been used in reconstructing the marker positions.

Markers positions were initially recorded in a steady state position for 2 sec-
onds (in order to acquire a static configuration) and, then, during the whole
trial. After each grasp, the subject kept in hand the object for some seconds.
A metronome has been used to set the rhythm of grasping and releasing the
cylinder during each acquisition.

It is worth noting that, before starting the hand tracking, each person grasped
the object several times in order to get familiar with that gesture.

3.2   Hand model

Several kinematic models, which describe human hand kinematics, have been
reported in literature [50]. One of the most important differences among them is
the simplifying hypothesis regarding the number of DOFs. Since the research ac-
tivity aims at developing an exoskeleton able to reproduce the finger trajectories
that the hand executes during the ADLs, the first step consists in determining a
suitable model which describes the particular fingers gestures during grasping.
The chosen kinematic model allows to obtain a suitable characterization of the

grasping movement using only few markers. In fact, in this phase of the research activity, it is important to acquire the hand movements without motion alteration due to the presence of the markers themselves on the hand.

The kinematic model presents 3 DOFs for each long finger which is, hence, modeled as an open kinematic chain. Since the exoskeleton does not effect the thumb, it is not considered in the study. Assuming the aforementioned hypotheses, the kinematic model of each finger is then be considered as a planar 3R mechanism (Fig. 3.5) which defines the fingertip pose $\mathbf{p}_f(\boldsymbol{\Theta}_f)$ as a function of the joint coordinates $\boldsymbol{\Theta}_f = [\theta_{f1}\ \theta_{f2}\ \theta_{f3}]^T$:

$$\mathbf{p}_f(\boldsymbol{\Theta}_f) = \left[p_f^x\ p_f^y\ \phi_f \right]^T = \begin{bmatrix} l_{f1}c_1 + l_{f2}c_{12} + l_{f3}c_{123} \\ l_{f1}s_1 + l_{f2}s_{12} + l_{f3}s_{123} \\ \theta_{f1} + \theta_{f2} + \theta_{f3} \end{bmatrix}; \qquad (3.1)$$

where, e.g. $c_{12} = cos(\theta_{f1} + \theta_{f2})$ and $s_{12} = sin(\theta_{f1} + \theta_{f2})$, $\mathbf{p}_f$ is the fingertip pose[1], the subscript $_f$ defines the finger ($f = 1, 2, 3, 4$ starting from the index and excluding the thumb) and l_{f1}, l_{f2}, l_{f3} are the phalanx lengths[2].

In Fig. 3.5, through the reference systems $\{O_0, x_0, y_0, z_0\}$, $\{O_{f1}, x_{f1}, y_{f1}, z_{f1}\}$, $\{O_{f2}, x_{f2}, y_{f3}, z_{f2}\}$, $\{O_{f3}, x_{f3}, y_{f3}, z_{f3}\}$ (which are, respectively, the wrist positions and the centre of rotation trajectory of MCP, PIP and PIP joints), the phalanx lengths l_{f1}, l_{f2}, l_{f3} and the distance vector between the wrist and the MCP joint $\mathbf{l}_{f0}$, the 3R mechanism can be easily adapted to different hand characteristics.

The described 3-DOFs kinematics model, which will be an essential input in the optimization procedure, can be obtained by processing MoCap data reported in Sections 3.1.1 and 3.1.2. Even if the chosen protocol allows to put only few markers on the hand, it is affected by tissue deformations during flexion/extension movements. So, a procedure, which provides the finger joints COR trajectories, has been required. In the following, the procedure to obtain the COR trajectories starting from the markers ones, will be reported. Markers trajectories themselves represent the starting point in defining the hand model. Such model exploits indeed the coordinates of every marker placed on the hand with respect to the 3D coordinate system defined during the calibration of the acquisition system (in the following, referred to as the "camera frame").

---

[1]The pose of each fingertip is defined with respect to the MCP joint. Referring to Fig. 3.5, the position should therefore be expressed as $^1\mathbf{p}_{4f}$. The simplified notation $\mathbf{p}_f$ will be adopted in the following for sake of readability.

[2]In Fig. 3.5 the subscript $_f$ has not been reported to have a more discernible picture.
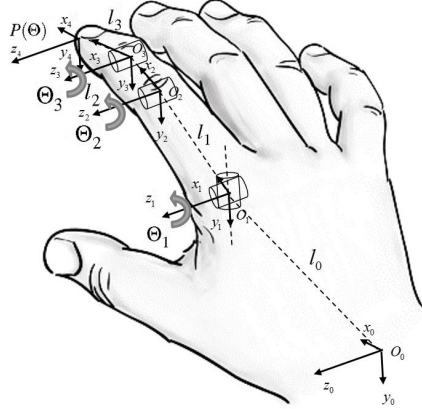
Figure 3.5: Hand kinematic model (the subscript $_f$ has not been reported, since the reference frame symbols refer to only one finger).

3.2.1 Finger trajectory definition

The first step to be taken is to refer all the acquired data to a common origin; since the finger moves with respect to the knuckle, the position of MCP marker on the finger has been chosen as the point all the measurements will be referred to (such frame, with origin in the finger MCP marker and whose axes are parallel to those of the camera frame, will be called the "finger frame"). Let $\mathbf{p}_m^C$ denote the 3D position of the generic marker (denoted by m) in the camera frame (denoted by C); then, the position of the same marker in the finger frame (represented by apex F) is given by

$$\mathbf{p}_m^F = \mathbf{p}_m^C - \mathbf{p}_{MCP}^C .\tag{3.2}$$

It is reasonable to assume that during subsequent opening and closure gestures of a finger, motion takes place always on the same plane, whose normal axis coincides with the knuckle axis. The idea is to determine the direction of such axis in order to align the acquired trajectory with the horizontal plane. To this aim, it is possible to determine the plane Π that best fits the acquired measurements (in a least square sense).

Consider the standard 3D plane equation

$$ax + by + cz + d = 0 \ . \tag{3.3}$$

Let $\mathbf{p}_\Pi = [x \ y \ z \ 1]^T$ denote a point on the plane, using an augmented vector representation. The vector $\mathbf{X}_\Pi = [a \ b \ c \ d]^T$ contains the unknowns of the problem. If a point $\mathbf{p}_\Pi$ lies on the plane, it satisfies

$$\mathbf{p}_\Pi^T \mathbf{X}_\Pi = 0 \ . \tag{3.4}$$

Given N points $[x_i \ y_i \ z_i \ 1]^T$, $i = 1, \cdots, N$, it is possible to write the following linear system:

$$P_\Pi \mathbf{X}_\Pi = \mathbf{e} \ , \tag{3.5}$$

where

$$P_\Pi = \begin{bmatrix} x_1 & y_1 & z_1 & 1 \\ \vdots & \vdots & \vdots & \vdots \\ x_N & y_N & z_N & 1 \end{bmatrix} \ , \tag{3.6}$$

and $\mathbf{e} \in \mathbb{R}^N$ is an error vector to be minimized (if all the points lie on the plane, then $\mathbf{e} = \mathbf{0}$). The solution vector is the closest vector to kernel of P_Π, which is given by the right-singular vector corresponding to the minimum singular value obtained from the singular value decomposition of P_Π. Once the coefficients of Eq. 3.3 have been determined, the direction of the normal to the plane is given by $\mathbf{n} = [a \ b \ c]^T$.

The above-mentioned considerations can be applied to the acquisitions of the markers on each finger; in particular, denoting with ${}^i\mathbf{p}_{TIP}^F = [{}^i x_{TIP}^F \ {}^i y_{TIP}^F \ {}^i z_{TIP}^F]^T$, $i = 1, \cdots, N_{TIP}$ the generic acquisition of the marker TIP in finger frame, the best fitting plane Π_{TIP} can be determined. The projection of each acquisition on such plane is given by:

$$ {}^{i,\Pi}\mathbf{p}_{TIP}^F = {}^i\mathbf{p}_{TIP}^F - \left(\mathbf{n}_{TIP}^T \left({}^i\mathbf{p}_{TIP}^F - \mathbf{p}_{TIP} \right) \right) \mathbf{n}_{TIP} \ , \tag{3.7} $$

where $\mathbf{n}_{TIP}$ is the normal to plane Π_{TIP} (i.e. the knuckle axis) and $\mathbf{p}_{TIP}$ is a generic point on such plane (which can be determined from its equation).

3.2.2   COR definition

The finger tip trajectory ${}^{i,\Pi}\mathbf{p}_{TIP}^F$ represents the pose $\mathbf{p}_f$ of the finger model. However, the projections of PIP and DIP markers trajectories on the best fitting
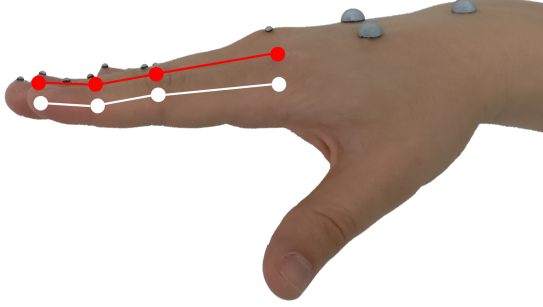
Figure 3.6: Difference between MCP, PIP, DIP and TIP markers positions (in red) and the respective joints CORs (in white).

plane Π_{TIP} are affected by surface motions of the markers around the joints and do not exactly correspond with the PIP and DIP COR (Fig. 3.6).

Through the application of the algorithm proposed in [51], the COR of the finger joints can be hence determined. Such algorithm, basing on the proposed protocol, employs an optimization routine which minimizes the time-variance of the internal links lengths, considering a linear (empirically validated) relationship between local movements of the surface marker around a joint and the joints flexion/extension. A brief explanation of the main steps leading to the COR positions for each finger joint is reported below. As mentioned above, an in-depth discussion of this method is reported in [51]. Referring to Fig. 3.7, and considering a generic long finger flexion/extension movement, surface motions cause changes in length and orientation of the distance vector between markers (L_{4-k} with $k = 1, 2, 3$[3] corresponding to, respectively, proximal, intermediate and distal phalanges), while the vector denoting the distance between CORs (l_k) maintains a quite constant length even if it changes its orientation. Vector d_{4-k}, which points from the surface marker M_{4-k} to the intersegmental joint COR C_{4-k}, also is supposed to maintain a constant length while rotating around C_{4-k} during grasping gestures. Taking the aforementioned considerations, the following relationship between the geometrical parameters reported in Fig. 3.7

---

[3]The specific notation adopted to denote the phalanges has been chosen since the optimization routine starts exploiting the TIP marker position (marker number 4) and, finally, uses MCP marker (number 1).
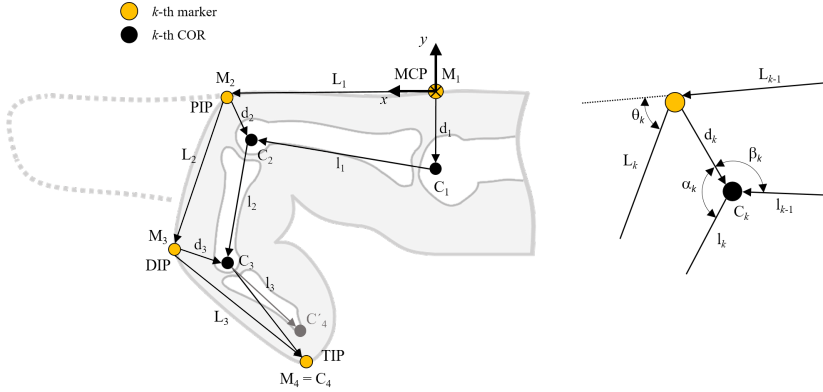
Figure 3.7: Schematic model of the geometric relationship between markers and COR relationship during flexion/extension gesture.

exists at any time instant t:

$$\mathbf{L}_{-k+4}(t) = \mathbf{l}_{4-k}(t) - \mathbf{d}_{3-k}(t) + \mathbf{d}_{4-k}(t), \qquad (3.8)$$

which can be written in the differential form:

$$\Delta\mathbf{L}_{4-k}(t) = \Delta\mathbf{l}_{4-k}(t) - \Delta\mathbf{d}_{3-k}(t) + \Delta\mathbf{d}_{4-k}(t). \qquad (3.9)$$

Referring to the local frame with the same origin of link l_{-k+4} and considering that, in this frame,

$$\Delta\mathbf{d}_{3-k}(t) = \mathbf{d}_{3-k}(t) \times \Delta\beta_{3-k}\mathbf{k}_{3-k}(t), \qquad (3.10)$$

where the operator $\times$ represents the cross-product, Eq. 3.9 becomes

$$\Delta\mathbf{L}_{4-k}(t) = -\mathbf{d}_{3-k}(t) \times \Delta\beta_{4-k}\mathbf{k}_{4-k}(t) + \mathbf{d}_{4-k}(t) \times \Delta\alpha_{4-k}(t)\mathbf{k}_{4-k}, \quad (3.11)$$

where $\Delta\beta_{3-k}$ is the vector representation of an infinitesimal change in the rotation angle of $\mathbf{d}_{3-k}$ relative to $\mathbf{l}_{4-k}$ (about z_{3-k} axis of $(3-k)$-th frame and denoted by $\mathbf{k}_{3-k}$ versor) and $\Delta\alpha_{4-k}$ represents an infinitesimal change in the rotation angle of $\mathbf{d}_{-k+4}$ also relative to $\mathbf{l}_{-k+4}$ (see Fig. 3.7). It is worth noting

that, since d_{3-k} and d_{4-k} have constant lengths, the magnitude of change in the surface link vector $|\Delta L_{4-k}|$ have a linear relationship with $\Delta \alpha_{4-k}$ as well as $\Delta \beta_{3-k}$. In addition, the dependence of $\Delta \beta_{3-k}$ to $\Delta \alpha_{4-k}$ can be obtained by geometrical considerations. Finally, each $\mathbf{C}_{4-k}$ position with respect to $\mathbf{M}_{4-k}$ one can be inferred by

$$\mathbf{d}_{4-k}(t) = \arg\min_{\mathbf{d}_{4-k}} \left(\Delta \mathbf{L}_{4-k}(t, \theta_{4-k}, \mathbf{d}_{4-k}) \right). \tag{3.12}$$

Where $\Delta \mathbf{L}_{4-k}(t, \theta_{4-k}, d_{4-k})$ (its direct dependence on θ will be explained in the following) is the objective function to be minimized and $\mathbf{d}_{4-k}(t)$ is calculated as that distance between COR $\mathbf{C}_{4-k}$ and marker $\mathbf{M}_{4-k}$ which minimizes the variation in length between C_{4-k} and $\mathbf{C}_{3-k}$. In order to minimize Eq. 3.11 with respect to $\mathbf{d}_{4-k}$, α_{4-k} has to be defined at any time. The results proposed in this thesis endorsed the use of a linear function to characterize such value. It has been parameterized as a function of θ_{4-k} as

$$\alpha_{4-k}(t) = p_{4-k} \theta_{4-k}(t), \tag{3.13}$$

where, according with [51], p_{4-k} is a joint-specific time-invariant value within the range from 0.27 to 0.47 for PIP and DIP joints and equal to 0.75 for the MCP joint. The aforementioned optimization routine allows, starting from the position of the TIP marker, and exploiting the positions of the other acquired markers on the hand, to define the CORs positions of finger joints. The proposed procedure introduces an initial small error since $\mathbf{M}_4$ and $\mathbf{C}_4$ has been considered coincident (see Fig. 3.7).

3.2.3 Alignment with horizontal plane

The following step is the rotation of the projected data in order to align them with the horizontal plane; such operation can be performed by simply rotating them of an angle given by

$$\theta_{TIP} = cos^{-1} \left(\mathbf{z}^T \mathbf{n}_{TIP} \right) , \tag{3.14}$$

where $\mathbf{z} = [0\ 0\ 1]^T$, about the axis

$$\mathbf{a}_{TIP} = \mathbf{n}_{TIP} \times \mathbf{z} . \tag{3.15}$$
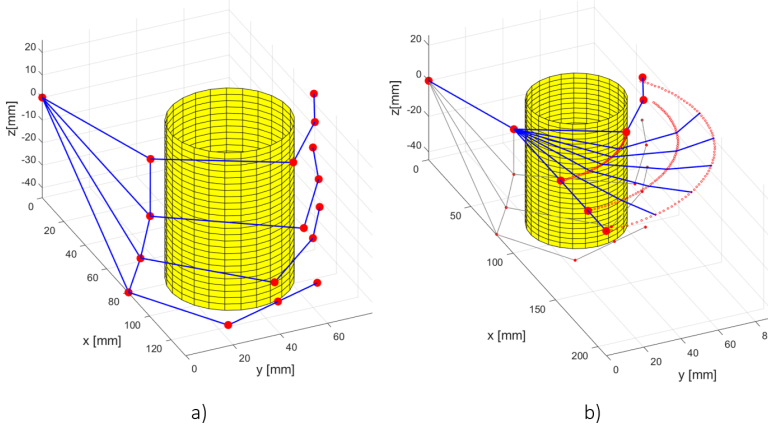
Figure 3.8: Link segment model (a) and index joints COR trajectories (b) of the hand grasping object.

Since the direct kinematics function is defined in the range $[0° \ − 90°]$, where $0°$ coincides with the complete extension of the finger and $−90°$ indicates that the finger is completely closed, a suitable rotation about the **z** axis can then be used in order to bring the acquired trajectory within desired range (in the following, an apex h will indicate data rotated on a horizontal plane and within the correct angular range).

The discussed simplifying assumptions lead to define the link segment model of the hand, which is used to determine the objective function of the optimization procedure. Figure 3.8 shows an example of the calculated joints positions during the flexion/extension of one of the subjects involved in the study.

3.3   Optimization process

Hereinafter the procedure adopted to define the particular shape of the exoskeleton components is discussed. The new shape of the mechanism is, then, able to reproduce the trajectory of the user, acquired with the MoCap system introduced in Section 3.1, very closely. The procedure can be conceptually separated into two parts. A preliminary data manipulation step is required in order to define the object function in a suitable format that can be fed to the optimization

algorithm. This step is crucial since it directly leads to the determination of the objective function, whose minimization constitutes the second part of the whole process. Sections 3.3.1 and 3.3.2 illustrate these two steps in details.

3.3.1 Target trajectory definition

For any user, the goodness of the developed exoskeleton can be established by evaluating the matching of the trajectories of the contact point between the hand and the device (point EE). Indeed, since the exoskeleton is a single-DOF mechanism, such condition is sufficient to ensure that the device follows the natural hand trajectory during normal use. Hence, the optimization process aims at determining the geometry of a device which minimizes the tracking error relative to such point, for the whole range of motion.

The position of EE can be calculated from the hand kinematic model. The hand exoskeleton direct kinematics function, on the other side, allows the computation of the position of the key points of the exoskeleton itself with respect to the fixed 2D coordinate system centered in Ox_1y_1 (Fig. 3.2). It is worth noting that the position of the contact point EE on the exoskeleton cannot be directly computed exploiting the direct kinematics function unless the complete hand-exoskeleton closed kinematic chain is taken into account. This is because the triangular-shaped component of the exoskeleton, connected to it with rotational joint 1 (the "end-effector", violet component in Fig. 3.9), is free to rotate (actually constituting an additional degree of freedom for the exoskeleton alone) unless the exoskeleton itself is placed on the hand. Hence, no direct comparison between outputs of the direct kinematics function and trajectories acquired using the motion analysis system is possible. However, from the hand kinematic model, it is possible to reconstruct the time-varying position defined by the joint 4 trajectory, which is the trajectory of an ideal exoskeleton that would precisely guide the hand motion with no slip and without exerting unwanted forces on the user's hand, based on purely geometrical considerations. The reconstructed trajectory, obtained as explained below, will be used to determine the objective function of the optimization algorithm.

In the following, joint 4 trajectory, since it characterizes the particular movement of component E (Fig. 2.1), will be denoted by "point E".

Referring to Fig. 3.9, when the exoskeleton is placed on the hand, the end-effector and the phalanx of the finger constitute a single rigid body: it is indeed such component that follows the natural motion of the finger without slipping. Hence, the position of a virtual marker EE (representing the connection between
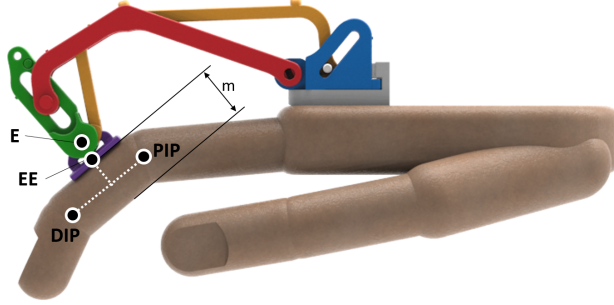
Figure 3.9: (a): end-effector; (b): finger phalanx.

the finger and the device) can be defined as follows:

$$^{i,F}\mathbf{p}_{EE}^h = \frac{^{i,F}\mathbf{p}_{DIP}^h + ^{i,F}\mathbf{p}_{PIP}^h}{2} + R_{\mathbf{z}}(\frac{\pi}{2})\frac{m}{2}\ \frac{^{i,F}\mathbf{p}_{DIP}^h - ^{i,F}\mathbf{p}_{PIP}^h}{||^{i,F}\mathbf{p}_{DIP}^h - ^{i,F}\mathbf{p}_{PIP}^h||}\ ,\qquad(3.16)$$

where m is the thickness of the second phalanx (Fig. 3.9). Hence, once the position of EE is determined, the time-varying direction of the vector $\mathbf{q}_i = ^{i,F}\mathbf{p}_{DIP}^h - ^{i,F}\mathbf{p}_{EE}^h$ can be exploited to reconstruct the reference trajectory for the exoskeleton point E. Refer to Fig. 3.10: let $\boldsymbol{\xi} = [0\ \xi\ 0]^T$ denote the vector
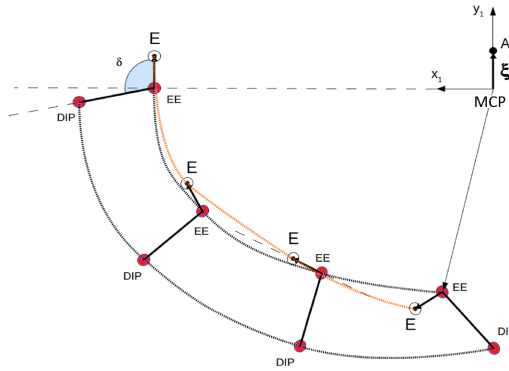
Figure 3.10: Reconstruction of the desired E trajectory.

distance between exoskeleton joint 1 of component A (named "point A" in the

following) and MCP joint; then, when the hand is completely open, the (fixed) angle between $\mathbf{q}_i$ and the line passing through E and EE can be computed as follows:

$$\delta = cos^{-1}\left(\frac{\boldsymbol{\xi}^T\mathbf{q}_1}{||\boldsymbol{\xi}^T\mathbf{q}_1||}\right). \tag{3.17}$$

Then, for the generic i-th acquisition, it is possible to determine the desired point E position as follows:

$$^{i,A}\mathbf{p}_E^{\star} = {}^{i,F}\mathbf{p}_{EE}^h + R_{\mathbf{z}}(\delta)\mathbf{q}_i\,\frac{\xi}{||\mathbf{q}_i||} - \boldsymbol{\xi}. \tag{3.18}$$

Note that the desired trajectory is computed with respect to the reference frame centered in A, so that it can be directly compared with the output of the exoskeleton direct kinematics function.

Finally, the obtained reference points have been interpolated in order to obtain a continuous and sufficiently smooth trajectory. Since each index i corresponds to a different acquisition frame (where frame $i + 1$ has been acquired $1/f_s$ seconds after frame i, where f_s is the sampling frequency of the acquisition system), and by observation of the natural motion of the hand, it is quite straightforward to realize that the x- and y- components of $^A\mathbf{p}_E^{\star}$ (taking into account all the acquired frames) exhibit a sinusoidal trend with respect to time (Fig. 3.11). However, interpolation of each component and subsequent reconstruction of the planar xy trajectory resulted in an unacceptable difference between the acquired and the interpolated trajectories. Instead, resorting to polar coordinates:

$$\begin{cases} \rho(i) = \sqrt{\left(^{i,A}p_E^{x,\star}\right)^2 + \left(^{i,A}p_E^{y,\star}\right)^2} \\ \beta(i) = atan2\left(^{i,A}p_E^{y,\star},\ ^{i,A}p_E^{x,\star}\right) \end{cases} \tag{3.19}$$

the desired trajectory can be expressed as a function of a single variable $\rho = g(\beta)$, eliminating the time dependency. This way, interpolation can be executed on the complete xy trajectory, yielding the continuous $\rho^{\star} = g(\beta^{\star})$ reference trajectory and avoiding the influence of time dependency on the result.

3.3.2   Determination of the optimal exoskeleton

Numerical optimization is used to define the dimensions and the shape of a *transparent* exoskeleton, i.e. a device which is capable of closely reproducing the hand trajectory of the user, without forcing it to unnatural motion.
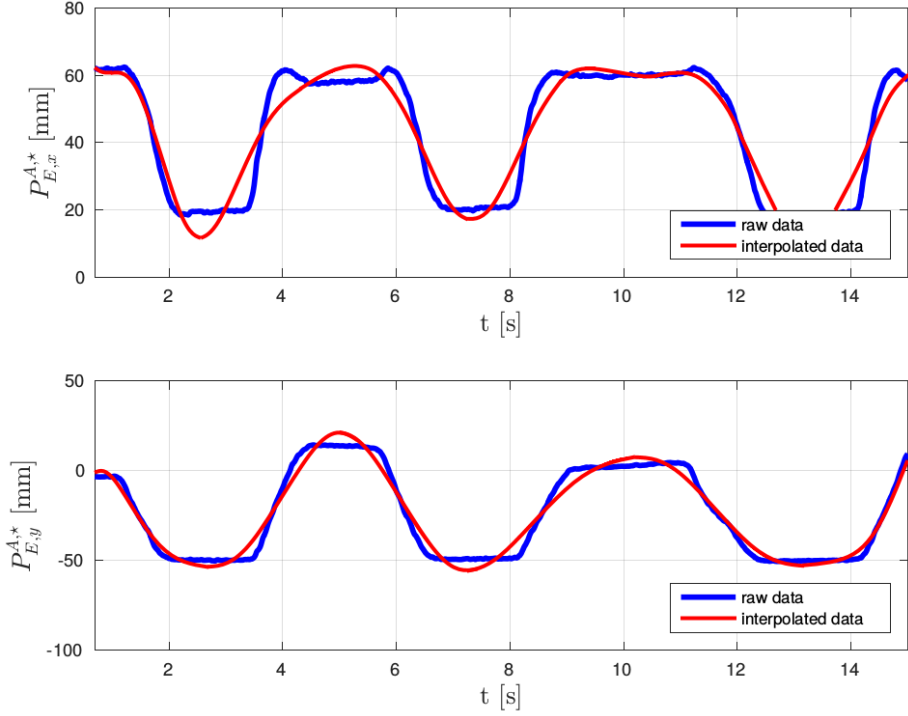
Figure 3.11: x- and y- components of $^A\mathbf{p}_E^\star$ as a function of time.

The optimization process requires an in-depth analysis of the kinematics of the single-DOF mechanism, which has been discussed in Section 2.1.

As reported in Eq. 2.11, $\tilde{\mathbf{q}}$ denotes the vector composed of the x- and y-axis positions of joints 2, 3, 4, and 5 of the exoskeleton (see Fig. 3.2) with respect to the frame centered in A (reference frame 1), and the two angular values which indicate the rotation of frame 3 and frame 4 about their respective z-axes. Being the exoskeleton a 1-DOF mechanism, given the physical dimensions of the device's parts the components of $\tilde{\mathbf{q}}$ can be determined using the exoskeleton direct kinematics as a function of α_2 angular value (Eq. 2.11), being $\mathbf{S}$ a set of relevant dimensions of the exoskeleton components (Eq. 2.10), which will constitute the free variables of the optimization problem.

Thus, this phase consists in *1)* the determination of a (minimum) set of com-

ponents dimensions $\mathbf{S}$ which enable the computation of $\tilde{\mathbf{q}}$ given any value of α_2 within the complete range of motion of the device, and *2)* the choice of such dimensions in order to closely reproduce the patient's trajectory obtained through the motion capture system.
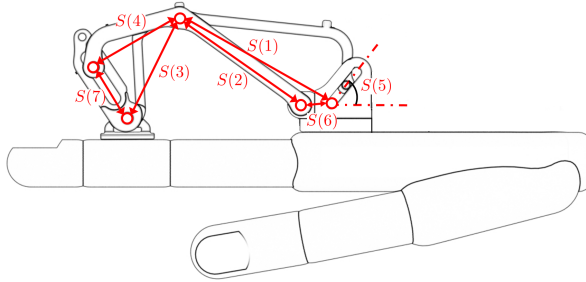
Figure 3.12: Choice of the optimization variables.

Optimization variables and objective function definition

The set of variables $\mathbf{S}$ chosen in this context is shown in Fig. 3.12; the reported lengths are independent from the value of the angle α_2 (i.e. are independent from the configuration of the device). In Section 2.1 it has been demonstrated that the shown seven variables are sufficient to completely determine the components of $\tilde{\mathbf{q}}$ given any value of α_2. Additionally, it is worth noting that the (fixed) open-hand length $||\mathbf{P}_E^A||$ depends only on the anatomy of the patient, it is equal to the distance between EE point and MCP marker, and can be thus determined from the acquired data.

The value of each component of $\mathbf{S}$ is chosen to achieve the minimization of a function weighing the error between the hand trajectory computed with the exoskeleton direct kinematics function and the acquired reference trajectory. Let such reference trajectory $\rho^\star = g\left(\beta^\star\right)$ be sampled using $K+1$ angular steps $\beta_k^\star$, $k = 0, \cdots, K$, where the step size k represents the trade-off between required computational resources and reconstruction accuracy (indeed, for increasing values of k the error will be evaluated for a higher number of points). Hence, given

a set $\mathbf{S}$, for any $\beta_k^\star$ the corresponding error can be computed as (Fig. 3.13):

$$e_k = e_k\left(\mathbf{S}, \beta_k^\star\right) = \left|\rho_{\mathbf{S}}\left(\beta_k^\star\right) - \rho^\star\left(\beta_k^\star\right)\right| , \tag{3.20}$$

being $\rho_{\mathbf{S}}\left(\beta_k^\star\right)$ the radius value obtained after conversion into polar coordinates of the coordinates of point ${}^A\mathbf{p}_E$ (joint position ${}^1\mathbf{p}_4$ in Sec. 2.1) computed exploiting the direct kinematics function for given $\mathbf{S}$ and $\beta_k^\star$. Hence, the determination
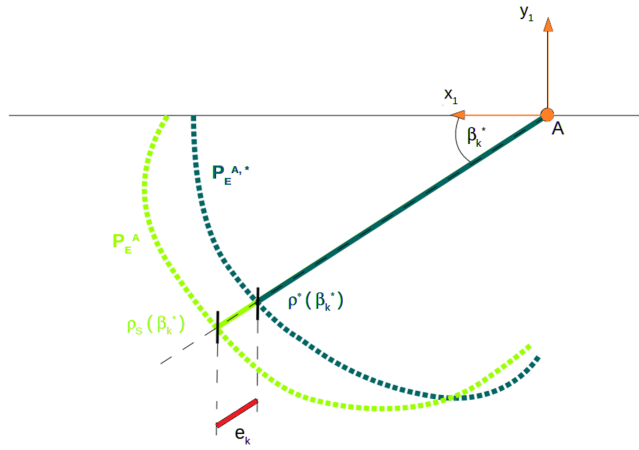
Figure 3.13: Graphical representation of the error between computed and reference trajectories.

of the optimal exoskeleton has been cast as an optimization problem using the following objective function:

$$\min_{\mathbf{S}} f\left(\mathbf{S}\right) = \min_{\mathbf{S}} \left(\max_k |e_k| + \gamma \sum_{k=0}^{K} \frac{|e_k|}{K+1}\right) , \tag{3.21}$$

weighing both the maximum and average errors, using the scale coefficient γ to set the relative weight of the two values within the objective function. In this study, γ has been set to 0.5, equally weighing maximum and average error.
Box constraints have been added to the free variables of the problem; such constraints, aiming at maintaining the final dimensions of the device limited, depend on the size and on the anatomy of the hand, and must be chosen ac-

cordingly for each user as a function of those parameters.

Furthermore, based on geometrical considerations, a suitable set of constraints has been taken into account so as to discard solutions leading to non working or even non-feasible (from a physical point of view) exoskeletons. In particular, these constraints influence the position of some of the key points of the device either in different configurations (open or closed hand), or for the whole range of motion (see Table 3.1 and refer to Fig. 2.1 and 3.2). In Table 3.1, subscripts

Open hand constraints	
${}^1\mathbf{p}_2^x \leq {}^1\mathbf{p}_4^x$	Right bound
${}^1\mathbf{p}_2^x \geq 0$	Left bound
${}^1\mathbf{p}_{2,min}^y \leq {}^1\mathbf{p}_2^x \leq {}^1\mathbf{p}_{2,max}^y$	Lower and upper bound
${}^1\mathbf{p}_3^x \geq {}^1\mathbf{p}_{3,min}^x$	Left bound
${}^1\mathbf{p}_3^y \leq {}^1\mathbf{p}_2^y$	Upper bound
${}^1\mathbf{p}_3^x \leq {}^1\mathbf{p}_3^{x\star}$	Right bound
$0 \leq {}^1\mathbf{p}_5^y \leq {}^1\mathbf{p}_{5,max}^y$	Lower and upper bound
${}^4\mathbf{p}_5^x \geq 0$	Left bound
${}^1\mathbf{p}_5^x \leq {}^1\mathbf{p}_{5,max}^x$	Right bound
Closed hand constraints	
$\frac{{}^1\mathbf{p}_4^y}{{}^1\mathbf{p}_4^x\ {}^1\mathbf{p}_2^x} - {}^1\mathbf{p}_2^y - {}^1\mathbf{p}_2^{y,max} \leq 0$	Lower bound
${}^1\mathbf{p}_5^y \leq {}^1\mathbf{p}_4^y$	Upper bound
Whole range of motion constraints	
$0 \leq {}^1\mathbf{p}_3^y \leq {}^1\mathbf{p}_3^{y,min}$	Lower and upper bound
${}^1\mathbf{p}_3^y \leq {}^1\mathbf{p}_5^{x,max}$	Right bound

Table 3.1: Optimization constraints.

min and *max* indicate minimum and maximum values, which must be chosen following the same considerations made for box constraints. Furthermore, since the geometrical constraints refer to joint relative positions, they are reported following the notation presented in Sec. 2.1

Optimization procedure

For what concerns the choice of the optimization algorithm, a direct search method has been used due to the complexity and non-differentiability of the

objective function to be minimized. Particularly, the strategy presented in [52], where the Nelder-Mead simplex method [48] is used to perform local searches over the function domain, has been employed. Each local search is terminated when particular conditions for the resulting simplex are met (i.e. when the latter is either small or flat [52]), and the starting point for the subsequent search is chosen accordingly to a probabilistic restart strategy aiming at maximizing the coverage of the whole domain, based on a memory of past starting and convergence points. Additionally, an adaptive penalty function allows to handle both equality and inequality constraints within the objective function. Hence, the idea is to perform a series of local searches (whose number can be influenced by a-priori setting the maximum number of iterations allowed) covering as much as possible of the function domain, and then comparing all the convergence points of such searches to determine the optimum. Even though convergence of the standard Nelder-Mead simplex method has been proved only in particular cases [53], the smart local search restarts linking allows to achieve good coverage of the function domain; additionally, the improvements made to the classical method (such as the constraints handling approach) highlight the de facto goodness of the strategy presented in [52] (the authors also show that their algorithm compares favorably with evolutionary algorithms in a realistic scenario), proving its usefulness for the minimization of discontinuous, non-convex, and constrained functions.

3.4   Tests and results

In this section, all the subjects whose hand has been studied in Section 3.1 will be taken into account to evaluate the precision of the proposed optimization strategy in following physiological finger gesture.

To check the reliability of the optimization algorithm, the error between the computed optimal trajectory of the exoskeleton and the target one has been assessed evaluating all the 13 subjects whose hand has been analyzed in motion (Section 3.1). The maximum calculated error among average values was 6.80 mm (mean value among all the subjects was 3.16 mm, standard deviation 1.47 mm).

Table 3.2 reports, for each subject, the length and width of the hand, the maximum and average values, and standard deviation of the error between the desired and the actual trajectory of exoskeleton point E relative to the index finger mechanism. The measurements of hand length (L) and width (W) represent, respectively, the distance between the medium finger tip and the wrist, and the

breadth of the palm (distance between MCP joints of index and small fingers). In addition, the percentage of the maximum and average values, and standard deviation of the error with respect to the finger length are given in the third last columns of Tab. 3.2. Considering the overall dimensions of the subjects hands (L and W), these three last columns allow to understand not only the goodness of the optimization results (reported in "Error" columns), but also the impact of these results on the finger kinematics ("Error/Finger Length" columns). In fact, the percentages of the maximum, average, and standard deviation errors provide a direct explanation of how the optimization results affect the finger when the exoskeleton is worn.

Subject ID	Features [mm]	Error [mm]			Error/Finger Length [%]		
	L x W	Max	Average	Std Dev	Max	Average	Std Dev
1	200 x 94	4.96	2.66	1.18	4.5	2.4	1.1
2	165 x 82	3.72	2.29	1.13	4.2	2.6	1.3
3	191 x 78	4.82	3.15	1.30	4.7	3.1	1.3
4	192 x 84	5.59	3.68	1.70	5.5	3.6	1.7
5	189 x 95	5.92	3.83	1.63	5.9	3.8	1.6
6	192 x 91	3.05	2.05	0.81	3.0	2.0	0.8
7	197 x 88	3.45	2.10	1.21	3.3	2.0	1.1
8	193 x 89	6.30	4.12	1.40	6.3	4.1	1.4
9	187 x 81	0.90	0.53	0.31	0.9	0.5	0.3
10	150 x 75	4.76	2.92	1.42	5.9	3.6	1.7
11	193 x 80	4.99	3.08	1.48	4.9	3.0	1.4
12	220 x 90	8.83	6.80	1.79	7.6	5.9	1.5
13	195 x 92	5.57	3.96	1.24	5.3	3.8	1.2

Table 3.2: Length (L) and width (W) of the hand, maximum, average and standard deviation of the error (between the desired and the actual trajectory for the index finger) and percentage (with respect to the finger length) error

Chapter 4

ABS hand exoskeleton prototypes: experimental results

This chapter is the dedicated to the description of the experimental results represented by the production and testing of three hand exoskeletons [54] [55]. Each manufactured prototype aimed to validate a specific part of the work. In particular, as well as it will be discussed in this chapter, the first device embodied the kinematic validation of the novel 1-DOF finger mechanism, the second prototype assessed the goodness of the optimization-based scaling procedure in following hand gestures and, finally, the last presented hand exoskeleton represents the final solution of a low-cost, fully portable and usable tool to assist people affected by hand disease.

In the following, each presented prototype will be presented considering the two main parts it is composed by: the mechanism, and the actuation system with the control unit and power supply.

The tests presented hereinafter were conducted under the supervision of health experts of the Rehabilitation Centre IRCCS Don Carlo Gnocchi. Informed consent and information sheet for the subject are available and attached at the end of the thesis (Annex A). According to the policy of the Don Carlo Gnocchi Foundation, ethical approval is not required for one-time qualitative tests. Written confirmation has been also obtained from the director of the centre, Prof. Carlo Macchi and this document is available upon request.

4.1 First prototype: kinematic validation

A first version of the hand exoskeleton (Fig. 4.1) has been designed and manufactured to test the embodiment of the kinematic model proposed in Chapter 2 [56].
A patient affected by SMA was the first user of the device, specifically developed for him.
Next subsections will describe, respectively, the mechanical design, and the electronics and the control strategy of the system.

Figure 4.1: The first version of the hand exoskeleton prototype worn by a patient.

Mechanical design

This prototype has been primarily designed to test the manufacturability of the developed kinematic chain discussed in Sec. 2.1. All the mechanical parts have been 3D-printed and internally produced by means of a 3D printing machine (Dimension Elite by Stratasys) in ABS thermoplastic polymer since it represents a satisfying trade-off between good mechanical characteristics, low weight and allows to manufacture components without considering technological constraints due to the particular production method as well as it may happen using subtracting processes.
Nevertheless, the embodiment of the 1-DOF mechanism required several choices

leading to a real, practically manufacturable and wearable mechanical solution. The first issue to face was represented by finding suitable dimensions to match the hand ones of the user and modifying the shape of the component in order not to touch the fingers while closing.

A general first customization of the mechanism allowed to overall adapt the kinematic model to each patient's finger. Starting from a 2D hand trajectories acquisition of the intermediate phalanges of the user (performed exploiting open source Kinovea software[1]), an optimization MATLAB-based algorithm minimized a constrained nonlinear multi-variable function [57] modifying the geometrical parameters and leading the mechanism to fit the acquired trajectories. The aforementioned optimization process is decribed in details in [37]. The specific routine is not discussed in the thesis since this optimization strategy has been preliminary exploited, in this context, to find a first-tentative exoskeleton actually wearable by a user but only in order to validate the kinematics chain of the finger mechanism. In fact, the goodness of the solution of this first optimization algorithm was strongly dependable on the initial state, resulting in a low adaptability of the system when it was far from the first tentative shape. The employment of the optimization strategy described in Chapter 3 allowed instead to avoid the issues arisen in the use of this first strategy. The exoskeleton designed to validate the second optimization algorithm will be presented in the next section.

Once the mechanism features was defined, virtual tests have then been carried out to assess, before manufacturing the device, the hand-exoskeleton kinematic coupling and interaction in simple opening and closing gestures. SolidWorks Motion Simulation tools allowed to investigate the overall behavior of the hand when the exoskeleton was worn by the user. Not only the kinematic interaction between the 1-DOF mechanism and the finger has been evaluated allowing to determine the suitable dimension of the mechanism, but also the occurrence of interpenetrations between the finger and the device has been checked, verifying mutual coupling during the whole range of motion. Referring to the quantities shown in Fig. 4.2, the defined dimensions of each component of the index finger mechanism are reported in Tab. 4.1, which collects the geometrical parameters for each part of each finger. Fig. 4.2 shows also the particular shape adopted in this exoskeleton version to avoid finger-mechanism contact during the use.

The mechanism reported in Fig. 4.2, is still representing a simplified model. During the design phase, mainly due to the passage from the simplified model to the real hand exoskeleton parts (designed for all the fingers), some important

---

[1]https://www.kinovea.org/
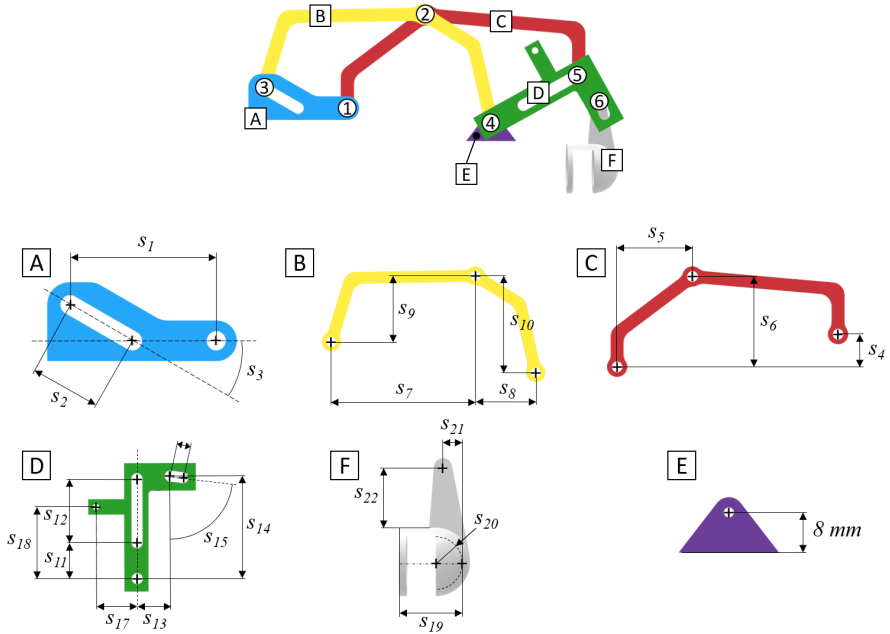
Figure 4.2: Exoskeleton mechanism parts

key issues have been faced (as long as maintaining the same kinematics). In particular, component C was split in two parts guaranteeing a symmetric load configuration during the use of the exoskeleton and obtaining a more stable solution. Components D was made in two parts as well, allowing them to be assembled together. component E, which represents the hand-exoskeleton interface, has been designed to wrap only the back side of the finger phalanx not to reduce the sense of touch, while a Velcro held the finger tight achieving a solid connection. Also the distal phalanx was then connected to the mechanism through a idler thimble (this additional DOF did not change the mechanism kinematics). In order to reduce the lateral encumbrances of each mechanism, pins and shafts were directly integrated in the ABS components as lateral rods. Finally, the shapes of all the components have been modified to avoid contact with the finger during hand closure. The re-design process of the mechanism is

Finger	A	C	B	F	D
	$[s_1..s_3]$	$[s_4..s_6]$	$[s_7..s_{10}]$	$[s_{11}..s_{18}]$	$[s_{19}..s_{22}]$
Little	[23.9,11.8,30°]	[9.6,25,22,65.4]	[44,19.9,22,29.4]	[10.3,18.4,9.6,29.4,82,3.7,11.8,20.6]	[8.8,5.1,5.1,12]
Ring	[32.5,16, 30]	[13,36,30,89]	[60,27,30,40]	[14,25,13,40,82,5,16,28]	[12,7,7,16.5]
Middle	[34.7,17, 30]	[13.9,38.4,32,95]	[64,28.8,32,42.7]	[14.9,26.7,13.9,42.7,82,5.33,17,30]	[12.8,7.5,7.5,17.6]
Index	[30.7,15.1, 30]	[12.3,34,28.3,84]	[56.7,25.5,28.3,37.8]	[13.2,23.6,12.3,37.8,82,4.7,15.1,26.4]	[11.3,6.6,6.6,15.5]

Table 4.1: Exoskeleton characteristics [mm]

shown in Fig. 4.3. The geometrical characteristics of the final mechanism parts are described in terms of maximum length l and height h.

	Index	Medium	Ring	Small
	$[l\ ,\ h]$	$[l\ ,\ h]$	$[l\ ,\ h]$	$[l\ ,\ h]$
A	[35 , 12]	[40 , 15]	[35 , 12]	[25 , 12]
B	[75 , 35]	[84 , 48]	[69 , 36]	[55 , 27]
C	[76 , 35]	[82 , 48]	[70 , 36]	[55 , 27]
F	[40 , 52]	[50 , 64]	[38 , 51]	[31 , 40]
Total	[120 , 42]	[130 , 50]	[115 , 41]	[90 , 30]

Table 4.2: Final mechanism characteristics for each finger [mm]

Actuation system

Since the whole system has been thought and developed under a low-cost concept, many solutions that could be found in the state of the art have been avoided due to their high costs. A specific cable-driven transmission has then been designed exploiting four servomotors which actuate the four long fingers. As visible in Fig. 4.1, both the transmission and the actuation system are placed on the hand backside, as well as the mechanisms are positioned on the fingers, and they do not impede objects handling. The four servomotors are in charge of opening the fingers at the same time by pulling a cable which has two connection points on each mechanism. Closing gesture is passively allowed releasing the same cables.

The reduction of the total mass, which was one of the main requirements of the device, has led to the choice of high power density actuators to be directly
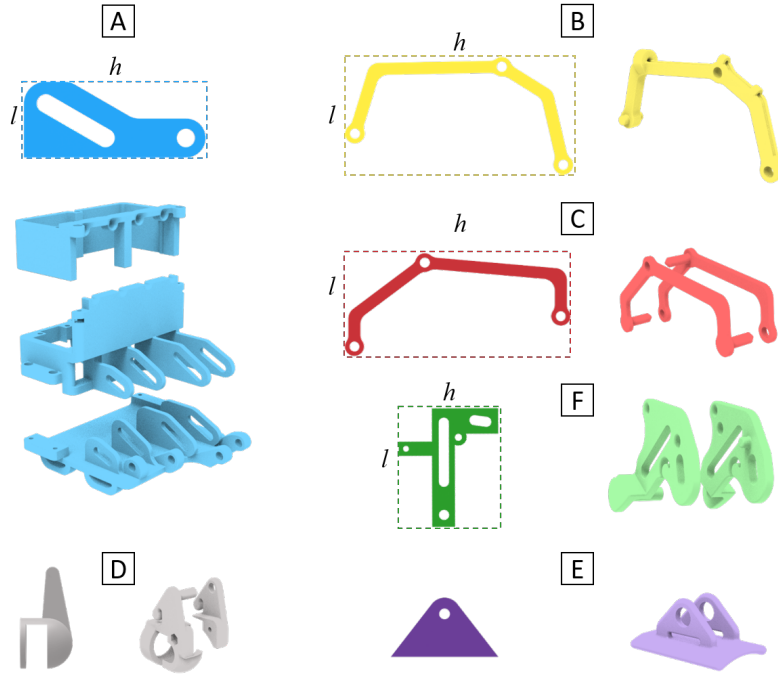
Figure 4.3: Re-design process of the exoskeleton parts.

mounted on the back of the hand. Four Savox SH-0254 servomotors[2], one per long finger, have been selected for their characteristics: maximum torque of 0.38 Nm [3.9 kg cm] and maximum angular speed of 7.69 rad/s [0.13 sec/60deg] at 6.0 V, with a size of 22.8x12x29.4 mm and weight of 16 g. These motors have been modified to allow for the continuous rotation of the shaft despite the resulting loss of position feedbacks. The actuators have undergone some experimental tests, which confirmed their characteristics and their capacity to easily actuate the exoskeleton, before they were mounted on the device. The control unit was based on a 6-channels MicroMaestro control board[3] which has been chosen for its cheapness, its lightness (only 5 g), its small dimensions (21x30 mm) and, above all, because its six channel matched the number of external devices that

_____

[2]http://www.savoxusa.com
[3]https://www.pololu.com

had to be connected to the board: the aforementioned four servomotors and two buttons, one for opening and one for closure triggering action. The control unit and the actuators were powered by a compact 4-cell Lithium battery (at 6.0 V), which was placed in an elastic band on the arm of the user, provided with a safety switch close to the buttons case, mounted instead on the forearm. Regarding the control strategy, the system was controlled by a simple script, stored and running directly on the MicroMaestro chip-set. The code had to continuously check for one of the two buttons to be pushed and held down and then react by sending the corresponding command to the actuators. This version did not include sensors for fingers position feedbacks and the bounds of the exoskeleton range of motion were manually managed by the user (keeping pushed or releasing the buttons) in order not to overcome their anatomical limits. Even thought there was one motor per finger, the possibility to move each of them independently from the others has not been considered for simplicity and all the long fingers were moved together.

Testing

The whole mechatronic system described in the previous sections has then been assembled and tested to evaluate the manufacturability of the adopted solution (Fig. 4.1). In fact, the single DOF mechanism, reported in Fig. 2.1, consists in a closed kinematic chain mechanism capable of performing a defined roto-translation of the end effector (joint 4), which is the connection point between hand and exoskeleton. In particular, the hand connection point is on the intermediate phalanx; if needed, also the distal phalanx can be connected through a thimble (maintaining the same kinematics). Such mechanism has a single DOF kinematics whose forward model has been studied in order to assess its capability to guide the user's long fingers during grasping movements. However, despite the simple kinematic model, the design process required several functional modifications from the model itself to the real prototype. Such modifications allow for the physical coupling of the components and guarantee their placing on the fingers, but a validation campaign needs to be carried out to verify the actual compliance between the model and the real device.

The same single-camera optical system exploited to evaluate the hand joints trajectory has been employed in this testing phase. Colored markers has been placed on the mechanism joints and open source Kinovea software was used to track markers trajectories. Finally, the acquired trajectories has been compared to the kinematic model ones.

Since the mechanism is the same for all the fingers, it consists of rigid bod-
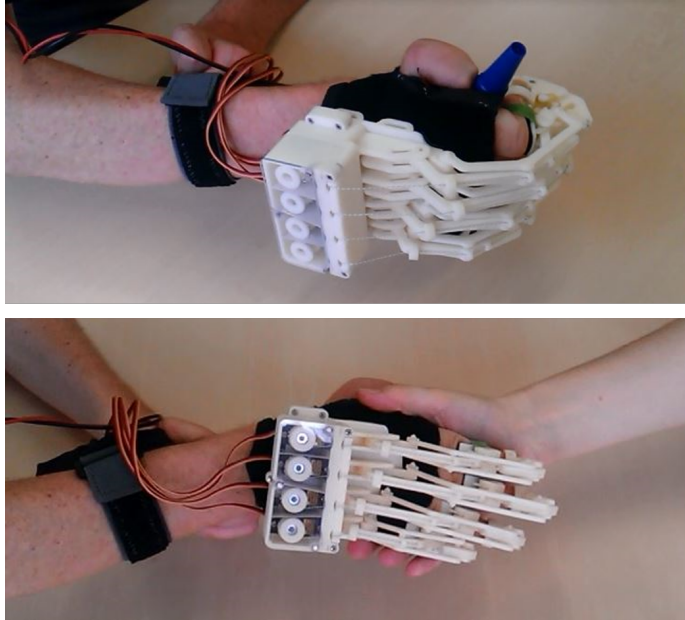
Figure 4.4: Testing phase of the exoskeleton prototype: grasping of a small object and shaking hands.

ies, and considering that the aim of the validation phase is the evaluation of the goodness of the prototype kinematics with respect to the modeled one, the comparison between real data and simulated trajectories are presented only for the index finger mechanism. Same considerations can be adopted for all other long fingers. In Fig. 4.5, the results of the comparison between the real and modeled exoskeleton trajectories are reported. The error results quite low, confirming the goodness both of the design process and the manufacturing one.

This phase played a key role for the research work, laying the groundwork in heading to a comfortable device completely and specifically designed on the patients' hand.
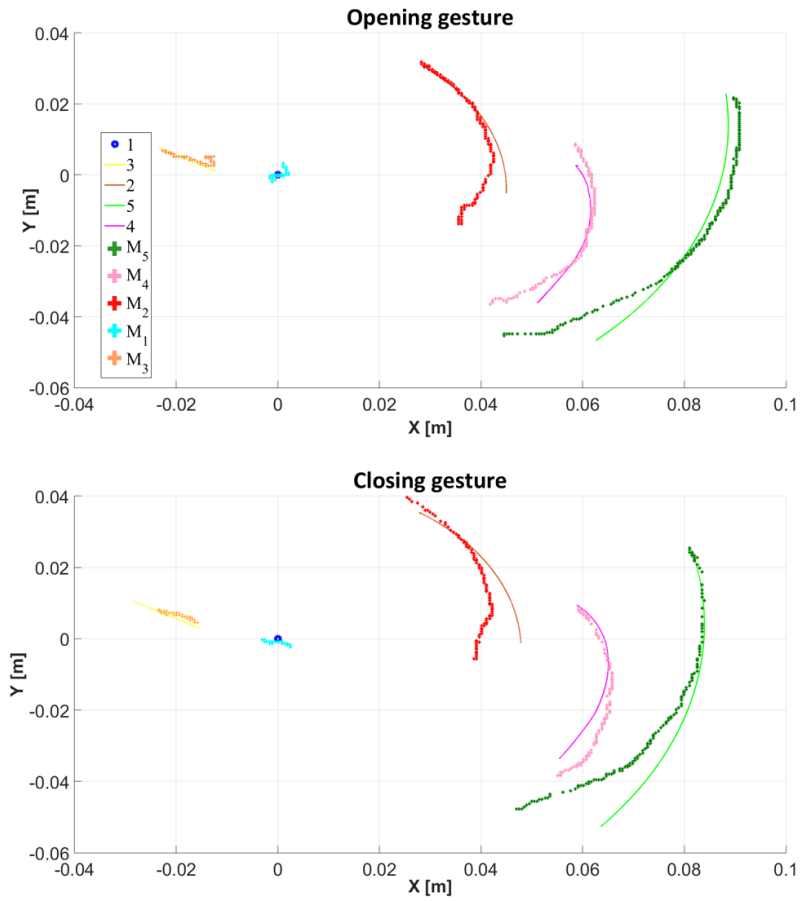
Figure 4.5: Comparison between the exoskeleton model trajectories and the real ones for the index finger during both opening and closing gestures.

4.2 Second prototype: optimization manufacturability assessment

According to the results obtained from the studies discussed in Chapter 3 and from the project specifications reported in Chapter 1, keeping in mind the wearability and adaptability requirements, a second prototype of the hand exoskeleton has been designed and built. The aim of this design phase is the manufacturing of a real device not only to validate the optimization-based strategy discussed in Chapter 3, but also to revamp the device presented in Section 4.1 reaching a lighter and more wearable system for the patients.

The high wearability of a system is hence endorsed by its transparency with respect to the hand natural kinematics, rising from a device which is not felt as a constraint, but whose use actually results straightforwardly intuitive. Both the optimization strategy, leading to a mechanism which replicates at best the fingers gestures, and the revamping design, heading to a lighter solution, contribute to a system completely accepted by the end user.

Mechanical design

The optimization procedure proposed and discussed in Chapter 3 has been applied to all the long fingers of one of the subjects whom the hand MoCap has been performed on. To automate the procedure, a parametric CAD model has then been developed. The possibility to adjust the geometry of the 3D model basing directly on those values obtained from the optimization routine leads to a completely automatic scaling procedure. In addition, as well as tested with the first prototype, a CAD model allows to simulate the wearing of the device and its kinematics (when it has been coupled with the hand), in order to improve the exoskeleton ergonomics basing on the particular user's hand even without facing the patient.

The prototype is, then, made in ABS through the Fused Deposition Modeling (FDM) technique. Another important advantage of the 3D-printing, in addition to those ones listed in the previous section, lies in the possibility of directly "print" the system from the CAD model, resulting, again, in a totally automatic procedure from the MoCap acquisition to the manufacturing of the device. In Fig. 4.6 some pictures of the devices exploited in validation phase are reported. In this prototype, the particular mechanical architecture of the exoskeleton has been slightly modified: only one contact point with the finger has been kept and the thimble has been removed. The new device does not envelop the finger itself avoiding uncomfortable constraint feeling and allows for touching objects

Figure 4.6: The optimized HES prototype worn by the user

without tactile hindrance.

In agreement with the physiotherapists of the Don Carlo Gnocchi Foundation, a passive DOF has been added upstream the finger mechanism (fig. 4.7) to support physiological ab/adduction during flexion/extension of the finger itself. This solution also improves the auto-alignment between finger and mechanism joints.
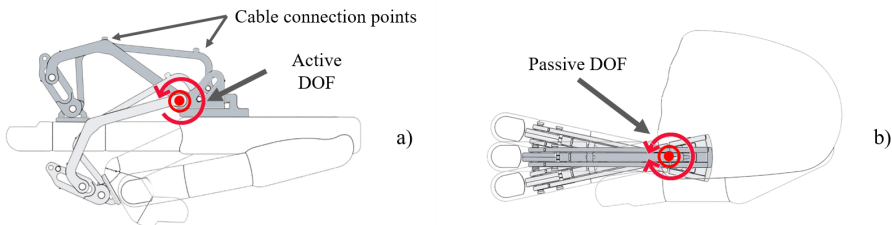
Figure 4.7: Lateral (a) and top (b) view of the finger mechanism mounted on the hand. The active and the passive DOF of the mechanism are highlighted in red.

Actuation system

The actuation system makes use of high power density actuators for the direct implementation on the back of the hand. This solution yields a compact system. With respect to the first exoskeleton version, in this new prototype the number of the servomotors is reduced from four to two: one for the index finger and one for the other three long fingers. This particular choice has let, improving the control system in further developments, to separately actuate index allowing for

pinch gesture. Since the mechanisms for each finger have different sizes, the opening and closing velocity is different for each finger. Through the design of a particular pulley with three different diameters (Fig. 4.8), it is possible to actuate middle, ring and small finger mechanism at the same time with the same motor. This solution allows to limit the weight of the whole system at 242 g, even though the new selected servomotors (Hitec HS-5495BH[4]) are different from those used in the first prototype being able to exert higher forces on the mechanism. They present a maximum torque of 6.4 kg/cm (0.628 Nm) at 6.0 V and 7.5 kg/cm (0.735 Nm) at 7.4 V with a size of 39.8x19.8x38.0 mm and a weight of 44.5 g. The maximum angular speed is 6.15 rad/s at 6.0 V and 6.67 rad/s at 7.4 V. The proposed actuation system has been tested in order to verify the real performances. The dimensions of the servomotors housing are 48x66x74 mm. Figure 4.8 shows the overall transmission developed to actuate the finger mechanism by means of two servomotors.
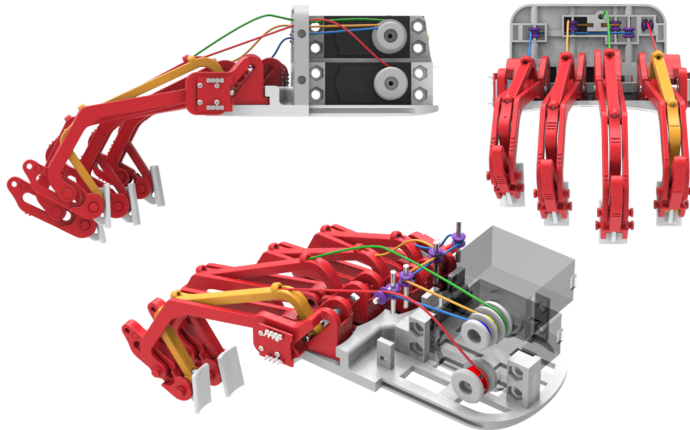
Figure 4.8: HES actuation system

The control system has been designed with a precise goal in mind: keeping its weight, complexity and costs as low as possible. Lightness, cheapness and simplicity are some of the main characteristics that make a device suitable for the application to a large number of people. Arduino Nano represented a good trade-off between performances, simplicity and cheapness. The 16 MHz-clock

---

[4]http://hitecrcd.com/products/servos/sport-servos/digital-sport-servos/
hs-5495bh-hv-digital-karbonite-gear-sport-servo/product

processor was enough powerful to work with signals whose maximum frequency is about 500Hz. The embedded board offered the possibility to directly connect lots of sensors already present on the market (drastically decreasing the complexity of connections) while its elementary programmability makes it easily re-configurable. Two 15-bit magnetic encoders are placed on joint 1 of the mechanism (Fig. 4.6) of the index and little finger, respectively and measure the value of the angle α_2, which identifies the single DOF of the mechanism.

The control strategy makes use of two inner control loops, which are added to take care of the grasping of objects and to indulge the hand motion if an unexpected muscular spasm occurs during the opening phase. Grasping of an object is detected calculating the length of the unrolled cable twice (the first time using the kinematic equations of the mechanism and the second one using the motors speed and the pulleys radius) and then comparing the differential measurement to a set threshold. Muscular spasms are detected, instead, when the instant motor speed falls below a set percentage of the nominal speed. In the first case the motors stop and hold their angular position while in the second case they invert their motion, from opening to closing.

Testing

This section presents the results obtained during the validation and testing phase of the prototype developed in accordance with the procedure discussed in Chapter 3. A real ABS prototype has been hence 3D-printed to test the manufacturability of the kinematic architecture and assess the goodness of the optimization strategy. The tests took place at the Don Carlo Gnocchi Foundation Rehabilitation Center in Florence, Italy, exploiting the same MoCap system used to acquire the motion of the hand alone; the same cameras configuration used for the hand motion acquisition phase was maintained for these tests.

The results shown in this section are relative to one of the volunteer subjects presented in Section 3.1, assumed as case study to validate the proposed optimization-based strategy. After having acquired the data according to the protocol discussed in Section 3.1, as reported above, a hand exoskeleton prototype, specifically tailored for the subject, has been designed and manufactured. For sake of brevity, the results related to one finger (index finger) are reported. The same assessment can be applied to all the other three long fingers as well. Figure 4.9 reports the joints trajectories of the considered patient's right index. Figure on the right has been obtained by the motion analysis campaign discussed in Section 3.1, which allows to define the hand kinematic model. Then, a whole flexion/extension gesture has been generated by the model. A MoCap has been

performed on the right index finger during three consecutive flexion/extension movements of the subject (markers positioning was the same reported in Fig. 3.3) and the relative trajectories are plotted in the background on the left of Figure 4.9. Taking the aforementioned trajectories as reference, the proposed
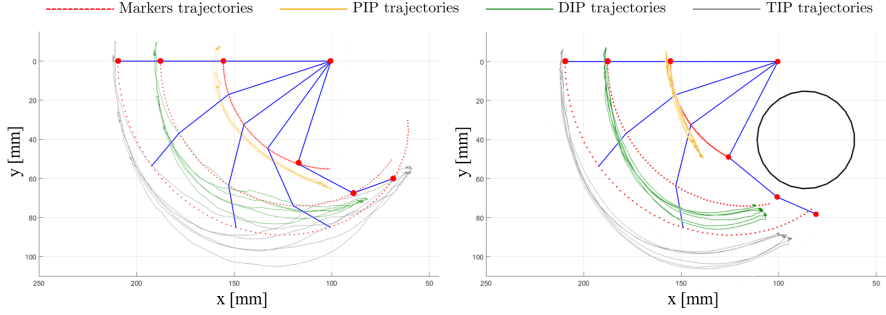
Figure 4.9: Hand kinematic model trajectories during a flexio/extension (on the left) and a grasping movement (on the right); markers trajectories, acquired through the MoCap, are reported in the background: PIP trajectory in yellow, DIP in green and TIP in grey

optimization procedure has been carried out (the maximum number of iterations was set to 300000).

Figure 4.10 reports the yielded mechanism trajectories actuating a complete flexion/extension movement. Computed trajectories have been compared with the real trajectories of the manufactured mechanism (exploiting again the BTS MoCap system): thanks to the precise additive manufacturing process, they are totally overlapping.

Point E in Fig. 4.10 (it corresponds to joint position $^1\mathbf{p}_4$ in Fig. 2.2) represents the end-effector which is in charge of following the finger movement when the exoskeleton is actuated. The more the trajectory of E point of the real device is similar to E point trajectory calculated from the hand kinematic model, the more the exoskeleton results comfortable for the user. So, comparing these two different trajectories means evaluating the comfort of the device. The desired trajectory (the one defined by hand kinematic model) has been hence compared with the real trajectory (directly tracked by means of the motion analysis). The results are graphically reported in Fig. 4.11. The error computed by the optimization algorithm through Eq. 3.21 (weighted combination of maximum and average error) is 7.62 mm, which corresponds to a maximum error of 4.96
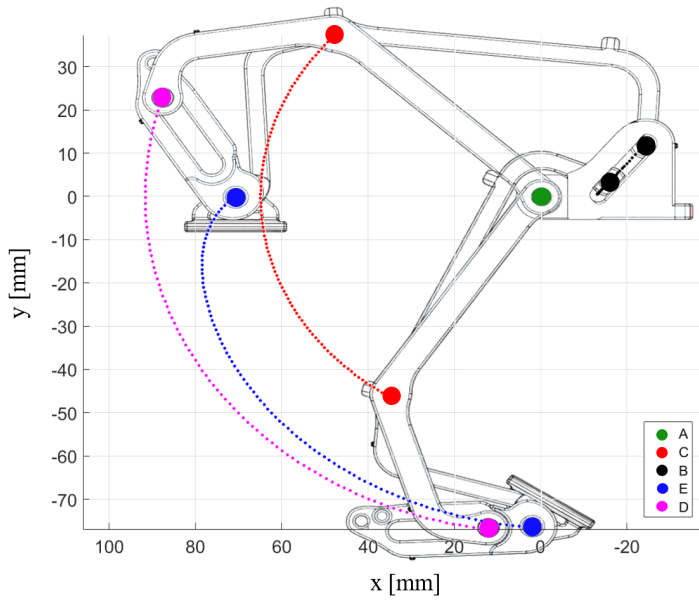
Figure 4.10: Joints trajectories of the resulting optimized exoskeleton.

mm, while the average error is 2.66 mm. The maximum error value is equal to the less than 2.4% of the total finger length. Such value can then be neglected even considering that, between the skin and the exoskeleton, slight relative displacements can occur softening the coupling.

Figure 4.12 reports the trend of the error in following the physiological computed trajectory by the exoskeleton. Also in this case, the desired trajectory is the one obtained by the hand kinematic model, while the actual one is the trajectory of point E of the exoskeleton acquired by the MoCap system.

The described testing campaign led to validate the optimization process yielding a mechanism fully design on the patient's anatomy and mobility. The importance of this part of the research project lies in the possibility (after having assessed its precision) of designing devices capable of being actually used without producing uncomfortable feeling in the user. The capability of replicating the natural finger trajectories is then essential during the rehabilitation process to make the patient reacquire the most natural mobility possible.
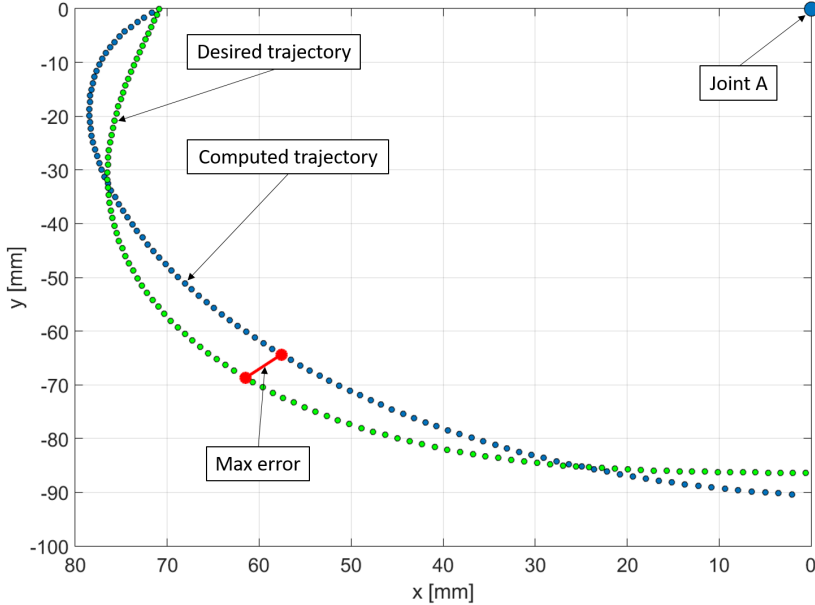
Figure 4.11: Difference between desired (computed through the hand kinematic model) and acquired (tracked through the MoCap system) trajectory of the E joint of the exoskeleton

4.3   Third prototype: final solution

This current version of the exoskeleton is represented by fully portable, wearable and highly customizable device that can be used both as an assistive hand exoskeleton and as a rehabilitative one. Both mechatronic design and control system are developed basing on the patients needs in order to satisfy users' daily requirements increasing their social interaction capabilities.

Mechanical design

The mechanics of this last exoskeleton has been revamped to achieve a more lightweight solution improving its wearability without influencing the obtained results in terms of accuracy while replicating hand gestures. The new system is actuated by a single servomotor and a specific cable driven transmission sys-
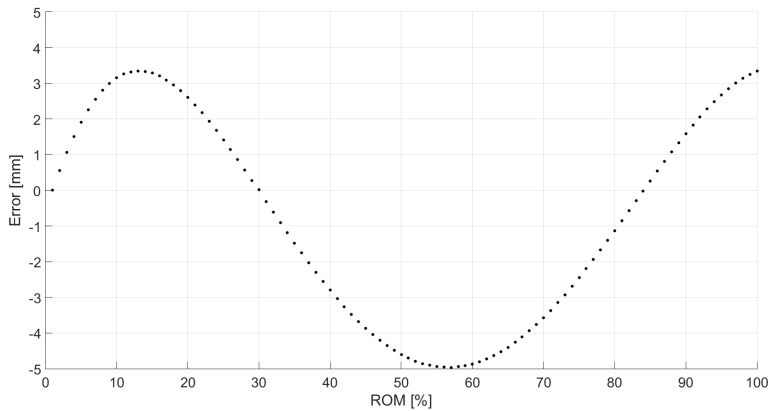
Figure 4.12: Trend of the error between desired and acquired trajectory of E joint of the robotic device during the flexion/extension ROM

tem has been developed to open all the four long fingers together at the same time. Different mechanisms velocities are obtained thanks to different pulleys diameters, which are calculated depending on users fingers dimensions. The mechanism kinematic architecture has been further modified by eliminating component D of Fig. 2.1. Thickness of components C and B has thus been increased to bear the load program these components are subjected to.
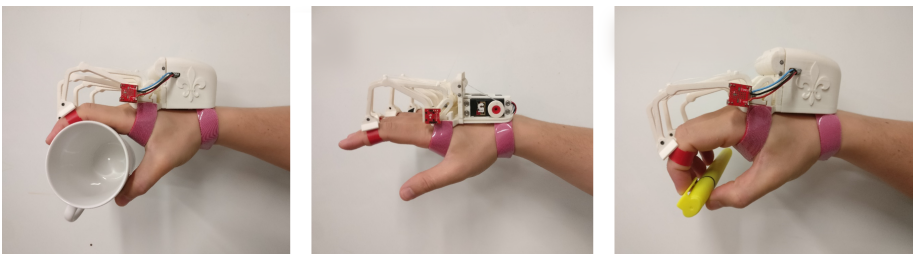
Figure 4.13: Final version of the exoskeleton prototype by the DIEF.

Actuation system

Both the electronics and the control system of this version has been deeply modified in order to give the patient the possibility to actuate the device by his own and to reduce the overall dimensions of the system.

The first important difference with respect to the previous systems is that, as reported above, another motor has been removed adopting a single-motor actuation system. Even though the motor has not been changed, the exploitation of just one actuator has brought with it some advantages: the total weight of the system has been remarkably reduced and the control code has resulted to be computationally lighter, not having to manage the coordination between motors. Nevertheless, the main difference of this prototype lies in the triggering system. Tests conducted on the second version of the prototype have hence stressed the importance for the user of being able to use both hands independently, pushing the buttons-based triggering action to be replaced with something which could allow for an autonomous control of each hand. An ElectroMyoGraphy (EMG)-based control system has been implemented following the most recent research trends in literature [58], [59], [60].

The EMG-strategy will not be discussed in details in the present work, but its general overview will be given in the following in order to describe the entirety of the designed device.

Firstly, according to the guidelines of simplicity on which this prototype was born, but also to the stringent constraints that the specific application imposes in terms of encumbrance and lightness, the electronics of the system has been reduced to the minimum necessary. The list of the selected components is provided below.

- MyoWare Muscle Sensors (AT-04-001) by Advancer Technologies[5] have been chosen for collecting EMG signals. This kind of sensors, which are small (20.8 x 52.3 mm) and low-powered devices, measures the electrical activity of a muscle, outputting either raw EMG signals or enveloped EMG signals, which are amplified, rectified and integrated.

- HS-5495BH High-Torque Servo by Hitec has been selected to be the only actuator of the system.

- Supermodified V3.0 for RC-servos from 01$^{\text{TM}}$ Mechatronics[6], which consists of a DC motor controller and a 15-bit magnetic encoder with overall

---

[5]https://learn.sparkfun.com/tutorials/myoware-muscle-sensor-kit
[6]https://www.01mechatronics.com/product/supermodified-v30-rc-servos

dimensions of 16x16x12 mm, has been used both for motor controlling and for collecting the angular position of the index finger (which is the only controlled DOF of the mechanism) and its angular velocity.

- Arduino Nano from Arduino has been chosen to be the embedded micro-controller of the system. This small board (18 x 45 mm), based on the ATmega328 from Atmel (16 MHz-clock processor, 8-bit AVR architecture, 32 kB of flash memory, 2 kB of SRAM memory and 1 kB of EEPROM memory), offers the possibility to easily connect and communicate to lots of electronics devices included, of course, all the aforementioned ones. Customized Arduino libraries have been used to interface with the HS-5495BH servo and the Supermodified motion control modules.

All the presented components, except for the MyoWare^{TM} Muscle Sensors, have been thought to be housed directly on the back of the users hand and their small dimensions have positively weighed on the choice.

Control architecture

A specific EMG-based control architecture has been developed letting the user the total control of the exoskeleton actuation without being forced to use the other hand (as it happened with the first and second prototypes).

Since the mechanism is already optimized for the tracking of the trajectories of the fingers, the control system focuses mainly on managing trigger actions. The proposed control strategy, whose pseudo code is reported in Algorithm 1 can be split in two main parts, which are sequentially executed every 33 ms. The first part of the code, which will be described hereinafter, takes care of classifying the user's intentions relying on the measurements of the forearm muscular activity captured by the EMG sensors. Once the current user's intention has been classified, the corresponding signal is passed to the second part of the code, which translates it into appropriate control commands for the actuation system. An outer control loop is in charge of continuously checking that, during functioning, the system does not overcome a fixed ROM, which is identified during the first phases of tuning when the anatomical limits of the user's hand are assessed. If these bounds are violated, the system stops and waits for a command that will move it back to a good configuration within the ROM (e.g. if closure bounds are reached, the system waits for an open command and rejects every other close commands). An inner control loop, which is only active during hand closing, is meant to check if an object is grasped. This is done evaluating closing velocity of the index finger: when it drops below a fixed threshold while the motor is still

---

Algorithm 1 Pseudo code of the control strategy

Every sample time interval

Input:

F_p = current finger position
F_v = current finger velocity
M_a = current muscular activity

Classification:

if M_a **compatible with** opening gesture **then**
| *open*
end
else if M_a **compatible with** closing gesture **then**
| *close*
end
else
| *rest*
end

Actuation:

if *open* **then**
  if F_p **compatible with** range of motion **then**
    | run motor to pull the cables to assist the hand opening
  end
  else
    | maximum opening reached: stop motor and wait for a new close command
  end
end
if *close* **then**
  if F_p **compatible with** range of motion **then**
    run motor to release the cables to follow the hand closing
    if F_v < velocity threshold **then**
      | object grasped: stop motor and wait for a new open command
    end
  end
  else
    | maximum closure reached: stop motor and wait for a new open command
  end
end
if *rest* **then**
| do nothing: wait for a new different command
end

---

running, it is reasonable to think that the hand has encountered an object or an obstacle. The control system intervenes stopping the motor, making it hold position and preventing the cable to be released more than necessary even if the user is keeping tightening the hand around the grasped object (keeping the hand tighten can indeed be classified as a closure intention as it activates the same muscles bands). It has been observed that too much cable released during object grasping usually introduced remarkable delays in controlling actions and led to issues of interweaving. Real-time information about the position and the velocity of the index finger is collected by means of the magnetic encoder mounted on the exoskeleton in correspondence of the MCP joint of the finger.

For the considered scenario, an accurate classification of user's intentions starting from sEMG signals represents a high challenging task. The human hand can indeed perform lots of different movements which require high dexterity. In addition, the muscles that converge on the tendons for the handling of the hand are many and very close to each other. Finally, signals coming from sEMG are usually very low and noisy. These are the main reasons that make the use of high computational power machines with long training phases necessary to teach complex algorithms to precisely discriminate every possible hand movement from the others and to teach the user how to emit appropriate muscle signals. However, linking the exoskeleton to something which is usually heavy and fixed in place (e.g. a workstation) is definitely far away from representing a wearable solution. The proposed strategy for EMG classification is, instead, thought to be implemented on an embedded micro-controller board, which can be directly mounted on the system, and not to require long training phases. To reach these goals, a trade-off between the number of different movements that can be classified and the computational power provided by the defined hardware had to be reached. As a result of the aforementioned reasons, only hand opening, hand closing and hand resting have been considered as possible user's intentions to be classified. Hand resting, which represents the safe mode of the system because it does not imply any motion, has been thought to enclose every EMG pattern different from hand opening and hand closing, including Unwanted Movements (UMs) similarly to the base idea of what is presented in [61].

Among all the other EMG signals features that literature recommends to extract [62], a preliminary Principal Components Analysis (PCA) has anyway identified the EMG envelope, which is directly output by the EMG sensors and which is known to work well with microcontrollers analog-to-digital converters, as a representative feature to discriminate between the three gestures. The choice of limiting the possible user's intentions to three, along with the possibility to

exploit the EMG envelope, turned out to be very advantageous to reduce the computational power required by the classifier: these gestures can be indeed discriminated with the use of just two EMG sensors placed on the antagonist muscle bands responsible of fingers/wrist extension and flexion and so, since the input signals are just two (one per sensor), the classification problem results to be bi-dimensional. Fig. 4.14 shows an example of the positioning of the EMG sensors attached to a healthy subject's forearm.
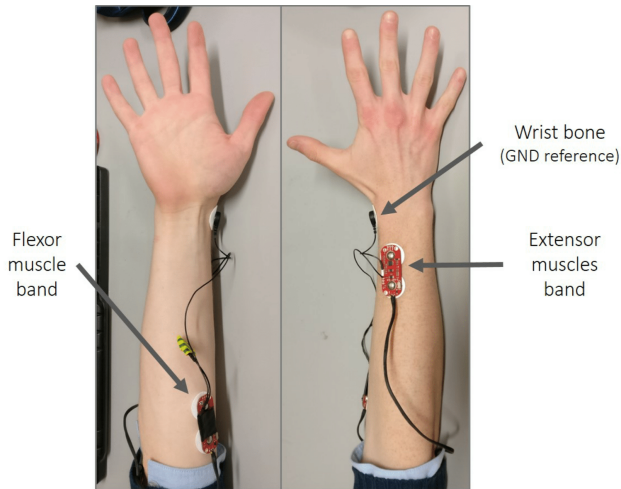
Figure 4.14: An healthy subject wearing the EMG sensors. One sensor is placed on the fingers/wrist extension muscles band, the other one on the flexor muscles band. An electrode is placed on the wrist bone and serves as ground reference.

For the classification phase a Point-in-Polygon algorithm has been chosen for its good performance and its light code (Algorithm 2). This algorithm is a ray-casting to the right: it takes as inputs the number of the polygon vertices, their coordinates and the coordinates of a test point; each iteration of the loop, the line drawn rightwards from the test point is checked against one of the polygon edges and the number of time this line crosses the edge is counted; once the loop has ended if the number of crosses is an odd number of times, then the point is outside, if an even number, the point is inside.

Although it is a fairly simple classifier, it still requires to be tuned by means of a preliminary training phase who will likely take place at the hospital/rehabilitation center before the patient gets discharged. A custom Qt Graphical User Interface

---

Algorithm 2 Point-in-Polygon algorithm

Input:

int N_v = number of the polygon vertices
float V_x = array of x-coordinate of all vertices
float V_y = array of y-coordinate of all vertices
float T_x = x-coordinate of the test point
float T_y = y-coordinate of the test point

int j = $N_v - 1$ bool inside = false **for** (*int* i = *0;* i < N_v; i ++) **do**
   if (((V_y [i] < T_y *and* V_y [j] ≥ T_y) *or* (V_y [j] < T_y && V_y [i] ≥ T_y
)) *and* (V_x [i] ≤ T_x *or* V_x [j] ≤ T_x)) **then**
     inside ^= (V_x [i] + (T_y − V_y [i]) / (V_y [j] − V_y [i]) ∗ (V_x [j] −
     V_x [i]) < T_x)
   end
   j = i
end
return inside

(GUI), visible in Fig. 4.15, has hence been designed to represent a user-friendly tool which can be used to easily and quickly upload on the micro-controller from a standard PC all the data needed by the classifier. In particular, it allows to collect EMG data concerning different gestures, to display them within a scatter plot on a 2D Cartesian plane on whose axis are reported the signals from the EMG sensors and straightforwardly draw the polygons which delimit the clouds of points belonging to the same gesture. Choosing the number of vertices, the shape and the size of the polygons represent a key-point of the classification phase which is meant to be done manually by a professional who have followed the patient during previous supervised physiotherapy sessions. Properly tuning these parameters on patient's needs can hence improve classification accuracy and disturb rejection.
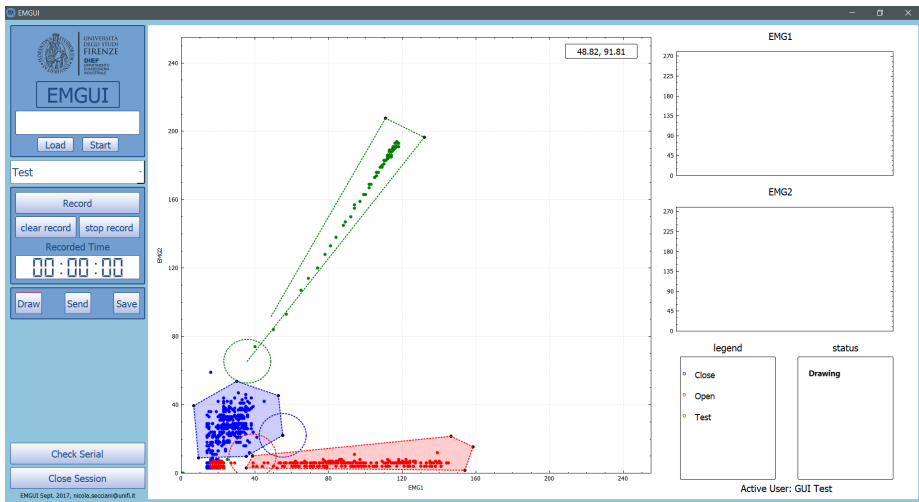
Figure 4.15: Example of the classification training phase exploiting the developed custom GUI.

Chapter 5

Aluminum hand exoskeleton prototype

In Chapter 4, an overview of three ABS-designed prototypes has been presented and their main features have been discussed. In particular, after the design of a first tentative mechanical solution which allowed for the kinematic chain validation (Section 4.1) and the first development of this device embodied by a new system tailored on the user's hand (Section 4.2), a fully wearable and portable hand exoskeleton has been reached with the third prototype (Section 4.3).

However, even if the portability of the hand exoskeleton is strictly related to its weight, size and adaptability to the user's kinematics, its usability (meant as the reliability the device provides during its prolonged use) relies on the employed materials. In particular, since the exoskeleton functioning is based on a rigid kinematic chain acting on the patient's fingers, the stiffness of the device plays an important role in applying suitable forces on the hand for the ADLs fulfillment.

This chapter, deals with a new design of the hand exoskeleton presented in the previous chapters. Making use of aluminum alloy components and exploiting novel topology optimization techniques, the structural features of the proposed new device guarantee increased performances (in terms of exerted forces without exceeding stresses bearable by the system and deformation suitable to the use) maintaining an acceptable weight for the users.

5.1   Topology optimization

Structural optimization problems are often faced in many areas of engineering and several mathematical methods have been developed and exploited in tackling this issue. They can be classified into three main groups (a graphical explanation is provided in Figure 5.1) [63]: parametric optimization (that changes the size of the elements) [64], shape optimization (that changes the shape of the structures) [65] and topological optimization (that changes the topology of the structures) [66].
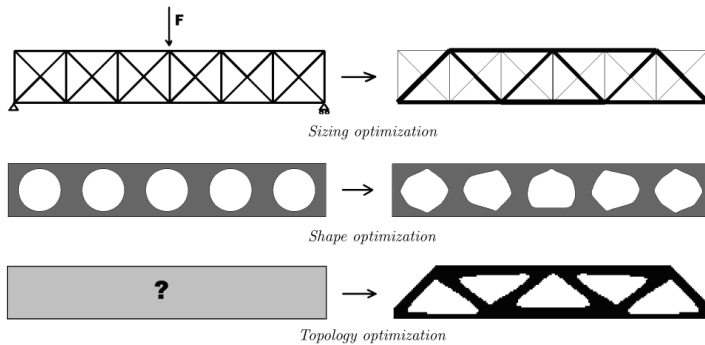
Figure 5.1: Sizing, shape and topology optimizations

Topology optimization techniques are widely used in civil [67] and automotive [68] engineering applications, while they are quite new in the medical field [69]. They can thus be surely considered one of the most challenging and promising method in structural optimization, especially considering the limited available space and the weight constraint along with the necessity to apply the optimized components on the human body.

Such a process leads to determine the optimal distribution of a given amount of material in the design domain to get the optimal connectivity; shape and number of holes are maximized or minimized keeping the specified structural performances [70]. Topology optimization allows for the change of structures topology and it has the capability of generating a large number of degrees of freedom available for the design variable settings, so that the optimal design can be obtained without prior knowledge [71].

Topology optimization problems are solved using the density method, also known as the Solid Isotropic Material with Penalization (SIMP) method, where a

pseudo material density is the design variable [72]. The material density is defined between 0 and 1, where 0 represents the void state and 1 is the solid state. The SIMP method applies a power-law penalization for the relationship between stiffness and density in order to set elements density.

The Level Set Method (LSM) is then used to solve the problem arising from the introduction of pseudo material density, since it is an excellent tool for modeling time-varying objects and following shapes that change topology. The application of Level Set techniques for topology design has also been proposed recently [71]. This method is a conceptual framework for using level sets as a tool for numerical analysis of shapes and surfaces. The contours of a parametrized family of Level Set functions are used to generate the boundaries of a structure, and the topology can change with changes in the Level Set function. By the exploitation of the LSM, it is possible to perform numerical computations involving curves and surfaces on a fixed Cartesian grid without parameterization of these objects [73].

Topology optimization, being very flexible and customizable, allows to consider:

- various external loads;

- various imposed mechanical constraints (boundary conditions);

- various optimization objective (compliance, volume);

- various optimization constraints (natural frequencies, stress, volume fractions).

The research work presented throughout this chapter investigates the topology optimization potentialities in the design of biomedical devices. This approach could be quite effective to obtain, thanks to innovative design processes, a considerable mass and stress reduction. This aspect can lead to a remarkable impact on the patient, who is able to wear a lightweight and comfortable device with high performances in terms of assistance. In addition, the use current modern manufacturing techniques, such as additive manufacturing, enables the realization of complex three-dimensional shapes, impossible to be produced in the past.

5.2   General architecture

The test case described in this chapter is a generic finger mechanism used in the hand exoskeleton presented in Chapter 4. After the optimization process described hereinafter and whose principal steps are reported below, the whole prototype has been completely re-designed in order to be manufactured in aluminum alloy.

As mentioned before, the steps that have been followed in the optimization process were the following.

- Definition of test case including physical and geometric features, boundary conditions and external loads.

- Static analysis on the standard non optimized model as benchmark tests.

- Definition of design space, an extended area that can change during the topology optimization.

- Definition of objective function and optimization constraints for the static characteristics.

- Topology optimization that differs from the other structural optimization techniques, because it allows to change the topology of structures layout (through the density method, a pseudodensity is introduced and a topology optimization algorithm solves the problems arising from the density method application).

- Surface rendering, to smooth surfaces after optimization process.

- Comparison with standard configuration in terms of obtained results as weight and stress.

5.3   Model description

All the steps, introduced in section 5.2, are described in detail in next sections.

5.3.1   Test case definition and benchmark test

In the test case definition, four different aspects must be considered and defined: geometry of the system, material of the studied components, boundary conditions and loads applied to the device.

Referring to the prototypes presented in Chapter 4, the mechanism of the device reported in section 4.2 (Fig. 4.6) has been chosen as reference for the re-design process. This mechanism represented, in fact, a good trade-off between comfort for the patient (component F is not present allowing for the tactile feeling) and mechanical stiffness (component D guarantees an additional support in case of accidental lateral loads which has been modeled as explained in the following). Then, for this analysis, it is supposed that the structural components of the finger mechanisms are fully constituted by a material with linear elastic isotropic properties (see Table 5.1[1]), i.e. Cl31Al aluminum alloy.

Yield Point $(R_e)^2$	170 - 220 N/mm^2
Tensile Strength (R_m)	310 - 325 N/mm^2
Elongation (A)	2 - 3 %
Young's Modulus (E)	approx. $75 \cdot 10^{3}$ N/mm^2
Density (ρ)	2700 kg/m^3

Table 5.1: Cl31Al material properties according to the material manufacturer's data sheet.

Boundary conditions

The boundary condition applied to the Finite-Element Analysis (FEA) has been defined to replicate an isostatic system. Each analyzed component has been indeed constrained replicating the ones of the kinematic model while the pose of the system has been fixed applying a torque on joint 1. This torque has been calculated by Eq. 2.48 and it represents the action of the actuation system which hold the position of the device and exerts 20 N on the end effector.

Loads application program

The first aspect that must be considered in designing a device which is meant to be an aid for an impaired person is how much strength is required to be exerted. Determining a suitable output force for the normal manipulation tasks during ADLs is still an important aspect in the hand exoskeletons design. In literature

---

[1]These properties refer to the particular material employed in the manufacturing process. Since the aluminum alloy powder has been melted trough a Selective Laser Melting Additive Manufacturing machine, such properties are related to the specific process.

there is a variety of output forces the devices can exert [33], [74].

On one side, studies on hand grasping have evaluated that healthy subjects are able to generate a maximum grabbing force up to 300 N (female) and 450 N (male) [74], [75]. Such force values result a challenging goal for hand exoskeleton systems, since they would demand for a heavy and bulky actuation system, leading to a non fully portable device. On the other side, when hand impairments occur, these force values decrease and, depending on the severity of the impairment, can be close to zero. With this second aspect in mind, the proposed exoskeleton has not been developed to generate the maximum grip strength of a healthy individual but it has been thought to manipulate object usually handled during the everyday life.

In [76], several objects has been assessed to define benchmarks in grasping and manipulating (e.g. picking up and holding a phone or a mug). Considering a weight target up to 1.5 kg and a coefficient of friction of 0.255 (values determined by [76]), a grabbing force of 14.7 N results suitable in manipulating most of the objects.

Thus, as regards the performance of the exoskeleton, each finger mechanism is required to express a 20 N force. This value is identified as a conservative choice and a suitable output for the normal manipulation tasks during ADLs even when only one finger is required in these tasks.

Since the hand exoskeleton studied in this research activity presents only 1 DOF per finger, holding an object becomes mandatory, while controlling and changing the position and orientation of the object could be neglected in this case. Assuming to hold a non-absolutely rigid object, exerting a uniform pressure on it, the object itself initially changes its shape and position with respect to the hand in order to assume a stable pose. Thus, the object results form-closed [77] (i.e. it is impossible to move the object because each point is in contact with the hand) if the stiffness is low and force-closed [77] (i.e. the hand applies forces on the object only through some contact points) if its stiffness is high. However, the aforementioned condition presents the inherent limitation in grabbing very soft objects or objects with an irregular shape. A very soft object could be squeezed too much before reaching the stable position while an objects with an irregular and thin shape might not be properly grabbed. In these cases, the 1-DOF per finger mechanism does not guarantee the required precise grasping procedure.

The dynamic analysis of the multibody system discussed in section 2.3 allows to calculate reaction forces an torques which one component exerts on the others during the use of the exoskeleton when 20 N force is expressed by each finger. The presented study regards the hand closure, since such movement stresses the
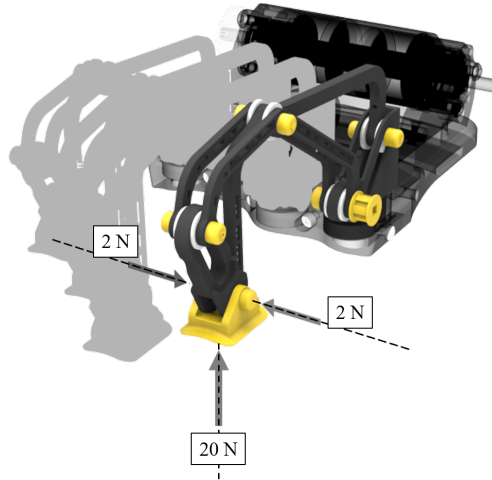
Figure 5.2: Loads.

most the mechanism. In fact, during the hand extension, reaction forces would take into account only the necessity of lifting the finger.

Referring to the kinematic chain of Fig. 4.6 and taking into consideration the notation reported in section 4.1, which identifies the mechanism components by letters from A to D (component F is not included) and the mechanism joints by numbers from 1 to 5 (again, joint 6 is not considered since component F is not present), the external load applied to the mechanism in order to model the interaction with the finger are the ones reported in Fig 5.2. In particular, 20 N force has been applied to the mechanism along y_4 direction at joint 4. In addition, a 2 N lateral load has been imposed along z_4 direction at the same point. Since the effect of the interaction between the hand and the device, modeled as a 20 N force on the end effector, is variable during the finger flexion (y_4 direction is variable with respect to the Ox_1y_1), it was necessary to evaluate the poses of the mechanism that maximize the modules of the joint reactions. Eq. 2.67 has hence been exploited to calculate reaction forces for all configurations - defined by varying the value of angle α_2, which defines the position of the mechanism. Finally, the worst case has been considered: each component has been studied in that configuration it results stressed at the most.

Table 5.2 reports the joints reaction values which maximize the module of, at

least, one reaction force acting on the joints; such values are expressed, both in the components evaluated with respect to the different reference systems (centered on each joint) and in module. The values of the torque acting on joint 1 are also present.

α_2 [°]	$^B R_{3x}$ [N]	$^B R_{3y}$ [N]	$^B R_3$ [N]	$^B R_{2x}$ [N]	$^B R_{2y}$ [N]	$^B R_2$ [N]	$^C R_{2x}$ [N]	$^C R_{2x}$ [N]	$^C R_2$ [N]
25.04	4.91	15.83	**16.57**	-11.84	-34.59	**36.56**	2.36	36.48	**36.56**
23.83	5.08	15.77	**16.57**	-11.71	-34.64	**36.56**	2.57	36.47	**36.56**
0.92	6.50	12.84	**14.39**	-6.84	-32.83	**33.54**	6.44	32.91	**33.54**
23.83	5.08	15.77	**16.57**	-11.71	-34.64	**36.56**	2.57	36.47	**36.56**
0.06	6.45	12.64	**14.19**	-6.53	-32.64	**33.29**	6.53	32.64	**33.29**
42.05	1.93	16.07	**16.19**	-13.02	-22.72	**32.22**	0.08	35.21	**35.21**

α_2 [°]	$^B R_{4x}$ [N]	$^B R_{4y}$ [N]	$^B R_4$ [N]	$^C R_{1x}$ [N]	$^C R_{1y}$ [N]	$^C R_1$ [N]	$^D R_{5x}$ [N]	$^D R_{5y}$ [N]	$^D R_5$ [N]	$^C M_1$ [Nmm]
25.04	6.93	18.76	**20**	-2.36	-36.48	**36.56**	0	0	**0**	**-824.98**
23.83	6.62	18.87	**20**	-2.57	-36.47	**36.56**	0	0	**0**	**-817.48**
0.92	0.34	20.00	**20**	-6.44	-32.91	**33.54**	0	0	**0**	**-597.33**
23.83	6.62	18.87	**20**	-2.57	-36.47	**36.56**	0	0	**0**	**-817.48**
0.06	0.08	20.00	**20**	-6.53	-32.64	**33.29**	0	0	**0**	**-587.50**
42.05	11.09	16.64	**20**	-0.08	-35.21	**35.22**	0	0	**0**	**-876.78**

Table 5.2: Reaction forces on the mechanism joints. $^i R_j$ indicates the reaction force applied to component i on joint j, while $^i M_j$ represents the torque applied to component i on joint j.

Benchmark test

A preliminary static analysis on the non-optimized components must be carried out as a benchmark to understand the constraints to be set in subsequent optimization test.

In the following, the implemented optimization problem will be discussed referring to the index finger mechanism. Nonetheless, the described procedure can be applied to the other fingers mechanisms by changing the dimensions of the analyzed components.

Table 5.3 summarizes the results in terms of maximum stress and displacement

	Component B		Component C		Component D	
	Stress [MPa]	Disp. [mm]	Stress [MPa]	Disp. [mm]	Stress [MPa]	Disp. [mm]
Vertical load	35	0.17	117	2.55	13	0.005
Lateral right load	29	1.13	50	1.82	2	0.002
Lateral left load	29	1.13	50	1.82	2	0.002

Table 5.3: Benchmark test results in terms of maximum stress and displacement for the components B, C and D.
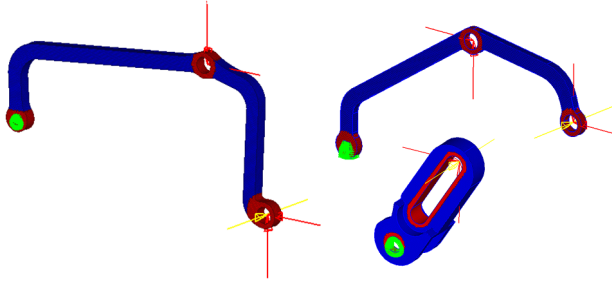
Figure 5.3: Definition of the design and non-design space.

on each mechanism component.

5.3.2 Design space definition

In the topology optimization, the design area denotes the set of elements that can be removed during the optimization, in contrast to the non-design space that remain unchanged. In the considered case study, the region around the holes must be kept as it is. These regions belongs to the non-design space and they do not change after the topology optimization. The design space is the area that changes during the topology optimization instead and it is usually expanded with respect to the basic model. This expansion provides to the solver much material to be used in the optimization with respect to the real case and a greater area which the material can be distributed within. An example of design and non design space are reported in the Figure 5.3. The blue volumes represent the design space and the red ones are the non-design space of the topological optimization.

5.3.3   Objective function and optimization constraints

In the formulation of optimization problems, some quantities can be used as objective function to be minimized (usually global quantities) and some others as constraints (usually local quantities): volume fraction, mass fraction, natural frequencies, stress and strains [70].
The minimization of objective functions is imposed to have a new optimized geometry and two main strategies have been tested in this work. First, the minimization of volume has been considered:

$$V(\rho_f) = \int_\Omega \rho_f \, d\Omega, \tag{5.1}$$

where ρ_f is the material density and Ω is the domain.
Secondly, the compliance minimization has been taken into account (see Eq. 5.2) and it is appeared as a very interesting and promising tool [78].

$$l(\boldsymbol{u}) = \int_\Omega \boldsymbol{f} \cdot \boldsymbol{u} \, d\Omega + \int_{\Gamma_T} \boldsymbol{t} \cdot \boldsymbol{u} \, ds, \tag{5.2}$$

where $\boldsymbol{f}$ are the body forces on the domain Ω and $\boldsymbol{t}$ are the external forces on the traction part of the boundary $\Gamma_T \subset \partial\Omega$.
The volume minimization turned out to be a critical approach, as it often generates convergence problems and the final geometries are quite irregular. Then, the compliance minimization has been chosen: through this method the optimized geometries results smoother and more regular. The convergence problems are reduced as well.
The compliance is the deformation energy of the structure and it can be considered as the reciprocal measure for the stiffness of the structure. It is defined for the whole structure, since the objective functions must be referred to a global parameter. The objective of the minimum compliance problem is to find the material density distribution that minimizes the structure deformation under the prescribed supports (boundary conditions) and loading conditions (rotational velocity).
The optimization constraints used in this work are on the maximum value of the stress, on the displacement and on the volume fraction. The volume fraction is defined as follow:

$$V_{fr} = \frac{V_{t,i} - V_{n,i}}{V_{d,i}} \tag{5.3}$$

where:

- V_{fr} is the volume fraction;

- $V_{t,i}$ represents the total volume at current iteration;

- $V_{n,i}$ is the initial non-design volume, that is the constant volume that remain unchanged after the topology optimization;

- $V_{d,i}$ represents the initial design volume.

This constraint on the maximum volume fraction is applied to reduce the design volume in particular areas where the solver tends to save too much material. On the other hand, a constraint on the minimum volume fraction has been set to guarantee the permanence of material, where the solver tends to eliminate all this part and generate an unphysical solution (non-connected geometries). The different constraints can be defined as follows:

$$
\begin{cases}
\sigma_r < \sigma_{max} \\
u_{min} < u_r < u_{max} \\
V_{fr,min} < V_{fr} < V_{fr,max}
\end{cases} . \tag{5.4}
$$

where:

- σ_{max} is the maximum values of stress in the optimized model;

- σ_r is the maximum allowable values of stress in the optimized model, equal or lower than the benchmark value, to be set in the optimization test;

- u_{max} is the maximum displacement for the optimized model, to be set during the optimization test;

- u_{min} is the minimum displacement for the optimized model;

- u_r is the maximum displacements allowable in the optimized model (this is the control parameter used to define the stiffness of the components;

- $V_{fr,max}$ is the maximum volume fraction for the optimized model, to reduce the material in particular areas;

- $V_{fr,mim}$ is the minimum volume fraction for the optimized model, to guarantee the material in particular areas;

- V_{fr} is the actual volume fraction of the topology optimization procedure.

5.3.4   Optimization algorithm

Topology optimization differs from the other structural and modal optimization techniques (shape and parametric), because it allows to change the topology of structures layout (e.g. by creating holes or cavity) [70]. Topology optimization is a mathematical technique that optimizes the material distribution for a structure with a given design space. This way a fictitious density of material is introduced.

Referring to a domain Ω it is possible to define the optimal design problem as the problem of finding the optimal choice of stiffness tensor $E_{ijkl}(x)$ which is a variable over the domain. Introducing the energy bilinear form (depending on the real displacement $\underline{u}$ and on the arbitrary virtual displacement $\underline{v}$):
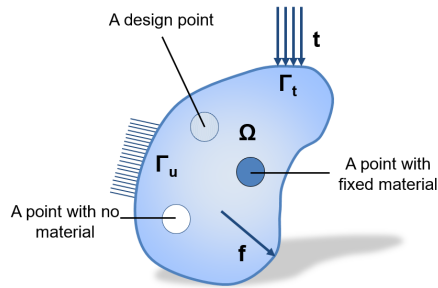
Figure 5.4: The generalized shape design problem of finding the optimal material

$$a(\boldsymbol{u}, \boldsymbol{v}) = \int_{\Omega} E_{ijkl}(\boldsymbol{x}) \epsilon_{ij} \epsilon_{kl}(\boldsymbol{v}) \, d\Omega \tag{5.5}$$

where $\epsilon_{ij}(\boldsymbol{u}) = \frac{1}{2} \left(\frac{\partial u_i}{\partial x_j} + \frac{\partial u_j}{\partial x_i} \right)$ and the load linear form:

$$l(\rho_f) = \int_{\Omega} \boldsymbol{f} \cdot \boldsymbol{v} \, d\Omega + \int_{\Gamma_T} \boldsymbol{t} \cdot \boldsymbol{u} \, ds, \tag{5.6}$$

the minimum compliance (maximum global stiffness) problem takes the form [70]:

$$\min_{\rho_f} l(\rho_f) \quad \text{s.t.} \quad a_E(\boldsymbol{u}, \boldsymbol{v}) = l(\boldsymbol{v}), \quad \forall \boldsymbol{v} \in U, \quad E \in E_{ad}. \tag{5.7}$$

U is the space of kinematically admissible displacement fields, $\boldsymbol{f}$ are the body forces (e.g. the weight of the system which has been neglected in this work due to its low value). E_{ad} represents the set of admissible stiffness tensors for design problem [70].

If the goal is to minimize the volume of the equation becomes:

$$V(\rho_f) = \int_\Omega \rho_f \ d\Omega, \tag{5.8}$$

and the minimum volume problem takes the following form:

$$\min_{\rho_f} V(\rho_f) \quad \text{s.t.} \quad a_E(\boldsymbol{u}, \boldsymbol{v}) = V(\boldsymbol{v}), \quad \forall \boldsymbol{v} \in U, \quad E \in E_{ad} \tag{5.9}$$

In this problem the physical size and the shape and connectivity of the structure are unknown.

Concerning the static loading condition, as anticipated before, body forces (e.g. the weight of the mechanism) have been neglected and there is thus only a static (boundary) loading condition due to the forces applied to the mechanism which model the interaction with the hand as follows:

$$\boldsymbol{t} = \begin{pmatrix} x \\ y \\ 0 \end{pmatrix}. \tag{5.10}$$

This problem has been solved using a tool of the engineering software *Altair HyperWorks*; this tool models and prepares the FEM analysis with a powerful interactive environment to analyze performance and display design. This software was used because it allows to perform very effectively complete modeling and optimization problem setup.

OptiStruct (Structural Analysis Solver) is a product of the engineering software *Altair HyperWorks*. Based on finite-element [79] and multibody dynamics techniques, Optistruct is an analysis solver for linear and non-linear structural problems. Light and innovative components designs could be developed, through the implemented optimization algorithms [80].

Optistruct solves topological optimization problems using the SIMP. Through this density method, a pseudo material density ρ_f is defined as the design variable. Under topology optimization, the material density ρ_f of each element varies continuously between 0 and 1, defining the element as being respectively either void or solid. Intermediate values of density represent fictitious material.

The SIMP method uses a power-law penalization for the relationship between stiffness and density, in order to set density toward 0 and 1 (void and solid) distribution [80]. The stiffness of the material is assumed to be linearly dependent on the density. In general, the optimal solution of problems involves large areas of intermediate densities in the structural domain. Techniques need to be introduced to penalize intermediate densities and to force the final design to be represented by densities of 0 or 1 for each element. The penalization technique used is the power law representation of elasticity properties, which can be expressed as follows [81]:

$$\tilde{K}(\rho_f) = \rho_f^p K \tag{5.11}$$

where:

- $\tilde{K}$ is the penalized stiffness matrix of a generic element used in FEM discretization;

- K represents the real stiffness matrix;

- p is the penalization factor ($p > 1$);

- ρ_f is the fictitious density.

A new topology optimization algorithm based on the LSM has been implemented in the recent versions of *Altair HyperWorks* to solve problems arising from the density method application and the pseudo density introduction [80]. In the level set method, the boundary of the design is represented as the isosurface (the zero level set) of a function defined on the finite element mesh. This function takes different values according to the different area (material region, boundary or region without material). The advantage of the level set model is to perform numerical computations involving curves and surfaces on a fixed Cartesian grid without having to parametrize these objects (Eulerian approach). Through the level set method it is easy to follow shapes that change topology. The domain is defined based on the value of the level set function:

$$\begin{cases} \phi(\boldsymbol{x}) > 0 : \boldsymbol{x} \in \Omega \\ \phi(\boldsymbol{x}) = 0 : \boldsymbol{x} \in \partial\Omega \\ \phi(\boldsymbol{x}) < 0 : \boldsymbol{x} \in D/\Omega \end{cases} \tag{5.12}$$

where:

- D is the design domain;

- Ω denotes the material region;

- $\partial\Omega$ represents the boundary of the material region Ω;

- D/Ω is the region with no material.

The dynamic motion of the boundary is governed by the level set equation:

$$\frac{\partial \phi}{\partial t} = V_n |\nabla \phi| \tag{5.13}$$

with:

- V_n stands for the normal velocity;

- $|\nabla \phi|$ represents the norm of the gradient of the level set function.

In other words, the material is removed following surfaces according to the level set method (see Figure 5.5): the red surface is the graph of the level set function ϕ determining the shapes (represented on the upper side of the figure), and the flat blue region represents the xy-plane. The boundary of the shapes are the zero level set of the function ϕ, while the shapes are the set of points in the plane for which ϕ is positive (interior of the shape) or zero (at the boundary).
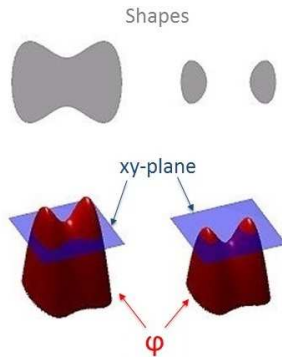

Figure 5.5: Level set method

5.3.5   Geometry reconstruction

After the optimization test, an iso surface of the new model can be created using *Ossmooth* [80]; this tool can be used to provide an iso-density surface based on the volumetric density from a topology optimization. The optimized model can be reimported in *Hypermesh* and the new geometry could be remeshed for a post-process reanalysis, to check the system performances. Finally, it is possible to render the whole component surfaces [82]. This is possible by exporting from the optimization results a Standard Tessellation Language (STL) file. This file format is supported by a wide range of software packages and it is used for computer-aided manufacturing and rapid prototyping. STL file describes the surface geometry of three-dimensional objects. The new models can be also imported in *SolidWorks* for the final rendering process.

5.4   Topology optimization results

In this section, the results on the topology optimization process are presented and discussed. Since the topology optimization-based design strategy headed to a rigid but lightweight system, the results assessment particularly focused on these two features comparing them to the non-optimized device ones.

The mechanism components are considered singularly and, for each one, the optimization variables chosen for the topology optimization are reported. Then, the goodness of the optimization outcome is evaluated in terms of maximum stress and displacement (both before and after the geometry reconstruction). Finally, a comparison between the mass of the parts before and after the optimization process is given.

Since the load program applied to the mechanism includes three forces (two of them acting on the same line of action), in this analysis the weighted deformation energy variable (Weighted Compliance) has been chosen as objective function. The solver thus provides a distribution that is such as to allow a minimum for all three load cases. Namely, minimizing the weighted compliance allows to consider the effect of all the three forces in the optimization process. In fact, being a linear problem, the solution deriving from the three separate cases can be added together to obtain a final distribution that ensures compliance with the imposed constraints. The weighted strain energy parameter then requires the definition of a value between 0 and 1 for the various load cases. Since none of the considered load cases represents a more important condition than the other, the unit value has been set for all loads.

5.4.1   Optimization model generation

Component B

The optimization analysis (whose optimization variable are reported in Tab. 5.4) has been carried out by imposing a limit on the constraint relative to the maximum permissible stress on the optimized component. With reference to the benchmark test, a maximum of 60 MPa has been set, which, compared to the yield strength of the material (170 MPa), yields a consistent safety factor of 3. In order to avoid unacceptable displacements, a constraint on the maximum allowable static displacement equal to 2.5 mm has been set. Larger displacements may in fact lead to the malfunctioning of the whole mechanism. In Fig. 5.6, the results of the optimization process are shown, while Tab. 5.5 reports the results in terms of stress and displacement with respect to the three different load cases.

The optimization algorithm suggests a hollow profile and this is in accordance with the constraints and loads imposed on the problem.

Responses	Constraints	Objective
Static Stress	$\leqslant$ 60 MPa	Min. W.Compliance
Static Displacement	$\leqslant$ 2.5 mm	
Volume Fraction	30% $\leqslant$ Volume $\leqslant$ 60%	
Weighted Compliance		

Table 5.4: Optimization variables chosen in component B topology optimization process.

	Stress [MPa]	Displacement [mm]
Vertical load case	50	0.34
Lateral right load case	44	2.23
Lateral left load case	44	2.23

Table 5.5: Component B optimization process results.
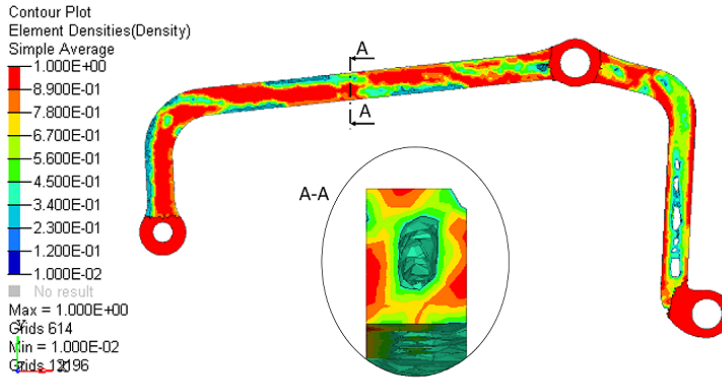
Figure 5.6: Component B optimized model.

Component C

Due to its quite lean section, this component results particularly stressed when the lateral loads act on it. As highlighted in the benchmark test, the maximum stress value was significantly higher than that one on component B. The safety factor has thus been reduced in the topology optimization (again, the optimization variable are reported in Tab. 5.6) to remain within the yield stress limits of the material. The stress when the lateral load is applied is higher with respect to the benchmark test (for this reason, no constraint on the volume fraction has been set) but it remains below the yield stress of the material. Figure 5.7 shows the optimized model, while in Tab. 5.7 the results are reported.

Responses	Constraints	Objective
Static Stress	$\leqslant$ 150 MPa	Min. W.Compliance
Static Displacement	$\leqslant$ 7.5 mm	
Weighted Compliance		

Table 5.6: Optimization variables chosen in component C topology optimization process.

Figure 5.7: Component C optimized model.

	Stress [MPa]	Displacement [mm]
Vertical load case	144	4.45
Lateral right load case	120	7.42
Lateral left load case	120	7.42

Table 5.7: Component C optimization process results.

Component D

Since the benchmark test has highlighted a quite low displacement value, the only one constraint set in this optimization procedure is on the static stress (Tab. 5.8). The optimized model is shown in Fig. 5.8. In Tab. 5.9 the results are reported.

Responses	Constraints	Objective
Static Stress	$\leqslant$ 150 MPa	Min. W.Compliance
Weighted Compliance		

Table 5.8: Optimization variables chosen in component D topology optimization process.
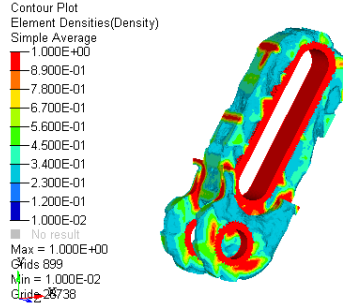
Figure 5.8: Component D optimized model.

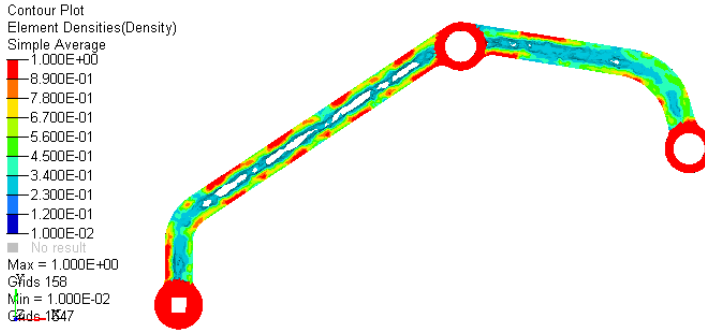|	Stress [MPa]	Displacement [mm]
Vertical load case	12	0.008
Lateral right load case	3	0.003
Lateral left load case	3	0.003

Table 5.9: Component D optimization process results.

5.4.2   Optimized device assessment

The geometries of the optimized models of each component, directly obtained by the solver, are dependent on the mesh and, thus, do not have a homogeneous surface as visible in Fig. 5.6, Fig. 5.7 and Fig. 5.8. The next phase is the reconstruction process of the geometries which will allow for the actual manufacturing of the components.

As reported in Section 5.3.5, after having checked the performances of the topology optimization results by using Ossmoth, the STL files of the exoskeleton parts have been imported in SolidWorks and the topology optimization outputs geometries have been made smoother (basing on the original surfaces generated by the solver). Finally, to let the kinematic assembly of the whole system free to move, some other changes to the geometries have been necessary allowing for the correct movement of the parts.

The results are presented in Fig. 5.9, where a comparison between original and optimized components is shown. At the bottom of the figure, the optimized process results of the back frame of the exoskeleton are reported. This part re-design is discussed in Appendix 6.

Figure 5.9: Reconstruction process results of the hand exoskeleton mechanism components. Component B and the back frame are represented in section view to highlight the internal holes.

		Stress [MPa]	Displacement [mm]
	B - single component	53	1.3
	B - mechanism	48	0.8
		Stress [MPa]	Displacement [mm]
	C - single component	135	5.6
	C - mechanism	113	0.7
		Stress [MPa]	Displacement [mm]
	D - single component	27	0.007
	D - mechanism	$1 \cdot 10^{-6}$	0.9

Table 5.10: Comparison between stress and displacement on the single components and the same component within the mechanism structure.

Once the optimized components have been modified, new static analyses have been carried out to verify the correct functioning of the parts by evaluating the stress responses (Fig. 5.11) and displacements (Fig. 5.10). This phase is mandatory not only to assess the optimization process, but also to check that the new components can bear the load conditions once manufactured.

The static analyses were carried out on the basis of the choices (in terms of applied loads and constraints) previously described in Section 5.3.1. The results related to stress and displacements are reported in Tab. 5.10 for each component. It is worth noting that, once the parts are assembled together, the system results more stable and rigid because part of the load acts on the joints. That confirms that the choice of analyzing each component separately from the other has been a conservative choice in the optimization process. What reported above is highlighted in Tab. 5.10 comparing stress and displacement on each component in both the described cases. In addition, Fig. 5.10 and Fig. 5.11
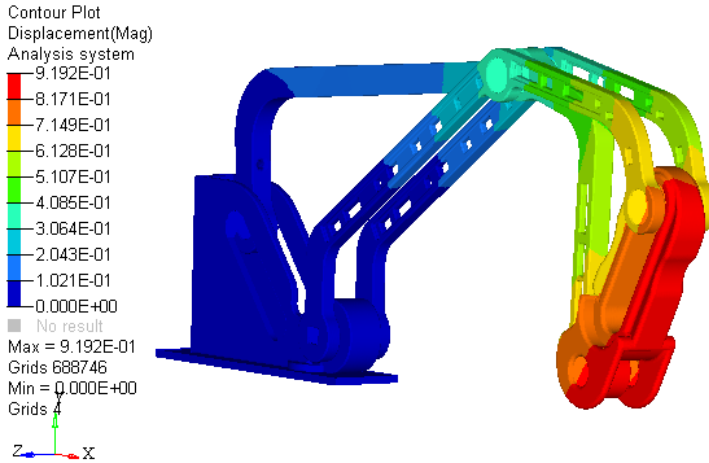
Figure 5.10: Displacement [mm] on the whole mechanism structure when 20 N (vertical) and 2 N (lateral) are applied on the end effector.

shows stress and displacement on the whole mechanism[3]. In this case the most critical condition, in terms of stress and displacement, resulted the configuration at $\alpha_2 = 0$. In conclusion, in Tab. 5.11 the comparison between the mass of the original components and the one of the optimized parts is reported. Even the reduction in mass results more than 20% for the whole index mechanism, it corresponds to less than 3 g. Considering this results, the optimization process may be evaluate as worthless in this application. However, the idea behind the presented topology optimization-based design process is not to save material (and weight) with respect to an already existing component (in this case the mass saving would be mandatory), but it is to design a device as light as possible in order not to hinder the patient's movements and not strain him in everyday life.

---

[3]A linear quasi-static analysis has been carried out on the whole system applying the loads as reported in the dedicated section. The constraints of the mechanism have been set by modeling the contact between each part.
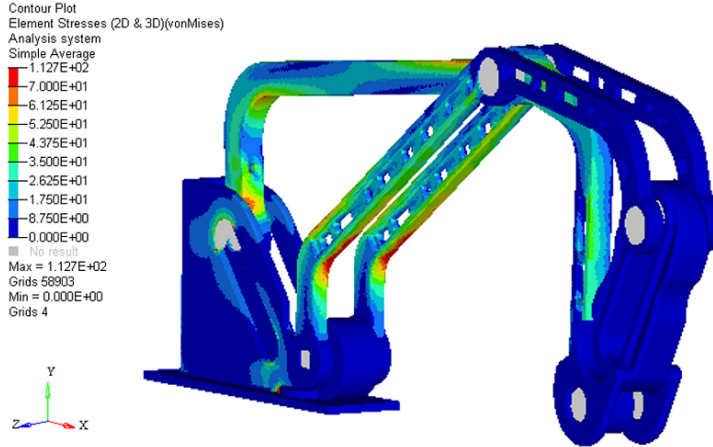
Figure 5.11: Stress [MPa] on the whole mechanism structure when 20 N (vertical) and 2 N (lateral) are applied on the end effector.

5.5   Design for manufacturing

Once the topology optimization process has been accomplished, the design for manufacturing phase of the whole exoskeleton has been carried out.

Firstly, the actuation system has been defined and commercial components has been identified, basing on the required performance in terms of output forces (20 N is the target force to be exerted by the finger) and room space (since the actuation system is placed on the hand, small dimensions and low weight are demanded).

Due to the particular and specific shape of the components of the exoskeleton (originated by the topology optimization process), Selective Laser Melting (SLM) additive technique has been adopted to manufacture such parts. In addition, Cl31Al aluminum alloy has been identified as a good trade-off between lightness and rigidity. However, this choice entails the adoption of other materials allowing for the reduction of the friction between moving parts.

In the remainders of this section, the design for manufacturing procedure which has led to the first aluminum hand exoskeleton prototype will be reported by analyzing three main steps.

- Design of the actuation system and commercial components identification;

	Original component	Optimized component	
	mass[g]	mass[g]	reduction%
A	4.46	3.81	14.6
B	2.33	1.78	23.6
C	4.22	3.23	23.5
Index mechanism	13.34	10.6	20.5
Back frame	109.50	73.88	32.5

Table 5.11: Comparison between the mass of the original and the optimized components.

- design of the back frame of the hand exoskeleton;

- design of joints and coupling systems.

5.5.1 Actuation system design

In order to maintain the whole system as compact as possible, two commercial electric servomotors have been placed directly on the back of the hand. In particular, they have been fixed side by side on component A (as it will be explained in details in the following), which serves as rigid connection of the mechanical device with the back of the hand, and a transmission system, exploiting gears and belts, directly actuates the fingers joints 1 (refer to Fig. 2.1 for joints and components nomenclature).

The overall conceived scheme is shown in Figure 5.12. The torque generated by motor M_1 is transmitted directly to joint 1 of the index finger mechanism through a toothed belt. Motor M_2, through the two gears G_1 and G_2, transmits the torque to another transmission shaft (schematically shown in green in Figure 5.12), which three toothed pulleys indicated with P_{lit1}, P_{rin1} and P_{mid1} are fixed on. Each pulley act, respectively on little, ring and middle fingers. The belt transmission allows each mechanism, even for an angle of a few degrees, to freely rotate around its vertical axis and thus support the movement of abadduction of the hand: a passive DOF is required to align the flexo/extension plane of action of the mechanism with the flexo/extension plane of each finger. The kinematic scheme of the aforementioned passive DOF is reported in Fig. 4.7, while its mechanical embodiment will be described in Sec. 5.5.2.

The exploitation of two motors for the whole system, rather than one per finger,
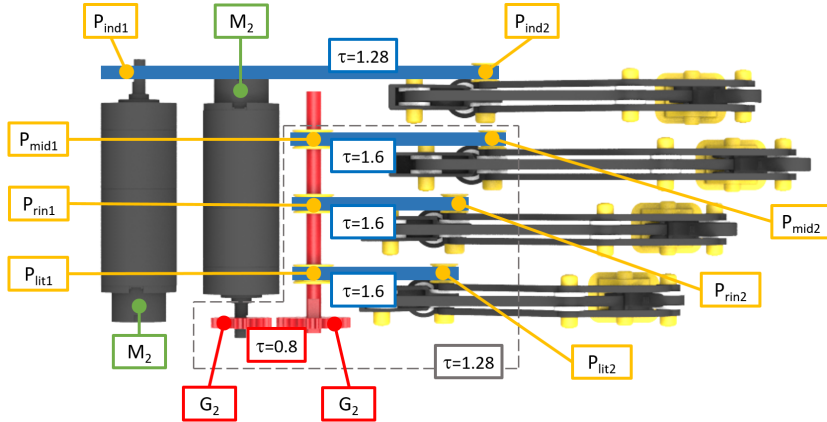
Figure 5.12: Overall actuation system scheme.

is justified by the fact that the index and the other three fingers (middle, ring and little finger) are separately actuated. This allowed to respect the constraint of low weight and encumbrances while not losing the effectiveness of the device. A study of the usual grasps carried out by the hand during the most common ADLs highlights hence that the independent use of the index finger provides a measurable advantage when precision grasps are involved, but basic prehensions are guaranteed (in terms of functionality) even without specific actuation for each individual finger [83].

Since the aim of the presented study is the design of a first prototype of hand exoskeleton particularly focusing on its finger kinematic structures and capability of withstanding the external forces generated by the interaction with the user, no differential gear has been included in the mechanical design. After all, the exploitation of a differential mechanism would allow for the adaptation of more objects without adding other motors. Its addition is hence considered in a new version of the device.

Actuators

The choice of motors starts by assessing the mode of operation of the actuation system. To perform ADLs, hand opening and closing at 0.5 Hz is targeted. In addition a whole opening and closing gesture corresponds to a 90° ROM of the fingers mechanisms, leading to an output speed of 1.57 rad/s . Exploiting,

finally, Eq. 2.52 in Sec. 2.2, it is possible to determine the trend of τ_2 with respect to the state variable α_2. By varying α_2 angle spanning the whole ROM (Fig. 5.13), the maximum output torque required at joint 1 has been identified as 0.88 Nm.
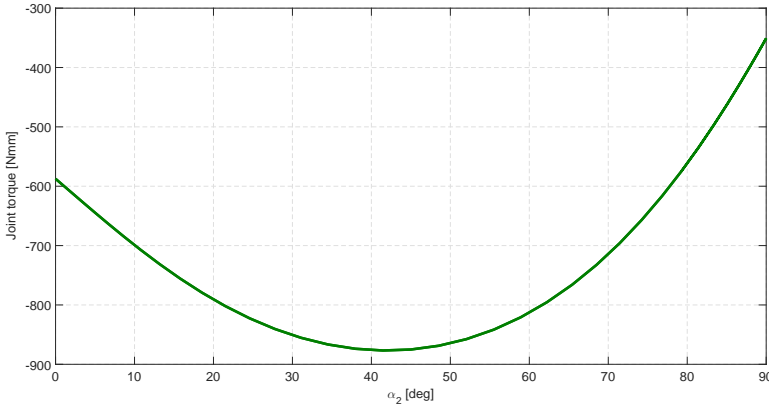
Figure 5.13: Hand exoskeleton actuation requests: torque on joint 1 to exert 20 N on the finger.

Basing on the aforementioned considerations, the maximum output power results 2.25 W.

An in-depth market analysis has then been carried out to find a solution matching all the specifications reported above. Other constraints were added to the choice also considering dimensional limits: it was estimated that each actuator, as a whole, did not exceed 25 mm in diameter and 80 mm in length to allow for positioning directly on the hand back. The identified solution is represented by the system consisting of 2224-018-SR DC motor, 22EKV-series planetary gear and IEH2-4096 encoder by MICROMO[4]. This solution results in a 22 mm diameter and 63.7 mm long actuation system (considering one actuator), which is compliant with the defined specifications.

---

[4]https://www.micromo.com/

Power transmission system

Referring to the specifically designed transmission (Fig. 5.12), since M_1 actuates the index finger, while M_2 is in charge of managing all the other three long fingers together, the transmission itself has been thought to provide the index finger with the torque that allows for 20 N force at the intermediate phalanx (1.44 Nm) and the other fingers equally share the same torque.

The idea behind this solution designates the index finger as a crucial tool for manipulation (according to the fact that one motor is entrusted with actuating it), other fingers only control the grasp.

The resulted gear ratios are shown in Fig. 5.12.

Gears   The gears definition can be conducted once the gear ratio is defined. Considering the set 0.8 gear ratio and an axis distance compliant with the overall dimension of the back frame (a suitable value has been evaluated as 18 mm), the radii (R_1 and R_2) of the two gears can be defined as follows:

$$\begin{cases} R_1 + R_2 = i \\ R_1/R_2 = \tau \end{cases} \tag{5.14}$$

R_1 and R_2 results, respectively, 8 mm and 10 mm.

The number of teeth of each gear is then defined considering the interference between the profiles. Assuming the use of gears having a 20° pressure angle, the interference between them, which results in a continuous and smooth coupling, is avoid if the following condition is followed.

$$z_1 \geqslant \frac{2\tau}{\sqrt{1 + \tau(2 + \tau)\sin^2(\alpha)} - 1} \geqslant 18. \tag{5.15}$$

This equation is applied to the smaller gear.

Setting $z_1 = 17$, the modulus has then been defined

$$m = \frac{2R_1}{z_1} = 0.78mm \Rightarrow 0.8mm \tag{5.16}$$

and the numbers of teeth are found

$$z_1 = \frac{2R_1}{m} = 20 \tag{5.17}$$

$$z_2 = \frac{2R_2}{m} = 25 \tag{5.18}$$

Belt A belt-based solution has been adopted for the power transmission on the index side and for the three motion transmissions from the shaft to the joints of the other three fingers. Such a transmission is guaranteed by synchronous belts that mesh toothed pulleys. A commercial solution of the components has been identified by Poggi-Trasmissioni Meccaniche S.p.A.[5]: synchronous belts with a pitch of 2.5 mm. Table 5.12 shows the external diameters of the pulleys and the gear ratios of the four transmissions.

	D_{e1} [mm]	D_{e2} [mm]
Index	7	9
Middle	7	11.5
Ring	7	11.5
Small	7	11.5

Table 5.12: Pulleys diameters.

5.5.2 Back frame design

In this section, the design phase of the frame of the exoskeleton which serves as interface between the back of the hand and the device will be described.

The frontal side of the component has to house the finger mechanisms. In particular, since the abduction and the adduction of each finger must be leave free, a passive joint letting this movement has been designed.

At the back, two motors housing has been placed, while the transmission system is located in between actuators flanges and finger mechanisms.

Figure 5.14 shows the designed solution of the back frame. It is worth noting that, in accordance with FEM analysis, in order to keep the diameter of the "ab/adduction joint" shaft as big as possible without enlarging the dimension of the frontal part of the back frame, no bushings are included for the coupling. They are instead replaced by low friction sheets, which has allowed to save space.

The coupling between the hand and the device is guaranteed by the use of two Velcro loop fasteners. Two holes has been obtained running athwart along

---

[5]http://www.poggispa.com/
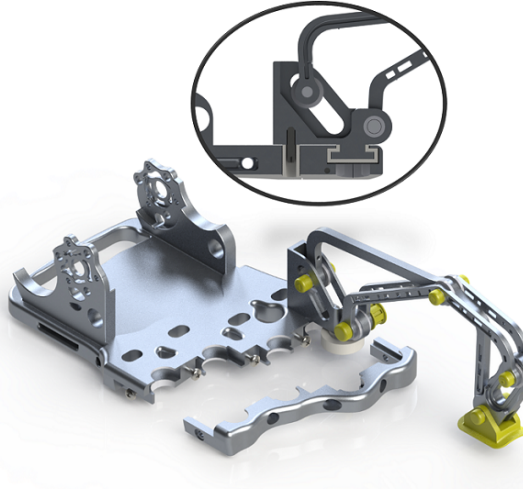
Figure 5.14: Design solution of the back frame.

the back frame. This solution represents an effective mechanical coupling but it is not ensure a comfortable wearing. An improvement of the whole system ergonomics represent an important future development of this research activity.

5.5.3   Joints couplings solutions

The manufacturing of the aluminum alloy prototype, compared to the previous ABS version, allows for a significant increase in the mechanical performances but has generated new design problems including the need of avoiding direct contact among moving parts.

For the joints design, two general guidelines were followed: the metal parts having relative movements each other must not be in contact and the components must be assembled and disassembled easily.

Even if fingers mechanisms present different dimensions depending on the finger they are coupled to, the adopted components for each joint are the same for all the four long fingers in order to exploit the same commercial components simplifying both the assembly process and the realization of those components not available on the market.

The choice of Teflon bushing, avoiding bronze ones, is due to the fact that the Cl31Al alloy does not allow for the second solution of coupling.

The axial locking of the pins have been obtained by ABS caps. In Figure 5.15 the technical drawing of the prototype is visible with all the design choices previously described. Figure 5.16 represents, finally, the render of the whole designed robotic system.
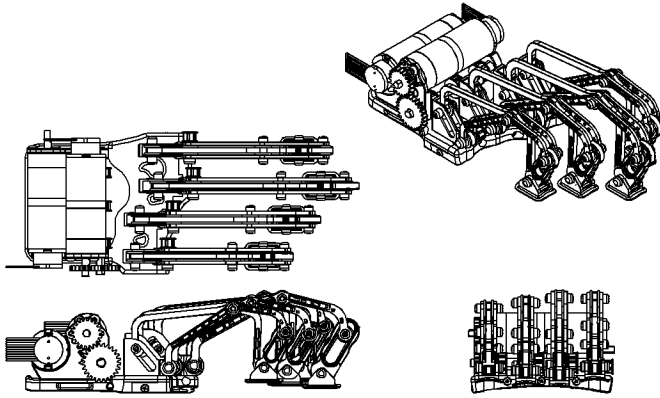
Figure 5.15: Hand exoskeleton design.
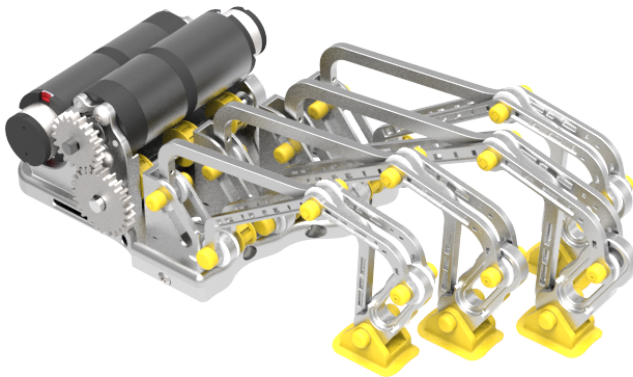
Figure 5.16: Hand exoskeleton design render.

5.6   Proof of concept

A real prototype of the designed hand exoskeleton has then been manufactured. Due to the specific shape of the topologically optimized components, an additive manufacturing process has been required. In particular, the M2 Cusing (Metal Laser Melting System) by Concept Laser[6], available at Certema Multidisciplinary Technological Laboratory[7], has been exploited for the purpose. Thanks to the collaboration between the Department of Industrial Engineering of the University of Florence and Certema Laboratory, embodied by the Additive Manufacturing Laboratory (AMLab) - a joint project between Certema and the University of Florence to promote and carry out advanced studies on the metal additive manufacturing aiming at creating knowledge and exploring the limits of the current technology -, the SLM technique has been used leading to the production of the aluminum alloy structural components of the hand exoskeleton system.

Since the focus of the this phase of the research activity was the design of a system, starting from the specific loading program the device was subject to, as lightweight as possible but rigid enough to withstand a prolonged use during rehabilitation tasks or ADLs performing, the proof of concept mainly focused on the production of the structural components. In order to validate the topology optimization-based strategy as a suitable design procedure to develop wearable systems, the optimized components needed to be manufactured and the overall mechanisms must to be coupled to verify their actual kinematic follows the modeled one. Fig. 5.17 shows the aluminum hand exoskeleton prototype worn by a user. Yellow and blue components are made of ABS (blue parts represent the actuators mock-up), while a Velcro system fastens the exoskeleton to the user's hand and fingers.

The manufactured components successfully comply with the topologically optimized models both in terms of weight and geometrical accuracy representing a solid basis for the future integration of sensors and actuation systems.

---

[6]urlhttps://www.concept-laser.de/en/products/machines.html
[7]http://www.certema.it/EN/index.html
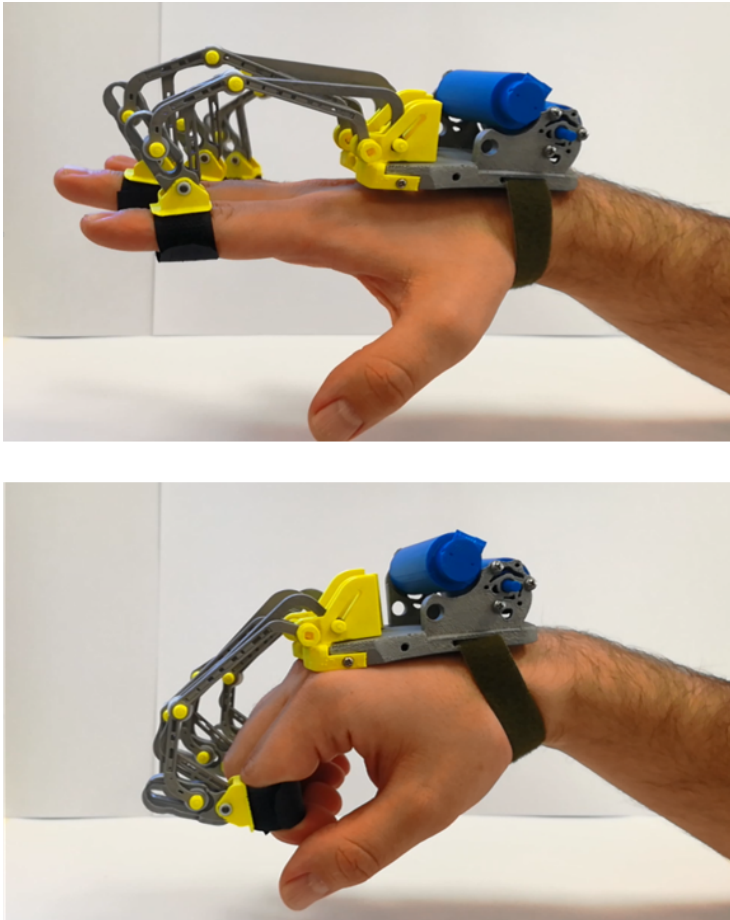
Figure 5.17: Hand exoskeleton prototype.

Chapter 6

Conclusion

This work collects the results of the research activity on wearable robotics carried out at the Mechatronics and Dynamic Modeling Laboratory of the Department of Industrial Engineering of the University of Florence during the years 2015-2018. The activity focused on the study of design strategies for hand exoskeletons, starting from the analysis of state-of-the-art solutions and leading to the development of new robotic devices.

Hand exoskeletons mechanical design constituted the main subject of the research, motivated by the issue that people who have lost or injured hand skills are deeply compromised in the possibility of an independent and healthy life with a sensitive reduction in the quality of their lives themselves. Since robotic devices, such as hand exoskeletons, may represent an effective solution for the patient affected by hand opening disabilities, or other mobility impairments, the focus was particularly given to the development of a robotic solution provider of an aid during prolonged and high-intensity rehabilitation treatments. Such systems also contribute to reduce costs and burden for the therapists, as long as being an effective aid in the execution of ADLs.

The overall research activity aimed not only to present the design of the hand exoskeletons developed by the University of Florence, but also, and actually mainly, to propose new user-centered and patient-based strategies which can be adopted in the production of wearable systems. Both the optimization-based scaling strategy (which, starting from the users' own gestures, leads to a tailor-made device) and the exploited topology optimization technique (which guarantees the design of a lightweight but rigid overall system) center the end-user on the design process and the proposed wearable systems (i.e. the ABS and aluminum alloy hand exoskeletons) are fully designed around him. In the first

part of the thesis, the hand kinematics plays the main role for the design of a tool as much wearable as possible, which guarantees a comfortable feeling even during the prolonged use. Achieving the aforementioned feature arose particularly hard when the constraints of the single DOF had to be maintained. The proposed solution resulted in a compact (due the 1 DOF per finger, cable-driven, single-motor system) device capable of precisely replicating the hand gestures. In the second part, the attention moved to the structural capabilities of the device. In this framework, with the surprising growth rate of AM technologies, which overcome the constraints of traditional manufacturing techniques, topological optimization has become one of the most powerful design tools. In fact, it allowed to achieve enhanced topological configurations capable, for instance, as in this case, to reduce mass while preserving product function and structural behavior. This phase of the research aims to demonstrate the effectiveness of topological optimization approaches applied to the design of patient-specific devices. The goal is minimizing the overall device mass assuring proper stiffness and strength, in order to increase device portability and obtain a more comfortable device when worn.

The satisfying results obtained highlight the goodness of the derived solutions, which may constitute a suitable alternative to existing hand exoskeletons. In addition, as reported above, the application of optimization procedures has been proved to be an important and interesting tool in the development of wearable devices. Nonetheless, there is still room for improvement: for instance, clinical trials exploiting the device presented in Section 4.13 may allow for the assessment of the impact the hand exoskeleton would have during real rehabilitation sessions. Also the aluminum alloy system, whose structural features have been discussed in Chapter 5, opens up the possibility for further improvements. A testing phase, employing a real actuation system, represents the first opened up point, which could lead to the necessity of improving the mechanical architecture of the whole exoskeleton in order to increase its usability and efficacy. The last, but not least, important issue which is worth being deepened in the near future is the assessment of the pose of the hand depending on the task it is required to accomplish. As reported in [84], the control of hand posture involves a few postural synergies leading to reduce the number of degrees measured by the hands anatomy and independently on the grip taxonomies. In this sense, considering the synergies occurred in some specific gestures [85] in the motion analysis assessment (Chapter 3) would allow the exoskeleton to guide the fingers with more effectiveness.

All these issues, whose resolution constitutes a natural continuation of the research activity carried out thus far, will be subjected to further investigation.

Appendix A

Parametric hand kinematic model

In this section, the hand gestures assessment discussed in [1] will be reported and described.

This study has been exploited in the implementation of a hand kinematic model which, basing on the exoskeleton users' hands anthropometry, leads to the generation of the long fingers trajectories that feed the optimization-based scaling procedure reported in Chapter 3. Even if this model does not represent one of the main objectives of the research activity proposed in this thesis, it embodies an useful tool to adapt the procedure presented in Chapter 3 when the studied subjects, due to specific pathologies, cannot realize the motion required to synthesize exoskeleton parameters.

With reference to the human hand, the model describes the analytic relationship between the angles joints (i.e the finger configuration) and the fingertip position. The fingers are discretely represented as chains of rigid bodies connected by revolute joints: the links embody the finger phalanges (modeled as cylinders) and the joints are the anatomic joints which provide the movement. This kinematic representation is the same adopted in Section 3.2.

In the presented model, hand links dimensions are parameterized to only hand length and width, with the relationships provided by [1]. As represented in Fig. 1, length l_h is defined as the distance between the medium fingertip and the wrist, while width b_h is the segment between the index and the small finger MCP joint extremities (namely, the maximum palm breadth). The relationships between the two parameters of the model (hand length and width) and the complete set of links necessary for the hand representation is specified in Tab. 1,
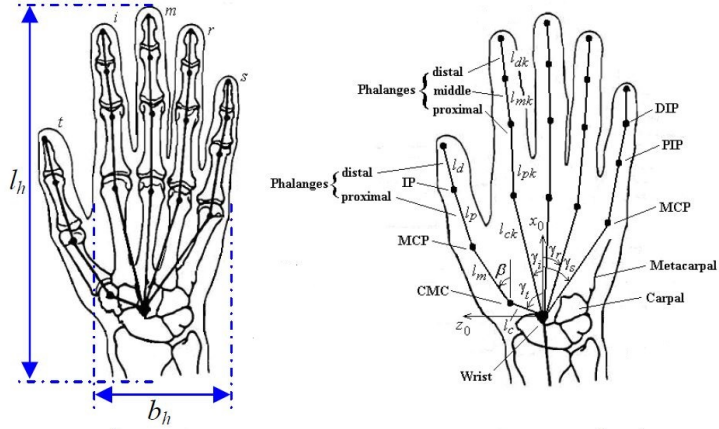
Figure 1: Hand parameterization (a) and anatomical terminology (b). Figure courtesy of [1].

where the rows identify the fingers and the columns distinguish the phalanges lengths. Where l_{ck}, l_{pk}, l_{mk} and l_{dk} represent respectively the metacarpus,

	l_c	l_p	l_m	l_d
Thumb	$0.5 \cdot \left(0.118 l_h + \sqrt{(0.073 l_h)^2 + (0.196 b_h)^2} \right)$	$0.196 l_h$	$0.251 l_h$	$0.158 l_h$
Index	$0.5 \cdot \left(0.463 l_h + \sqrt{(0.447 l_h)^2 + (0.251 b_h)^2} \right)$	$0.245 l_h$	$0.143 l_h$	$0.097 l_h$
Medium	$0.446 l_h$	$0.266 l_h$	$0.170 l_h$	$0.108 l_h$
Ring	$0.5 \cdot \left(0.421 l_h + \sqrt{(0.409 l_h)^2 + (0.206 b_h)^2} \right)$	$0.242 l_h$	$0.165 l_h$	$0.107 l_h$
Small	$0.5 \cdot \left(0.414 l_h + \sqrt{(0.368 l_h)^2 + (0.402 b_h)^2} \right)$	$0.204 l_h$	$0.117 l_h$	$0.093 l_h$

Table 1: Evaluation of the fingers segments according to [1].

proximal, middle and distal phalanges lengths of the k-th finger. Adopting this solution, being the number of measurements required limited to two, the capture and modeling of human hands becomes a simple and rapid procedure.
Considering the hand structural complexity, it is common practice in the development of kinematic models to simplify the representation by ignoring those

DOF which are scarcely interesting for the specific purpose. The presented kinematic model is based on the finger movement assumptions introduced in [1]; these hypotheses are different for the thumb and the long fingers, due to the fact that they present different skeletal structures and consequently show different kinds of motion. The thumb exhibits the most complex kinematic structure among the fingers. It presents a total of 6 DOF: a flexion-extension at the Proximal Interphalangeal (IP) joint, a flexion-extension and an ab-adduction at the MCP and CarpoMetaCarpal (CMC) joints, and a rotation around the proximal phalanx axis. In the model, the thumb carpal segment is assumed to be fixed and the metacarpal segment lies on a plane that is 45° oriented with respect to the palm of the hand.

Concerning the long fingers, they present 4 DOF each: one flexion-extension movement per joint, and one ab-adduction at MCP joints. In the model though, the ab-adduction at MCP joints has been neglected for ease, as it appears to be very narrow and therefore negligible for the current representation. In addition, this movement is let free by the hand exoskeleton. As a consequence of the previous assumptions, each long finger behaves as a three-link planar arm manipulator, presenting three revolute joints with parallel axes, and moving on the plane perpendicular to the aforementioned axes where the finger longitudinal dimension lies. The first step in the model implementation is the specification of a coordinates reference system; the reference system center is set in the wrist and the axes are oriented so that the XY plane aligns to the sagittal plane, the XZ is parallel to the frontal plane and the YZ completes the set laying on the transverse plane. Fig. 3.5 shows the reference frames of the described hand kinematic models.

Thumb and index trajectories

The procedure followed to obtain the complete fingers movements uses the D-H convention [9] to identify the joints position and orientation with respect to the wrist coordinate system (Fig. 2).

The relative position and orientation of two arbitrarily chosen links (i.e the fingers phalanges in this case) are gathered through the multiplication of the single matrices, as follows:

$$^{i-1}p = H_i^{i-1}\ {}^i p, \tag{1}$$

where $^i p$ is the position vector expressed in the i-th coordinate system, ^{i-1}p is the position vector expressed in the $(i-1)$-th coordinate system and H_i^{i-1} is the homogenous transformation matrix from the i-th to $(i-1)$-th coordinate
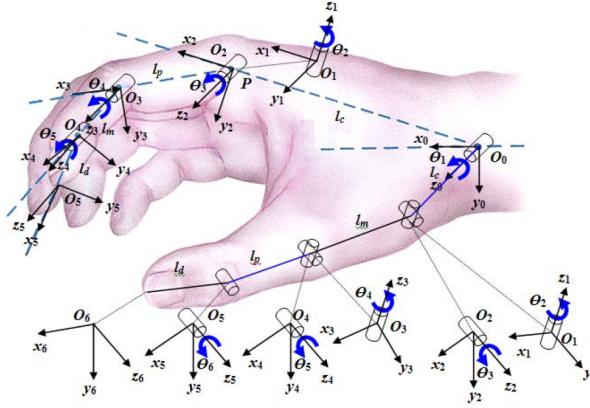
Figure 2: Denavit-Hartenberg convention for index and thumb. Figure courtesy of [1].

system, namely

$$H_i^{i-1}(\theta_i) = \begin{bmatrix} \cos(\theta_i) & -\sin(\theta_i)\cos(\alpha_i) & \sin(\theta_i)\sin(\alpha_i) & a_i\cos(\theta_i) \\ \sin(\theta_i) & \cos(\theta_i)\sin(\alpha_i) & -\cos(\theta_i)\sin(\alpha_i) & a_i\sin(\theta_i) \\ 0 & \sin(\alpha_i) & \cos(\alpha_i) & d_i \\ 0 & 0 & 0 & 1 \end{bmatrix}. \quad (2)$$

In addition, referring to the notation exploited in Fig. 3.5, a_i is the length of the i-th phalanx, d_i is the distance between O_i and O_{i-1} along z_{i-1} axis, α_i is the angle between z_{i-1} and z_i axes about x_i axis(to be taken positive when rotation is made counter-clockwise), θ_i is the flexion-extension angle of the i-th joint. As a consequence, the fingertip position can be obtained through the pre-multiplication of the successive joints matrices (each one relative to one link):

$$^0\boldsymbol{p} = H_1^0 \cdot H_2^1 \cdot \cdots H_{n-1}^n \cdot {}^{\boldsymbol{n-1}}\boldsymbol{p}. \quad (3)$$

In the proposed model, the D-H parameters are distinct for the thumb and the long fingers, due to the differences in their modeling. Tab. 2 and Tab. 3 reports these values. It is worth noticing that, being the number of generalized coordinates equal to the number of the finger DOF, the index and the thumb present respectively 3 and 2 variables. In Tab. 2 and Tab. 3, k is index for fingers (k = i, m, r, s, t where i = index finger, m = middle finger, r = ring finger, s = small finger and t = thumb), q_i is the generalized coordinate, θ_{ik} is

Joint	θ_{ik}	α_{ik}	a_{ik}	d_{ik}
1	0°	-90°	$l_{ck} \cdot \cos(\theta_k)$	$l_{ck} \cdot \sin(\theta_k)$
2	0°	90°	0	0
3	q_1	0°	l_{pk}	0
4	q_2	0°	l_{mk}	0
5	q_3	0°	l_{dk}	0

Table 2: D-H parameters for the long fingers.

Joint	θ_{ik}	α_{ik}	a_{ik}	d_{ik}
1	35°	-135°	$l_{ct} \cdot \cos(\gamma_t)$	$l_{0t} \cdot \sin(\gamma_t)$
2	-19°	90°	0	0
3	8°	90°	l_{mt}	0
4	0°	-90°	0	0
5	q_1	0	l_{pt}	0
6	q_2	0	l_{dt}	0

Table 3: D-H parameters for the thumb.

the joint angle of finger k , γ_k is the angle of finger k at the root segment with respect to axis x_0.
The fingers trajectories are then obtained by linearly varying the generalized coordinates from the extension to the complete closure configurations. The values used to identify the two extreme positions are collected in [1] and reported in Tab. 4 and Tab. 5. The results obtained with this technique (in terms

	Maximum flexion	Maximum extension
q_1	90°	0°
q_2	100°	0°
q_3	60°	0°

Table 4: D-H parameters for the long fingers.

of generated trajectories) are processed in MATLAB environment and shown in Fig. 3. Rest fingers are reported in red, while the blue lines identify the moving segment. The circles represent the finger joints, the segments embody the hand bones. Fig. 1, on the left, reports the thumb trajectory; this finger movement lies on a plane 45 ° orientated to the hand palm while, according

	Maximum flexion	Maximum extension
q_1	$60°$	$0°$
q_2	$110°$	$0°$

Table 5: D-H parameters for the thumb.
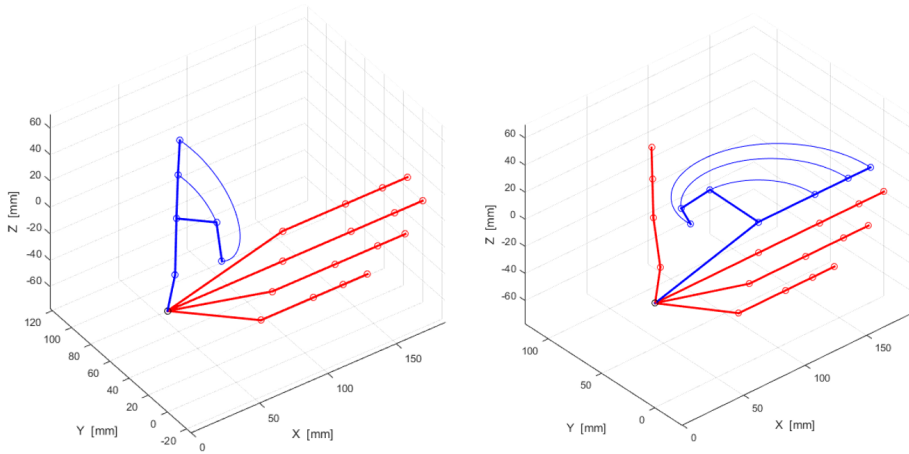
Figure 3: Thumb (on the left) and index (on the right) trajectories.

to the model assumptions, the carpal and metacarpal segments are fixed. The index movement lies, instead, on a plane perpendicular to the hand palm and parallel to the chosen XY plane.

Appendix B

Back frame topology optimization

Another important part of the hand exoskeleton that requires to be maintained as rigid and lightweight as possible is the part which connects the device with the back of the hand.

On one side, this component houses motors seats, transmission elements and the connection joints with the finger mechanisms. Thus, it must withstand all the stress coming from the actuation system and from the interaction with the fingers and should not warp in order to guarantee the kinematic mode of operation of the whole motion architecture directly connected to the user's hand. On the other side, since the actuation system housing is placed on the back of the hand, it should be a quite lightweight component which does not tire the user even if the exoskeleton is worn for a relative long time.

The topology optimization-based design strategy presented in Chapter 5 has hence been employed also in this case to obtain a resistant part with a low weight.

Again, the steps needed to be followed to implement the topology optimization process are the same discussed in Section 5.2. They are reported hereinafter for convenience.

- Definition of test case including physical and geometric features, boundary conditions and external loads.

- Static analysis on the standard non optimized model as benchmark tests.

- Definition of design space (area affected by the topology optimization).

- Definition of objective function and optimization constraints for the static characteristics.
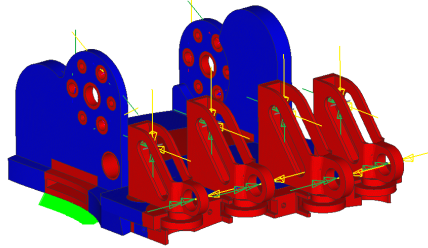
Figure 4: Back frame FEM model.

- Topology optimization.

- Surface rendering, to smooth surfaces after optimization process.

- Comparison with standard configuration in terms of obtained results as weight and stress.

All these steps are reported in the following and the whole procedure leading to the finel version of the back frame of the device (Fig. 6) is described.

The definition of loads, constraints and geometries of the design space come after the design choices which are described in Section 5.5. In particular, two loads configurations simulating the forces discharged on this component during opening and closing phases (of the finger mechanisms) are applied and studied. The actions generated by the opening phase are reported in green in Fig. 4 while those ones highlighted in orange represents the reaction forces (and torques) due to the closing gesture. For the application of the loads, components A of the four fingers mechanisms were inserted in the model in order to model the distribution of the forces to the frontal plate of the back frame. The load configuration on this components is hence known (please refer to 5.3.1) exploiting the procedure discussed in Section 2.3.

In particular, the load cases applied to the back frame of the hand exoskeleton results the following.

- *Loads on the frontal side:* referring to Fig. 4, the reaction forces coming from the fingers mechanisms have been modeled as force applied on joints 1 and 3 (referring to the kinematic architecture shown in Fig. 2.1) and torques acting on joints 1. In Tab. 6 the values of the forces acting on joints 1 and 3 of all the four fingers mechanisms are reported, while in Tab 7 torques applied to joints 1 are given.

Forces on joints 1	[N]	Forces on joints 3	[N]
$^{A}R_{1x,ind}$	2.64	$^{A}R_{3x,ind}$	4.79
$^{A}R_{1y,ind}$	36.46	$^{A}R_{3y,ind}$	15.87
$^{A}R_{1x,mid}$	2.92	$^{A}R_{3x,mid}$	5.31
$^{A}R_{1y,mid}$	40.40	$^{A}R_{3y,mid}$	17.58
$^{A}R_{1x,ring}$	2.64	$^{A}R_{3x,ring}$	4.79
$^{A}R_{1y,ring}$	36.46	$^{A}R_{3y,ring}$	15.87
$^{A}R_{1x,small}$	1.76	$^{A}R_{3x,small}$	3.20
$^{A}R_{1y,small}$	24.35	$^{A}R_{3y,small}$	10.60

Table 6: x- and y-components of the forces acting on joints 1 and 3 on component A. Such forces are expressed with respect to the body coordinate system of the hand exoskeleton back frame.

Torques on joints 1	[Nmm]
$M_{a,ind}$	876.7
$M_{a,mid}$	971.4
$M_{a,ring}$	876.7
$M_{a,small}$	585.6

Table 7: Maximum torques applied to joints 1.

- *Loads on the back side:* they represents the reactions that the actuation system exerts on their support flanges and they are reported in Tab. 8. This interaction has been modeled by decomposing the torques into three components (forces) applied in the seats of the fixing screws of the motor itself to reproduce the mechanical contact of these components.

The finite element model of the back frame has then been constrained, on the lower face of the plate, rigidly fixing all the elements around the hole for the elastic band that connects the object to the hand.
Once the constraints and loads have been defined and applied to the model, the design space has been chosen according to the choices made during the design process detailed in Section 5.5. In particular, the blue regions of Fig. 4 that have been considered as non-design space includes the areas around the fixing and centering holes of the two motors, the area around the shaft connecting the finger mechanisms to the motors, the four D components of the kinematic

Actuation system torques	[Nmm]
Motor 1	1125
Motor 2	1125

Table 8: Actuation system actions on the support flanges.

Responses	**Constraints**	**Objective**
Static Stress	$\leqslant 150$ MPa	Min. W.Compliance
Volume Fraction	Volume $\leqslant 30\%$	
Weighted Compliance		

Table 9: Optimization variables chosen in the hand exoskeleton back frame topology optimization.

system, since they are exploited only to simulate the load application, the front part, which presents the joint that allow for the ab/adduction gesture, the area around the hole where the elastic band runs. Also for this component, the objective function to be minimized has been the weight deformation energy (Weighted Compliance), as it leads to good results avoiding the generation of quite irregular geometries due to convergence issues. In this case, a solution that allow for a minimum deformation energy for all the set load cases (forces and torques generated by the opening and closing gestures and torques due to the actuation system working both to drive flexion and extension of the hand) has been required to the solver. In Tab. 9 the optimization variables are reported. Figures 5 and 6 show, respectively, the elements density of the optimized model and the final design of the back frame. Finally, Tab. 10 reports the comparison, in terms of stress and displacement, between the original and the optimized components. The comparison has been carried out taking into account two different load cases. "Mechanism-driven" case happens when the finger are moved to generate 20 N each for manipulation purposes. "Mechanism-driven" case consider the case when the actuation system is in charge of exerting 20 N per finger mechanism.

	Load cases	Original		Optimized	
		Stress [MPa]	Disp. [mm]	Stress [MPa]	Disp. [mm]
Mechanism-driven	Opening	8.8	0.003	114	0.007
	Closing	8.8	0.003	114	0.007
Motors-driven	Opening	99	0.1	99	0.2
	Closing	99	0.1	99	0.2

Table 10: Hand exoskeleton back frame benchmark test and optimization results.
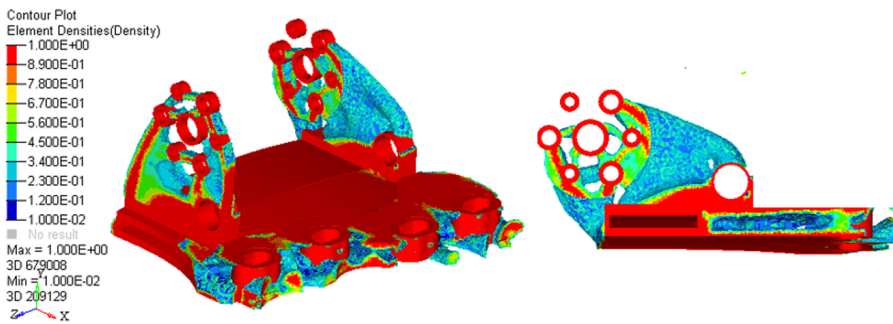
Figure 5: Hand exoskeleton back frame optimized model.
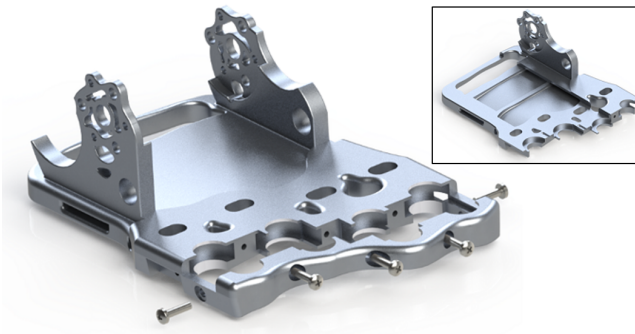
Figure 6: Reconstruction process results of the hand exoskeleton back frame. The section view highlights the internal holes.

Annex A

Informed consent

The tests were conducted under the supervision of health experts of the Rehabilitation Centre IRCCS "Don Carlo Gnocchi".

Informed consent and information sheet for the subject are available.

According to the policy of the Rehabilitation Centre IRCCS "Don Carlo Gnocchi", ethical approval is not required for the one-time qualitative tests conducted.

Written confirmation has been also obtained from the director of the center, Prof. Carlo Macchi. This document is available upon request.

FOGLIO INFORMATIVO E MODULO DI CONSENSO INFORMATO

ALLA PARTECIPAZIONE AL PROGETTO DI RICERCA

PER I SOGGETTI ADULTI

Titolo dello studio: *Test di controllo di un sistema di movimentazione per la mano con attuazione a cavi.*

Egr. Sig. / Gent.le Sig.ra

La informiamo che stiamo conducendo presso l'IRCCS Centro di Riabilitazione Don Carlo Gnocchi di Firenze, uno studio dal titolo: *Studio di un controllo ElettroMioGrafico (EMG) per un esoscheletro di mano.*

Per realizzare questo studio desideriamo avvalerci della collaborazione e della disponibilità di persone come Lei che soddisfano i requisiti idonei all'inserimento nella prova ergonomica di un dispositivo di guanto attuato per l'ausilio alla movimentazione della mano. Per questo motivo Le proponiamo di partecipare allo studio che sarà condotto sotto la responsabilità del Ing. Federica Vannetti.

Prima che Lei decida se accettare o rinunciare, La invitiamo a leggere con attenzione questo documento, qualora Lei desideri avere ulteriori informazioni e chiarimenti potrà rivolgersi all'Ing. Federica Vannetti (i cui recapiti sono indicati in fondo al presente documento) che Le dedicherà tutto il tempo necessario per chiarire ogni Suo dubbio, fermo restando che Lei potrà rivolgersi in qualsiasi momento anche agli operatori coinvolti nell'esecuzione dello studio.

Premesse e scopo dello studio

L'idea alla base del progetto è sviluppare un innovativo sistema di supporto per la movimentazione della mano di pazienti non autonomi in tale task. A tal scopo è stato ideato una nuovo esoscheletro attuato da cavi in grado di aprire la mano del soggetto che lo indossa per agevolare la presa di oggetti. Questo sistema è controllato mediante l'utilizzo di sensori EMG (superficiali) posti sull'avambraccio dell'utilizzatore.

Procedure previste dallo studio

- Esecuzione di esercizi di presa su oggetti di uso quotidiano (frutta, telefono, ecc…).
- Esecuzione di una "stretta di mano" fra Lei e un'altra persona che non indosserà alcun ausilio motorio.
- L'esecuzione del protocollo non richiede particolari capacità motorie.
- L'esecuzione dei vari task motori verrà ripresa con una telecamera.

Possibili benefici relativi alla partecipazione allo studio.

Lo studio è diretto alla valutazione di possibili sviluppi nel design del dispositivo.
Lo studio non altera in nessun modo lo status dei soggetti partecipanti.

Possibili rischi / effetti collaterali legati alla partecipazione allo studio.

Nessuno, data la natura dello studio di tipo non invasivo, assente di effetti permanenti e basato su task motori semplici ed eseguibili da qualunque soggetto normodotato.

Assicurazione

Data la natura non farmacologica dello studio, non è necessaria una copertura assicurativa aggiuntiva rispetto a quella già prevista dalla polizza generale di assicurazione per responsabilità civile stipulata dalla Fondazione Don Carlo Gnocchi.

Partecipazione allo studio

La Sua partecipazione è completamente libera e volontaria.

Se Lei acconsente a partecipare Le sarà chiesto di firmare il Modulo di Consenso Informato, allegato al presente documento, prima che Lei inizi a eseguire la procedura prevista dallo studio.

La firma del modulo allegato è al fine di garantire che Lei abbia ricevuto un'informazione completa e che abbia espresso liberamente la Sua volontà di partecipare; tale firma non implica alcun impegno da parte Sua a proseguire lo studio, non costituisce un vincolo di natura contrattuale, né rappresenta una rinuncia ai diritti che Le spettano.

Nel caso in cui Lei decida di ritirarsi dallo studio, dopo avere inizialmente accettato, potrà interrompere la Sua partecipazione in qualsiasi momento dandone comunicazione al responsabile dello studio senza dover fornire una giustificazione. La scelta di non partecipare, o di ritirarsi dopo l'iniziale accettazione, non comporta l'esclusione o la limitazione delle cure e dell'assistenza che Lei riceve presso le nostre strutture, né alcuna penalizzazione nel Suo rapporto con il personale che La assiste.

Qualora si venisse a conoscenza di nuovi dati o di risultati che possano influenzare la Sua partecipazione allo studio ne sarà tempestivamente informato/a; inoltre, il Responsabile dello studio potrà ritirarLa dallo studio qualora ritenga che tale decisione risponda al Suo migliore interesse.

Sul piano economico la partecipazione allo studio non determina alcun tipo di onere o di spesa aggiuntiva a Suo carico.

Precisiamo che non Le viene richiesto di partecipare a questo studio per ricevere assistenza clinica, o per ottenere beneficio personale di tipo diagnostico, in ogni caso le possibilità di cura di cui dispone il Centro della Fondazione a cui Lei afferisce saranno sempre a Sua disposizione.

Non è prevista l'assunzione di alcuna terapia farmacologica né la sospensione, lì dove presente, della stessa nei soggetti ritenuti idonei e partecipanti allo studio.

Trattamento dei dati personali

Titolari del trattamento e finalità

La Fondazione Don Carlo Gnocchi-Onlus, persona giuridica privata nella persona del legale rappresentante pro-tempore, Don Vincenzo Barbante, con sede legale in P.le R. Morandi, 6 – 20121 Milano, in accordo con le responsabilità previste dalle norme di pratica clinica (D.M. 15.7.1997, D. Lgs. 211/2003, D. Lgs. 200/2007) e di protezione dei dati personali (D. Lgs. 196/2003) nonché dalle disposizioni dell'Autorità Garante per la protezione dei dati personali tratterà in qualità di Titolare i dati personali del/della paziente, in particolare quelli sulla salute, nella misura indispensabile in relazione all'obiettivo dello studio ed in funzione della realizzazione dello stesso.

Responsabile del trattamento è stato designato il Dr. Francesco Converti (Direttore del Presidio Centro 1 della Fondazione a cui afferisce l'IRCCS di Firenze) che ha ricevuto istruzioni scritte anche per le finalità della tutela della riservatezza dei dati sensibili.

L'Ing. Alessandro Ridolfi sarà il rappresentate dell'Università degli Studi di Firenze, partner dello studio proposto.

Natura del conferimento dei dati

Il conferimento dei dati personali sopramenzionati è facoltativo, ma l'eventuale rifiuto, totale o parziale, al conferimento e al trattamento da parte Sua non Le consentirà di partecipare allo studio.

Natura dei dati e modalità di trattamento

Tutte le informazioni, personali e cliniche che La riguardano, raccolte durante questo studio sono confidenziali e saranno trattate nel rispetto della normativa vigente sopra richiamata. I dati relativi ad ogni soggetto verranno anonimizzati e resi ricollegabili per mezzo di un codice identificativo. Tale codici saranno utilizzati unicamente dai responsabili allo studio precedentemente menzionati.

I dati, trattati mediante strumenti anche elettronici, potranno essere diffusi in forma rigorosamente anonima attraverso riunioni, convegni e pubblicazioni scientifiche; in ogni caso il Suo nome o qualsiasi altro dettaglio idoneo a identificarLa, non saranno divulgati in quanto i dati potranno essere presentati esclusivamente in forma aggregata ovvero secondo modalità che non rendano identificabili i soggetti partecipanti allo studio.

Esercizio dei diritti
Lei potrà esercitare i diritti di cui all'art. 7 del D.Lgs. 193/2003 (accedere ai Suoi dati personali, chiederne l'integrazione, l'aggiornamento, la rettifica, la cancellazione, opporsi al trattamento, etc….) rivolgendosi direttamente al Responsabile del trattamento oppure tramite il personale da esso incaricato.
Nel caso in cui Lei si ritiri dallo studio, non saranno più raccolti ulteriori dati che La riguardano, fermo restando l'utilizzo di quelli eventualmente già acquisiti per determinare, senza alterarli, i risultati dello studio.

Per ulteriori informazioni, chiarimenti e comunicazioni:
Ing. Alessandro Ridolfi
Università degli Studi di Firenze - Dipartimento di Ingegneria Industriale (DIEF)
Ricercatore presso la Sezione di Meccanica Applicata
Via di Santa Marta 3
50139 Firenze (FI) ITALIA
Telefono +39 055 2758761
Cellulare +39 340 6104918 // +39 338 8756944
Fax +39 055 2758755
Email: a.ridolfi@unifi.it

La ringraziamo per la Sua disponibilità e la Sua collaborazione

MODULO DI CONSENSO INFORMATO per la partecipazione allo studio:

Test di controllo di un sistema di movimentazione per la mano con attuazione a cavi.
PER I SOGGETTI ADULTI

Io sottoscritto: __ Bianchini Massimo __
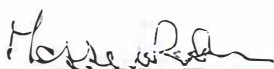*Cognome e Nome in stampatello del soggetto adulto partecipante.*

nato a, il: ___ Firenze __ 12/06/1963 __
Luogo e data di nascita del soggetto adulto partecipante.

DICHIARO QUANTO SEGUE:

1. ho letto e compreso il foglio informativo di cui questo modulo è parte integrante;

2. ho avuto la possibilità di porre domande e di chiedere spiegazioni all'Ing. Federica Vannetti dalla quale ho ricevuto risposte soddisfacenti;

3. mi sono state illustrate la natura, lo scopo e la durata dello studio, le procedure che saranno seguite, il trattamento previsto per i partecipanti e il tipo di collaborazione che ad essi sarà richiesta;

4. ho compreso che la mia partecipazione allo studio è libera e volontaria e che in qualsiasi momento posso decidere di ritirarmi dallo studio senza essere in alcun modo privato/a delle cure e dell'assistenza di cui ho bisogno e dell'eventuale accesso a nuove prospettive diagnostiche e/o terapeutiche e senza che siano compromessi i miei diritti e il mio rapporto con il medico e con gli operatori sanitari;

5. ai sensi del Decreto Legislativo n.196/2003 e successive modificazioni, acconsento al trattamento dei miei dati personali e sensibili raccolti nell'ambito di questo studio nei termini e nei modi indicati nel presente documento.

Tutto ciò premesso, nella mia piena capacità di intendere e di volere e senza alcuna forma di condizionamento o coercizione, accetto la proposta di partecipare allo studio descritto nel presente documento.

Luogo e data: Firenze, 20/11/2017   Firma: _____

PARTE RISERVATA ALL'OPERATORE CHE HA PRESENTATO L'INFORMATIVA

Io sottoscritta Ing. FEDERICA VANNETTI _____ *(Cognome e Nome in stampatello)*

DICHIARO:

a. di avere spiegato alla persona sopraindicata la natura e lo scopo dello studio, nonché le procedure che saranno adottate e il tipo di collaborazione che sarà richiesta;

b. di non avere cercato di influenzare o di costringere in alcun modo la persona sopra indicata per indurla a manifestare il suo consenso alla partecipazione allo studio;

c. di rilasciare alla persona sopraindicata una copia firmata e datata del presente modulo insieme al foglio informativo.

Luogo e data: Firenze, 20/11/2017   Firma: _____

References

[1] Y. Y. Huang and K. H. Low, "Initial analysis and design of an assistive rehabilitation hand device with free loading and fingers motion visible to subjects," in *2008 IEEE International Conference on Systems, Man and Cybernetics*, Oct 2008, pp. 2584–2590.

[2] W. H. Organization, "WHO global disability action plan 2014-2021: better health for all people with disability," World Health Organization, Tech. Rep., apr 2014.

[3] W. S. Harwin, J. L. Patton, and V. R. Edgerton, "Challenges and opportunities for robot-mediated neurorehabilitation," *Proceedings of the IEEE*, vol. 94, no. 9, pp. 1717–1726, 2006.

[4] L. Rosenstein, A. Ridgel, B. S. A. Thota, and J. Alberts, "Effects of combined robotic therapy and repetitive-task practice on upper-extremity function in a patient with chronic stroke," *The American journal of occupational therapy: official publication of the American Occupational Therapy Association*, vol. 1, no. 62, pp. 28–35, 2008.

[5] A. Heller, D. Wade, V. Wood, A. Sunderland, R. Hewer, and E. Ward, "Arm function after stroke: measurement and recovery over the first three months," *Journal of Neurology, Neurosurgery and Psychiatry*, vol. 131, no. 50, pp. 714–719, 1987.

[6] D. Wade, R. Langton-Hewer, V. Wood, C. Skilbeck, and H. Ismail, "The hemiplegic arm after stroke: measurement and recovery," *Journal of Neurology, Neurosurgery and Psychiatry*, vol. 46, no. 6, pp. 521–524, 1983.

[7] A. Sunderland, D. Tinson, L. Bradley, and R. Hewer, "Arm function after stroke. An evaluation of grip strength as a measure of recovery and a

prognostic indicator," *Journal of Neurology, Neurosurgery and Psychiatry*, vol. 52, no. 11, pp. 1267–1272, 1989.

[8] H. Nakayama, H. Jrgensen, H. Raaschou, and T. Olsen, "Recovery of upper extremity function in stroke patients: the Copenhagen Stroke Study," *Archives of Physical Medicine and Rehabilitation*, vol. 75, no. 4, pp. 394–398, 1994.

[9] Siciliano, Bruno and Khatib, Oussama, *Springer handbook of robotics.* Springer, 2016.

[10] P. Heo, G. M. Gu, and S. Lee, "Current hand exoskeleton technologies for rehabilitation and assistive engineering," *International Journal of Precision Engineering and Manufacturing*, vol. 13, no. 5, pp. 807–824, May 2012.

[11] M. Troncossi, M. Mozaffari-Foumashi, and V. Parenti-Castelli, "An Original Classification of Rehabilitation Hand Exoskeletons," *Journal of Robotics and Mechanical Engineering Research*, vol. 1, no. 4, pp. 17–29, 2016.

[12] R. A. Bos, C. J. Haarman, T. Stortelder, K. Nizamis, J. L. Herder, A. H. Stienen, and D. H. Plettenburg, "A structured overview of trends and technologies used in dynamic hand orthoses," *Journal of NeuroEngineering and Rehabilitation*, vol. 13, no. 1, p. 62, Jun 2016. [Online]. Available: https://doi.org/10.1186/s12984-016-0168-z

[13] L. Martinez, O. Olaloye, M. Talarico, S. Shah, R. Arends, and B. BuSha, "A power-assisted exoskeleton optimized for pinching and grasping motions," in *Northeast Bioengineering Conference*, 2010, pp. 1–2.

[14] S. Moromugi, Y. Koujina, S. Ariki, T. Okamoto, A.and Tanaka, M. Q. Feng, and T. Ishimatsu, "Muscle stiffness sensor to control an assistance device for the disabled," *Artificial Life and Robotics*, vol. 8, no. 1, pp. 42–45, 2004.

[15] J. Iqbal, N. Tsagarakis, A. Fiorilla, and D. Caldwell, "A portable rehabilitation device for the hand," in *International Conference of the IEEE Engineering in Medicine and Biology*, 2010, pp. 3694 – 3697.

[16] C. Jones, F. Wang, C. Osswald, X. Kang, N. Sarkar, and D. Kamper, "Control and kinematic performance analysis of an Actuated Finger Exoskeleton for hand rehabilitation following stroke," in *International Conference on Biomedical Robotics and Biomechatronics (BioRob)*, 2010, pp. 282–287.

[17] J. Li, R. Zheng, Y. Zhang, and J. Yao, "iHandRehab: An interactive hand exoskeleton for active and passive rehabilitation," in *International Conference on Rehabilitation Robotics (ICORR)*, 2010, pp. 1–6.

[18] Y. Hasegawa, Y. Mikami, K. Watanabe, and Y. Sankai, "Five-fingered assistive hand with mechanical compliance of human finger," in *International Conference on Robotics and Automation(ICRA)*, 2008, pp. 718–724.

[19] C. Schabowsky, S. Godfrey, R. Holley, and P. Lum, "Development and pilot testing of HEXORR: Hand EXOskeleton Rehabilitation Robot," *Journal of NeuroEngineering and Rehabilitation*, 2010.

[20] C. Jones, F. Wang, C. Osswald, X. Kang, N. Sarkar, and D. Kamper, "Control and kinematic performance analysis of an Actuated Finger Exoskeleton for hand rehabilitation following stroke," in *International Conference on Biomedical Robotics and Biomechatronics (BioRob)*, 2010, pp. 282–287.

[21] A. Wege, K. Kondak, and G. Hommel, "Mechanical design and motion control of a hand exoskeleton for rehabilitation," in *International Conference on Mechatronics and Automation (ICMA)*, 2005, pp. 155–519.

[22] A. Chiri, N. Vitiello, F. Giovacchini, S. Roccella, F. Vecchi, and M. Carrozza, "Mechatronic Design and Characterization of the Index Finger Module of a Hand Exoskeleton for Post-Stroke Rehabilitation," *IEEE/ASME Transactions on Mechatronics*, vol. 17, no. 5, pp. 884–894, 2012.

[23] A. Wege and G. Hommel, "Development and control of a hand exoskeleton for rehabilitation of hand injuries," in *International Conference on Intelligent Robots and Systems (IROS 2005)*, 2005, pp. 3046–3051.

[24] C. Takahashi, L. Der-Yeghiaian, V. Le, R. Motiwala, and S. Cramer, "Robot-based hand motor therapy after stroke," *Brain*, vol. 131, no. 2, pp. 425–437, 2008.

[25] M. Mulas, M. Folgheraiter, and G. Gini, "An EMG-controlled exoskeleton for hand rehabilitation," in *International Conference on Rehabilitation Robotics (ICORR)*, 2013, pp. 371 – 374.

[26] K. Rotella, M.F.and Reuther, C. Hofmann, E. Hage, and B. BuSha, "An orthotic hand-assistive exoskeleton for actuated pinch and grasp," in *Northeast Bioengineering Conference*, 2009, pp. 1–2.

[27] E. Brokaw, I. Black, R. Holley, and P. Lum, "Hand Spring Operated Movement Enhancer (HandSOME): A Portable, Passive Hand Exoskeleton for Stroke Rehabilitation," *Transactions on Neural Systems and Rehabilitation Engineering*, vol. 19, no. 4, pp. 391–399, 2011.

[28] A. Stilli, A. Cremoni, M. Bianchi, A. Ridolfi, F. Gerii, F. Vannetti, H. A. Wurdemann, B. Allotta, and K. Althoefer, "Airexglove a novel pneumatic exoskeleton glove for adaptive hand rehabilitation in post-stroke patients," in *2018 IEEE International Conference on Soft Robotics (RoboSoft)*, April 2018, pp. 579–584.

[29] H. Yap, F. Nasrallah, J. Lim, F. Low, J. Goh, and R. Yeow, "MRC-glove: A fMRI compatible soft robotic glove for hand rehabilitation application," in *International Conference on Rehabilitation Robotics (ICORR)*, 2015, pp. 735–740.

[30] P. Polygerinos, Z. Wang, K. Galloway, R. Wood, and W. C.J., "Soft robotic glove for combined assistance and at-home rehabilitation," *Robotics and Autonomous Systems*, vol. 73, pp. 135–143, 2015.

[31] R. Deimel and O. Brock, "A Novel Type of Compliant, Underactuated Robotic Hand for Dexterous Grasping," in *Proceedings of Robotics: Science and Systems*, 2014.

[32] S. Delph, M.A.and Fischer, P. Gauthier, C. Luna, E. Clancy, and G. Fischer, "A soft robotic exomusculature glove with integrated sEMG sensing for hand rehabilitation," in *International Conference on Rehabilitation Robotics (ICORR)*, 2013.

[33] K. Tong, S. Ho, P. Pang, X. Hu, W. Tam, K. Fung, X. Wei, P. Chen, and M. Chen, "An intention driven hand functions task training robotic system," in *International Conference of the IEEE Engineering in Medicine and Biology*, 2010.

[34] J. Iqbal and B. Khelifa, "Stroke rehabilitation using exoskeleton-based robotic exercisers: Mini Review," *Biomedical Research*, vol. 26, no. 1, pp. 197–201, 2015.

[35] M. Bianchi, M. Cempini, R. Conti, E. Meli, A. Ridolfi, N. Vitiello, and B. Allotta, "Design of a series elastic transmission for hand exoskeletons," *Mechatronics*, vol. 51, pp. 8 – 18, 2018. [Online]. Available: http://www.sciencedirect.com/science/article/pii/S095741581830031X

[36] L. Lucas, M. DiCicco, and Y. Matsuoka, "An EMG-Controlled Hand Exoskeleton for Natural Pinching," *Journal of Robotics and Mechatronics*, vol. 16, no. 5, pp. 1–7, 2004.

[37] R. Conti, E. Meli, A. Ridolfi, M. Bianchi, L. Governi, Y. Volpe, and B. Allotta, "Kinematic synthesis and testing of a new portable hand exoskeleton," *Meccanica*, 2017.

[38] Cheli, Federico and Pennestrí EttoreSiciliano, Bruno and Khatib, Oussama, *Cinematica e dinamica dei sistemi multibody. Vol. 1: Teoria.* CEA, 2006.

[39] C. Han, "A general method for the optimum design of mechanisms," *Journal of Mechanisms*, vol. 1, no. 3-4, pp. 301–313, 1966.

[40] S. Kramer and G.N.Sandor, "Selective Precision Synthesis. A General Method of Optimization for Planar Mechanisms," *ASME Journal of Engineering for Industry*, vol. 97, no. 2, pp. 689–701, 1975.

[41] V. N. Sohoni and E. J. Haug, "A State Space Technique for Optimal Design of Mechanisms," *ASME Journal of Mechanical Design*, vol. 104, no. 4, pp. 792–798, 1982.

[42] A. Bataller, J. Cabrera, M. Clavijo, and J. Castillo, "Evolutionary synthesis of mechanisms applied to the design of an exoskeleton for finger rehabilitation," *Mechanism and Machine Theory*, vol. 105, pp. 31–43, 2016.

[43] M. Sarac, M. Solazzi, E. Sotgiu, M. Bergamasco, and A. Frisoli, "Design and kinematic optimization of a novel underactuated robotic hand exoskeleton," *Meccanica*, vol. 52, pp. 749–761, 2017.

[44] M. Bianchi, N. Secciani, A. Ridolfi, F. Vannetti, and G. Pasquini, "Model-based approach in developing a hand exoskeleton for children: A preliminary study," in *Wearable Robotics: Challenges and Trends*, M. C. Carrozza, S. Micera, and J. L. Pons, Eds. Cham: Springer International Publishing, 2019, pp. 490–494.

[45] M. Bianchi *et al.*, "Kinematics-based strategy for the design of a pediatric hand exoskeleton prototype," in *Advances in Italian Mechanism Science*, G. Carbone and A. Gasparetto, Eds. Cham: Springer International Publishing, 2019, pp. 501–508.

[46] M. Bianchi, F. Fanelli, L. Giordani, A. Ridolfi, F. Vannetti, and B. Allotta, "An automatic scaling procedure for a wearable and portable hand exoskeleton," in *2016 IEEE 2nd International Forum on Research and Technologies for Society and Industry Leveraging a better tomorrow (RTSI)*, Sept 2016, pp. 1–5.

[47] M. Bianchi, F. Fanelli, E. Meli, A. Ridolfi, F. Vannetti, M. Bianchini, and B. Allotta, "Optimization-based scaling procedure for the design of fully portable hand exoskeletons," *Meccanica*, vol. 53, no. 11, pp. 3157–3175, Sep 2018. [Online]. Available: https://doi.org/10.1007/s11012-018-0858-7

[48] J. Nelder and R. Mead, "A simplex method for function minimization," *Computer Journal*, vol. 7, no. 4, pp. 308–313, 1965.

[49] F. Cordella, L. Zollo, A. Salerno, D. Accoto, E. Guglielmelli, and B. Siciliano, "Human hand motion analysis and synthesis of optimal power grasps for a robotic hand," *International Journal of Advanced Robotic Systems*, vol. 11, no. 37, pp. 1–13, 2013.

[50] I. M. Bullock, J. Borrs, and A. Dollar, "Assessing assumptions in kinematic hand models: A review," *International Conference on Biomedical Robotics and Biomechatronics (BioRob)*, pp. 139–146, 2012.

[51] X. Zhang, S. Lee, and P. Braido, "Determining finger segmental centers of rotation in flexion-extension based on surface marker measurement," *Journal of Biomechanics*, vol. 36, pp. 1097–1102, 2003.

[52] Luersen, M.A. and Le Riche, R. and Guyon, F., "A constrained, globalized and bounded Nelder-Mead method for engineering optimization," *Structural and Multidisciplinary Optimization*, vol. 27, no. 1, pp. 43–54, 2004.

[53] J. Lagarias, J. Reeds, M. Wright, and P. Wright, "Convergence properties of the Nelder-Mead simplex method in low dimension," *SIAM Journal of Optimization*, vol. 9, no. 1, pp. 112–147, 1998.

[54] N. Secciani, M. Bianchi, A. Meschini, A. Ridolfi, Y. Volpe, L. Governi, and B. Allotta, "Assistive hand exoskeletons: The prototypes evolution at the university of florence," in *Advances in Italian Mechanism Science*, G. Carbone and A. Gasparetto, Eds. Cham: Springer International Publishing, 2019, pp. 307–315.

[55] N. Secciani, M. Bianchi, A. Ridolfi, F. Vannetti, and B. Allotta, "Assessment of a hand exoskeleton control strategy based on user's intentions classification starting from surface emg signals," in *Wearable Robotics: Challenges and Trends*, M. C. Carrozza, S. Micera, and J. L. Pons, Eds. Cham: Springer International Publishing, 2019, pp. 440–444.

[56] M. Bianchi, F. Fanelli, R. Conti, L. Governi, E. Meli, A. Ridolfi, A. Rindi, F. Vannetti, and B. Allotta, "Design and motion analysis of a wearable and portable hand exoskeleton," in *Wearable Robotics: Challenges and Trends*, J. González-Vargas, J. Ibáñez, J. L. Contreras-Vidal, H. van der Kooij, and J. L. Pons, Eds. Cham: Springer International Publishing, 2017, pp. 373–377.

[57] R. H. Byrd, J. C. Gilbert, and J. Nocedal, "A trust region method based on interior point techniques for nonlinear programming," *Mathematical Programming*, vol. 89, no. 1, pp. 149–185, Nov 2000. [Online]. Available: https://doi.org/10.1007/PL00011391

[58] J. Lobo-Prat, P. N. Kooren, A. H. Stienen, J. L. Herder, B. F. Koopman, and P. H. Veltink, "Non-invasive control interfaces forintention detection in active movement-assistive devices," *Journal of NeuroEngineering and Rehabilitation*, vol. 11, no. 1, p. 168, Dec 2014. [Online]. Available: https://doi.org/10.1186/1743-0003-11-168

[59] A. A. Adewuyi, L. J. Hargrove, and T. A. Kuiken, "Evaluating emg feature and classifier selection for application to partial-hand prosthesis control," *Frontiers in Neurorobotics*, vol. 10, p. 15, 2016. [Online]. Available: https://www.frontiersin.org/article/10.3389/fnbot.2016.00015

[60] M. Bianchi, T. Buetzer, F. Fanelli, N. Secciani, A. Ridolfi, O. Lambercy, F. Vannetti, and B. Allotta, "Development of an EMG triggered hand exoskeleton for assistive and rehabilitation purposes," in *Proceedings of the 2016 IEEE/RSJ International Conference on Intelligent Robots and Systems (IROS 2016)*, october 2016.

[61] X. Li, S. Chen, H. Zhang, O. W. Samuel, H. Wang, P. Fang, X. Zhang, and G. Li, "Towards reducing the impacts of unwanted movements on identification of motion intentions," *Journal of Electromyography and Kinesiology*, vol. 28, pp. 90 – 98, 2016. [Online]. Available: http://www.sciencedirect.com/science/article/pii/S1050641116300189

[62] B. Hudgins, P. Parker, and R. N. Scott, "A new strategy for multifunction myoelectric control," *IEEE Transactions on Biomedical Engineering*, vol. 40, no. 1, pp. 82–94, Jan 1993.

[63] N. Olhoff, "On optimum design of structures and materials," *Meccanica*, vol. 31, no. 2, pp. 143–161, Apr 1996. [Online]. Available: https://doi.org/10.1007/BF00426257

[64] S. Degertekin, "Improved harmony search algorithms for sizing optimization of truss structures," *Computers and Structures*, vol. 92-93, pp. 229 – 241, 2012. [Online]. Available: http://www.sciencedirect.com/science/article/pii/S004579491100277X

[65] R. Drazumeric and F. Kosel, "Shape optimization of beam due to lateral buckling problem," *International Journal of Non-Linear Mechanics*, vol. 47, no. 3, pp. 65 – 74, 2012. [Online]. Available: http://www.sciencedirect.com/science/article/pii/S002074621100268X

[66] P. Hajela and E. Lee, "Genetic algorithms in truss topological optimization," *International Journal of Solids and Structures*, vol. 32, no. 22, pp. 3341 – 3357, 1995. [Online]. Available: http://www.sciencedirect.com/science/article/pii/002076839400306H

[67] W. Prager, "A note on discretized michell structures," *Computer Methods in Applied Mechanics and Engineering*, vol. 3, no. 3, pp. 349 – 355, 1974. [Online]. Available: http://www.sciencedirect.com/science/article/pii/004578257490019X

[68] M. N. Sudin, M. M. Tahir, F. R. Ramli, S. A. Shamsuddin, and H. T. Jaya, "Topology optimization in automotive brake pedal redesign," *International Journal of Engineering and Technology*, vol. 6, no. 1, 2014.

[69] M. Bianchi, F. Buonamici, R. Furferi, and N. Vanni, "Design and Optimization of a Flexion/Extension Mechanism for a Hand Exoskeleton System," in *ASME 2016 International Design Engineering Technical Conferences and Computers and Information in Engineering Conference*, august 2016.

[70] M.P. Bendsøe, O. Sigmund, *Topology Optimization: Theory, Methods and Applications.* Springer, 2003.

[71] M. Y. Wang, X. Wang, and D. Guo, "A level set method for structural topology optimization," *Computer Methods in Applied Mechanics and Engineering*, vol. 192, no. 1, pp. 227 – 246, 2003. [Online]. Available: http://www.sciencedirect.com/science/article/pii/S0045782502005595

[72] L. Shu, M. Y. Wang, Z. Fang, Z. Ma, and P. Wei, "Level set based structural topology optimization for minimizing frequency response," *Journal of Sound and Vibration*, vol. 330, no. 24, pp. 5820 – 5834, 2011. [Online]. Available: http://www.sciencedirect.com/science/article/pii/S0022460X11006079

[73] S. Osher and R. P. Fedkiw, "Level set methods: An overview and some recent results," *Journal of Computational Physics*, vol. 169, no. 2, pp. 463 – 502, 2001. [Online]. Available: http://www.sciencedirect.com/science/article/pii/S0021999100966361

[74] L. Dovat, O. Lambercy, R. Gassert, T. Maeder, T. Milner, T. Leong *et al.*, "HandCARE: a cable-actuated rehabilitation system to train hand function after stroke," *IEEE Transactions on Neural Systems and Reahabilitation Engineering*, vol. 16, no. 6, pp. 582–591, dec 2008.

[75] V. Mathiowetz, N. Kashman, G. Volland, K. Weber, M. Dowe, and S. Rogers, "HandCARE: a cable-actuated rehabilitation system to train hand function after stroke," *IEEE Transactions on Neural Systems and Reahabilitation Engineering*, vol. 66, no. 2, pp. 69–74, feb 1985.

[76] K. Matheus and A. Dollar, "Benchmarking Grasping and Manipulation: Properties of the Objects of Daily Living," in *IEEE/RSJ International Conference on Intelligent Robots and Systems (IROS)*, Taipei, Taiwan, Oct. 2010, pp. 5020–5027.

[77] D. Prattichizzo and J.C. Trinkle, "Grasping," in *Handbook of Robotics*. New York: Springer, 2016, pp. 955–988.

[78] S. Wang, K. Lim, B. Khoo, and M. Wang, "An extended level set method for shape and topology optimization," *Journal of Computational Physics*, vol. 221, no. 1, pp. 395 – 421, 2007. [Online]. Available: http://www.sciencedirect.com/science/article/pii/S0021999106002968

[79] Olek Zienkiewicz and Robert Taylor, *The Finite Element Method*. Butterworth-Heinemann, 2013.

[80] "Altair HyperWorks official web site," http://www.altairhyperworks.com/, accessed: 2018-09-12.

[81] G. Rozvany, "Aims, scope, methods, history and unified terminology of computer-aided topology optimization in structural mechanics," *Structural and Multidisciplinary Optimization*, vol. 21, no. 2, pp. 90–108, 2001.

[82] G. Treece, R. Prager, and A. Gee, "Regularised marching tetrahedra: improved iso-surface extraction," *Computers and Graphics*, vol. 23, no. 4, pp. 583–598, 1999.

[83] F. Montagnani, M. Controzzi, and C.Cipriani, "Independent Long Fingers are not Essential for a Grasping Hand," *Scientific Reports*, vol. 6, 2016.

[84] M. Santello, M. Flanders, and J. Soechting, "Postural hand synergies for tool use," *Journal of Neuroscience*, vol. 18, no. 23, pp. 10 105–10 115, 1998. [Online]. Available: https://www.ncbi.nlm.nih.gov/pubmed/9822764#

[85] M. Santello, M. Bianchi, M. Gabiccini, E. Ricciardi, G. Salvietti, D. Prattichizzo, M. Ernst, A. Moscatelli, H. Jrntell, A. M. Kappers, K. Kyriakopoulos, A. Albu-Schffer, C. Castellini, and A. Bicchi, "Hand synergies: Integration of robotics and neuroscience for understanding the control of biological and artificial hands," *Physics of Life Reviews*, vol. 17, pp. 1 – 23, 2016. [Online]. Available: http://www.sciencedirect.com/science/article/pii/S1571064516000269